BODY SURFACE LEAD REDUCTION ALGORITHM AND ITS USE IN INVERSE PROBLEM OF ELECTROCARDIOGRAPHY

A THESIS SUBMITTED TO
THE GRADUATE SCHOOL OF NATURAL AND APPLIED SIENCES
OF
MIDDLE EAST THECHNICAL UNIVERSITY

BY

FOUROUGH GHARBALCHI NO

IN PARTIAL FULFILLMENT OF THE REQUIREMENTS
FOR
FOR THE DEGREE OF MASTER OF SCIENCE
IN
BIOMEDICAL ENGINEERING

JANUARY 2015

Approval of the Thesis

BODY SURFACE LEAD REDUCTION ALGORITHM AND ITS USE IN INVERSE PROBLEM OF ELECTROCARDIOGRAPHY

submitted by **FOUROUGH GHARBALCHI NO** in partial fulfillment of the requirements for the degree of **Master of Science in Biomedical Engineering Department, Middle East Technical University** by,

Prof. Dr. Gülbin Dural Ünver
Dean, Graduate School of **Natural and Applied Sciences** _____

Prof. Dr. Işık Hakan Tarman
Head of Department, **Biomedical Engineering** _____

Assoc. Prof. Yeşim Serinağaoğlu Doğrusöz
Supervisor, **Electrical and Electronics Engineering Dept., METU** _____

Prof. Dr. Gerhard Wilhelm Weber
Co-supervisor**, Institute of Applied Mathematics., METU** _____

Examining Committee Members:

Prof. Dr. Nevzat G. Gençer
Electrical and Electronics Engineering Dept., METU _____

Assoc. Prof. Dr. Yeşim Serinağaoğlu Doğrusöz
Electrical and Electronics Engineering Dept., METU _____

Prof. Dr. Gerhard Wilhelm Weber
Co-supervisor**,** Institute of Applied Mathematics., METU _____

Prof. Dr. Tolga Çiloğlu
Electrical and Electronics Engineering Dept., METU _____

Assist. Prof. Dr. Ergin Tönük
Mechanical Engineering Dept., METU _____

Date: 26.01.2015

I hereby declare that all information in this document has been obtained and presented in accordance with academic rules and ethical conduct. I also declare that, as required by these rules and conduct, I have fully cited and referenced all material and results that are not original to this work.

Name, Last name: FOUROUGH GHARBALCHI NO

Signature :

ABSTRACT

BODY SURFACE LEAD REDUCTION ALGORITHM AND ITS USE IN INVERSE PROBLEM OF ELECTROCARDIOGRAPHY

Fourough Gharbalchi No
M.S. Department of Biomedical Engineering
Supervisor: Assoc. Prof. Yeşim Serinağaoğlu Doğrusöz
January 2015, 97 pages

Determining electrical activity of the heart in a non-invasive way is one of the main issues in electrocardiography (ECG). Although several cardiac abnormalities can be diagnosed by the standard 12-lead ECG, many others are *not* detectable by this fixed lead configuration. One alternative to compensate for the imperfection of standard 12-lead ECG in detecting many of the most informative signals is Body Surface Potential Mapping (BSPM), which measures ECG signals from a dense array of electrodes (32-256 electrodes) over the body surface.

However, besides having no standard lead-set configuration, this method suffers from the need for a large number of leads to perform with an acceptable accuracy. Therefore, despite having the potential to be used in clinical applications, BSPM has not been a practically accepted method.

This study aims to propose a specific lead-set configuration, whose acquired data is sufficient to be used in inverse problem of ECG to reconstruct epicardial potentials with high accuracy. Towards this end, in our study, a lead reduction algorithm is

proposed and implemented. As a result of applying the lead reduction algorithm on 23 different data-sets related to 23 different stimulation sites on the surface of the heart, 23 exclusive lead-set configurations corresponding to these 23 data-sets are obtained. Then, by selecting the most repeated leads, two common lead-set configurations, one consisting 64 and the other consisting of 32 leads, are obtained.

To assess the performance of the proposed common lead-set configurations, inverse problem of ECG is solved using the data obtained by these lead-sets and the results are compared to those of exclusively optimal lead-sets, and the original complete lead-set. Mean and standard deviation values of Correlation Coefficient (CC) values obtained at each time instant between the true epicardial potentials and the inverse solutions are used to compare the results. By examining these mean and standard deviation of CC values, it has been observed that, instead of large number of leads, small number of leads optimally located on the surface of the torso would be sufficient to reconstruct the epicardial potentials accurately.

Additionally, inverse problem of ECG is solved using four different regularization algorithms, namely, Tikhonov Regularization, Truncated Total Least Squares (TTLS), Lanczos Truncated Total Least Squares (LTTLS), and Lanczos Least Squares QR (LLSQR), using data from the original complete lead-set, exclusively optimal and common lead-sets (32 and leads). Mean and standard deviation values of Correlation Coefficient (CC) for these inverse solutions are calculated and compared for three different data-sets. It is observed that LTTLS method reconstructs the epicardial potentials better than the TTLS and LLSQR methods.

Keywords: Lead reduction algorithm, Tikhonov regularization, Truncated Total Least Squares (TTLS) method, Lanczos Truncated Total Least Squares (LTTLS) method, Lanczos Least Squares QR (LLSQR) method, regularization parameter selection methods.

ÖZ

VÜCUT YÜZEYİ KAYIT NOKTALARININ AZALTILMASI ALGORİTMASI VE TERS ELEKTROKARDİYOGRAFİ PROBLEMİNE UYGULAMASI

Fourough Gharbalchi No

Yüksek Lisans, Biyomedikal Mühendisliği Bölümü

Tez Yöneticisi: Assoc. Prof. Yeşim Serinağaoğlu Doğrusöz

Ocak 2015, 97 sayfa

Kalbin elektriksel aktivitesini non-invazif bir şekilde belirlemek, elektrokardiyografideki (EKG) temel konulardan biridir. Kalpteki anormalliklerden bazılarının standart 12 kanallı EKG yöntemi ile teşhis edilebilmesine karşın, başka birçok anormallikler, bu sabit ölçüm noktası yapılandırması tarafından tespit edilememektedir. 12 kanallı EKG'nin gövde üzerinden detaylı bilgi taşıyan sinyallerin pek çoğunu algılayamama sorununu gidermek için bir altertatif, Vücut Yüzeyi Potansiyel Haritalaması (VYPH) yöntemidir. Bu yöntemde EKG sinyalleri vücut yüzeyinden çok kanallı (32-256) bir elektrot dizisinden ölçülmektedir.

Ancak, bu yöntemin iyi tanımlanmış bir kayıt noktası yapılandırmasının olmamasının yanı sıra, kabul edilebilir bir doğrululuğa ulaşabilmek için çok sayıda elektrot kullanılması da gerekmektedir. Bu nedenle, VYPH'nin klinik uygulamalarda kullanılabilme potansiyeli olmasına rağmen, bu yöntem pratik uygulamalarda kabul görmemiştir.

Bu çalışmada hedef, ters EKG probleminin çözümünde epikart potansiyel dağılımlarının yüksek doğrulukla elde edilebilmesini sağlayacak belirli bir kayıt

noktası yapılandırmasının önerilmesidir. Bu çalışmada, sözü geçen hedefe yönelik olarak bir kayıt noktası azaltma algoritmasi önerilmiş ve uygulanmıştır. Bu kayıt noktası azaltma algoritması, kalp üzerinde 23 farklı noktadan uyarılma sonucu elde edilen 23 farklı veri kümesine uygulanmış, bunun sonucunda 23 tane birbirinden farklı ve veriye özel kayıt noktası yapılandırması elde edilmiştir. Daha sonra, belirlenen bu kayıt noktalarından her veride en çok tekrar edilen kanallar seçilmiş ve biri 64 kanallı, diğeri 32 kanallı olmak üzere iki tane "ortak" (her veriye uygulanabilecek) kayıt noktası yapılandırması elde edilmiştir.

Elde edilen ortak kayıt noktası yapılandırmalarının performanslarını değerlendirebilmek amacıyla, her bir veri kümesi için ters EKG problemi hem ortak, hem de kendisine özel olan kayıt noktası yapılandırmalarından elde edilmiş VYPH kullanılarak çözülmüştür. Sonuçlar ayrıca tüm kayıt noktalarına ait VYPH kullanılarak elde edilen ters EKG çözümleriyle de karşılaştırılmıştır. Bu karşılaştırmalarda, çözümlerle gerçek epikart potansiyelleri arasında her zaman anında ayrı olarak hesaplanan korelasyon katsayılarının (KK) ortalama ve standart sapma değerleri kullanılmıştır. KK değerlerinin ortalama ve standart sapmalarının kıyaslanması sonucunda görülmüştür ki, çok sayıda kayıt noktası kullanmak yerine, az ama yeterli sayıda ve en uygun şekilde yapılandırılmış kayıt noktalarının kullanılmasıyla, epikart potansiyel dağılımlarının doğru bir şekilde elde edilmesi mümkün olmaktadır.

Ayrıca, bu çalışmada ters EKG problemi dört farklı düzenlileştirme yöntemi kullanılarak çözülmüştür. Bunlar, Tikhonov, Kesilmiş En Küçük Kareler Toplamı (TTLS), Lanczos Kesilmiş En Küçük Kareler Toplamı (LTTLS) ve Lanczos En Küçük Kareler QR (LLSQR) düzenlileştirme yöntemleridir. Bu yöntemlerle ters EKG problemi asıl (çok kanallı), veriye özgün elde edilmiş az kanallı, ortak elde edilmiş az kanallı (64 ve 32) kayıt noktası yapılandırmaları kullanılarak çözülmüş, çözümler birbirleriyle ve gerçek epikart potansiyelleriyle karşılaştırılmıştır. Bu karşılaştırmalar, yine KK ortalama ve standart sapma değerleri ile ve üç farklı veri seti için yapılmıştır. Sonuçlar incelendiğinde LTTLS yönteminin epikart potansiyel dağılımlarını TTLS ve LLSQR yöntemlerine göre daha iyi bir şekilde elde etmeye yaradığı görülmüştür.

Anahtar Kelimeler: Kayıt noktası azaltma algoritması, Tikhonov düzenlileştirmesi, Kesilmiş En Küçük Kareler Toplamı (TTLS), Lanczos Kesilmiş En Küçük Kareler Toplamı (LTTLS), Lanczos En Küçük Kareler QR (LLSQR), düzenlileştirme parametresi seçim yöntemleri.

To My Family

ACKNOWLEDGEMENTS

I am using this opportunity to express my special appreciation and thanks to my advisor Assoc. Prof. Yeşim Serinağaoğlu Doğrusöz. You have been a tremendous mentor for me. I am thankful for your aspiring guidance, invaluably constructive criticism and friendly advice during this study.

Besides my advisor, I am grateful to my co-adviser Prof. Dr. Gerhard Wilhelm Weber for his continuous support, patience, motivation, enthusiasm, and immense knowledge.

I would also like to thank my parents for their endless love and support during this study. Thank you for all of the sacrifices that you've made on my behalf.

Special thanks to my friend, Mehdi Sadighi. Words cannot express how grateful I am to him. I would like appreciate his kindness and support he has shown during the past one year it has taken me to finalize this thesis.

Last but not least, I would like to thank my friends, Mürsel Karadaş, Azadeh Kamali Tafreshi, Raha Shabani, Cihan Göksu, and Sasan Sokhanvar. They were always supporting me and encouraging me with their best wishes

This study is part of the project 111E258 that is supported by Turkish Scientific and Technological Research Council (TUBITAK).

TABLE OF CONTENTS

LIST OF TABLES

TABLES

LIST OF FIGURES

FIGURES

LIST OFABBREVIATIONS

ECG	Electrocardiography
BSPM	Body Surface Potential Mapping
TTLS	Truncated Total Least Square
LTTLS	Lanczos Truncated Total Least Square
LLSQR	Lanczos Least Square QR
CC	Correlation Coefficient
MCC	Maximum Correlation Coefficient
RDMS	Relative Difference Measurement Star

CHAPTER 1

INTRODUCTION

According to World Health Organization (WHO) report, an estimated 17 million people die of cardiovascular diseases, namely, heart attack and stroke, around the world every year [1]. There are over 2 million people in Turkey who are suffering from various types of heart diseases, and each year 160-170 thousand people die as a result of heart failure [2]. The yearly growing number of patients not only in Turkey, but also around the world has motivated researchers to seek for clinically practical methods to attain detailed and precise information about the electrical activity of the heart.

To obtain and understand the electrical activity of the heart is important in order to diagnose the problem and treat it before it leads to death. Determining electrical activity of the heart in non-invasive way is one of the main issues in Electrocardiography (ECG). Although several cardiac abnormalities are diagnosable by standard 12-lead ECG, many others are *not* detectable by this fixed lead configuration. An alternative to compensate for the imperfection of standard 12-lead ECG in detection of many of the most informative signals from the torso surface is Body Surface Potential Mapping (BSPM). This method is an ECG technique that records the potentials from a wide region of the chest using 100-200 or even more electrodes. There is no standard configuration for the BSPM approach. Although, this method has the potential to be used in clinical applications, due to the large number of employed electrodes, it has no uptake in practical approaches. The attachment of large number of leads makes the BSPM approach practically hard to apply. However, since the acquired electrical signals of the heart using BSPM approach are quite accurate and contain invaluable information, when they are

employed to solve the inverse problem of ECG, the results are also accurate. In other words, solving inverse problem of ECG using BSPM provides accurate information about the electrical sources on the surface of the heart.

Same as many other bioelectric signals, measured heart signals from the torso surface are noise contaminated, attenuated and smoothed due to inhomogeneity inside of the thorax. Thus, inverse problem of ECG is ill-posed and it needs to be regularized to give meaningful and stable solutions. Several regularization algorithms are proposed in literature to solve inverse problem of ECG. In this study, Tikhonov, Truncated Total Least Squares (TTLS), Lanczos Truncated Total Least Squares (LTTLS), and Lanczos Least Squares QR (LLSQR) regularization methods are used to solve the inverse problem of ECG to reconstruct potentials on the epicardial surface.

In this study, lead reduction algorithm is proposed and implemented to choose the leads whose acquired signals are informative and eliminate those whose signals have small or no contribution to understand the electrical activity of the heart. During the selection process Tikhonov regularization along with Maximum Correlation Coefficient (MCC) method as regularization parameter selection approach is used.

In this study, 23 data-sets each resulting from 23 different stimulation points are used. Given each of these 23 data-sets to the lead reduction algorithm as inputs, 23 exclusive lead-set configurations are obtained which are different from each other. Consequently, 23 different configurations with 32 and 64 number of leads are resulted.

This study aims to propose one specific lead-set configuration, consists of 64 or 32 leads, whose acquired data is qualified enough to be used to reconstruct epicardial potentials with high accuracy. By selecting the most repeated leads among all of 23 different lead-set configurations, 32 and 64 reduced lead-sets, namely, common lead-sets, appropriate for different data-sets are selected.

To assess the performance of these *common* lead-sets, the inverse problem of ECG is solved using the data obtained by these common lead-sets. Then the obtained solutions for common lead-set are compared with the solutions obtained by exclusive

configurations optimal for each data-set by calculating mean of Correlation Coefficient values between real epicardial potentials and related inverse solutions.

1.1 Scope of the Thesis

The aim of this study is to propose a lead-set configuration that works for different data-sets in order to effectively estimate the epicardial potentials on the surface of the heart, the latter is the result of the solution of inverse problem of electrocardiography (ECG). In this study, a new method to reduce the number of measurement leads attached to the surface of the torso is proposed and implemented. To this end, our proposed lead reduction algorithm is applied on 23 different data-sets related to 23 different stimulation sites. Since the data-sets are different from each other, application of the lead reduction algorithm on these data-sets results in 23 different lead-set configurations. The inverse solutions obtained by these lead-sets are compared quantitatively using Correlation Coefficient (CC) and Relative Difference Measurement Star (RDMS) to the real epicardial potentials. Later, having considered all 23 lead-set configurations according to number of lead number repetitions, the most repeated leads are chosen to form one common lead-set whose acquired data can produce a proper answer for all lead-sets.

The lead reduction algorithm employs Tikhonov regularization during lead selection process. To assess the performance of the common lead-set, four regularization methods, Tikhonov, Truncated Total Least Squares (TTLS), Lanczos Truncated Total Least Squares (LTTLS) and Lanczos Least Squares QR (LLSQR) are applied on the data obtained by this common lead-set. The results then are compared by calculating mean of Correlation Coefficient (CC) values between real epicardial potentials and the potentials related to inverse solution. The regularization parameter selection method used for above-mentioned regularization methods is Maximum Correlation Coefficient (MCC).

In this study, 30 dB Signal to Noise Ratio (SNR) is added to all of the data-sets prior to application of any method. In addition to the visualization software used in this study, MAP3D, all the data is provided by Utah Eccles Harrison Cardiovascular Research and Training Institute (CVRTI) [3].

1.2 Contribution of the Thesis

Nearly all of the lead-set configurations provided in the literature to derive Body Surface Potential Map (BSPM) suffer from the need of large number of electrodes that have to be attached to the torso surface in order to obtain data. This study proposes a lead-set configuration that is able to acquire many of the most informative signals related to the electrical activity of the heart. As it is stated in the previous section, all of the data used in this study is provided by Utah Eccles Harrison Cardiovascular Research and training Institute [3]. Tikhonov regularization and TTLS method used in this study are modified version provided by regularization toolbox [4], since the provided versions in the toolbox are suitable for over-determined systems but the systems in this study turn to be under-determined systems. The other regularization methods, LTTLS and LLSQR, are implemented to solve inverse problem of ECG, related to different lead-sets. In this study the lead reduction algorithm is newly proposed and implemented.

1.3. Outline of the Thesis

In Chapter 2, theory and literature survey about lead selection methods and different regularization methods to solve inverse problems of electrocardiography (ECG) or other kinds of inverse problems are discussed and explained.

In Chapter 3, the proposed and implemented method for lead reduction is explained, thoroughly. Additionally, the methods which are used in this study to solve the inverse problem of ECG are presented completely. The regularization parameter selection method used during regularization process MCC, which is also explained in Chapter 3.

Chapter 4 contains the results of the lead reduction algorithm for all 23 data-sets presenting the mean and standard deviation values of CC between real epicardial potentials and reconstructed potentials using data acquired by reduced lead-sets. Furthermore, this chapter includes MAP3D images of reconstructed potentials through Tikhonov regularization for different lead-sets. Finally, four different regularization methods, Tikhonov, TTLS, LTTLS, and LLSQR are applied to three

different data-sets. Mean and standard deviation of CC values are then calculated for these reconstructed potentials and presented in separate tables.

Chapter 5 includes conclusions of this study and future work.

CHAPTER 2

REVIEW AND BACKGROUND

In this chapter, first electrophysiology of the heart is discussed, including anatomy of the heart and its electrical activity, action potential generation and propagation. Then, after an introduction to the major methods of electrocardiography (ECG), the electrode selection approach which is one of the main subjects of this study, is discussed. Afterwards, forward and inverse problems of electrocardiography are defined. Later on, different methods to solve the inverse problem of ECG are introduced. To solve the inverse problem of ECG is another main subject of this study.

2.1 Anatomy of the Heart

Heart is the electro-mechanical pump of the body. The human heart lies within the thorax, in mediastinum. It pumps blood though vessels to the whole body. All parts of the body are fed by oxygen and nutrition received through blood flow, which the heart is responsible for. Thus the heart is a vital organ whose failure, most probably, causes death.

A healthy adult heart beats about 72 times, pumping 4.7-5.7 liters of blood per minute. It weights between 250-300 gr in females and between 300-350 gr in males [5, 6].

As it is illustrated in Figure 2.1, the heart consists of four chambers, which are filled and discharged with blood in every beat. Two atria and two ventricles compose four chambers of the heart. In every single cardiac cycle, the two atria receive blood and contract forcing the received blood to enter the corresponding ventricles, then

ventricles contract pumping the blood out of the heart. There are two blood circulation systems in the body; pulmonary and systemic. During pulmonary circulation, deoxygenated blood fills the right atrium through vena cava, then by contraction, right atrium forces the blood to the right ventricle. After passing the tricuspid valve, the blood enters the right ventricle, which afterward contracts and sends the blood out via pulmonary valve to pulmonary arteries leading to lungs. Simultaneously, oxygenated blood from the lungs enters the left atrium through pulmonary veins, and left atrium forces the blood through the mitral valve into the left ventricle, whose subsequent contraction pumps the blood through aortic valve into the aorta, leading to a systemic circulation.

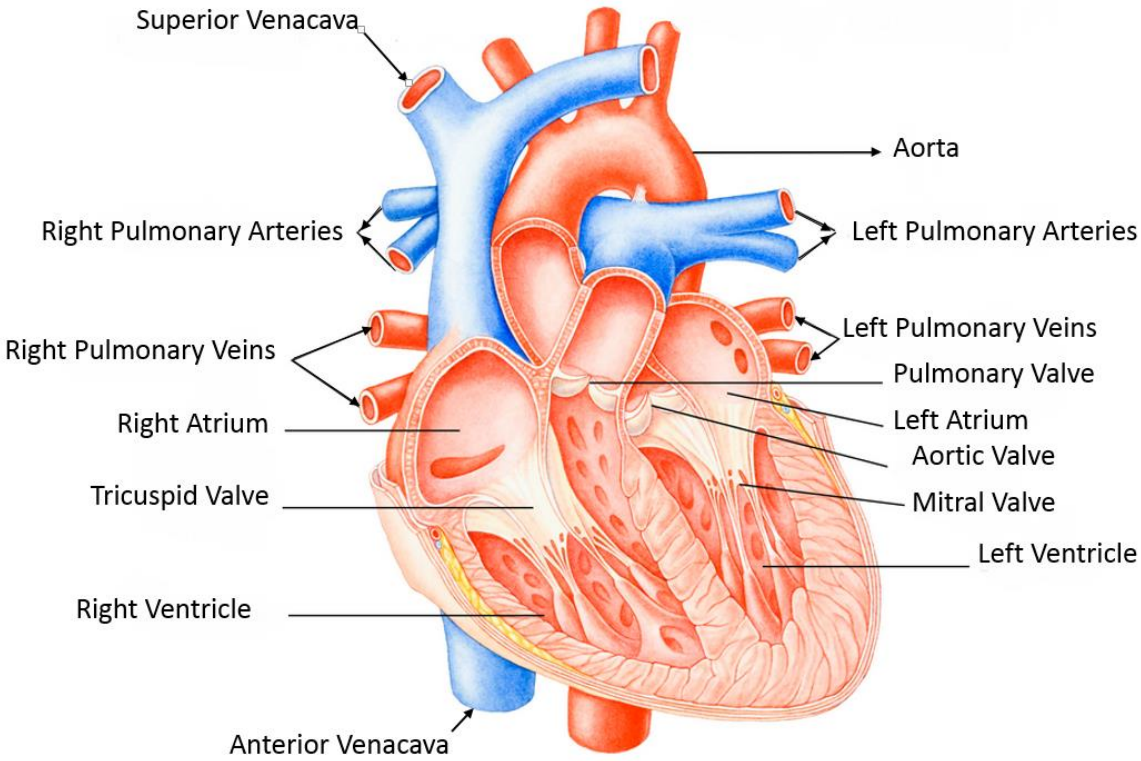

Figure 2.1: The anatomy of the heart and the vessels [7].

As it can be inferred from Figure 2.1, there are four heart valves; the tricuspid valve which prevents backflow of blood to the right atrium from the right ventricle. The pulmonary valve blocks the blood pumped to left pulmonary arteries from flowing back to the right ventricle, the mitral valve is the one way port to the left ventricle

and has the same prohibitive function, and the aortic valve restricts blood flow direction only towards the aorta.

The heart tissue is composed of four layers as it is illustrated in Figure 2.2.

1. *Pericardium*: the outermost double layer membrane of the heart, which encloses the heart.
2. *Epicardium*: inner layer of the heart tissue that is in contact with the surface of the heart. Usually the epicardial potentials are used to build electrical model of the heart which is used to solve forward and inverse problem of ECG.
3. *Myocardium*: muscular tissue of the heart made of cardiac muscle. Myocardium is the middle layer of the wall of the heart. This layer contracts spontaneously to pump the blood out of the heart. The myocardial potentials are determined by solving three dimensional electrocardiography imaging.
4. *Endocardium*: innermost layer of the heart which provides protection to the valves and heart chambers.

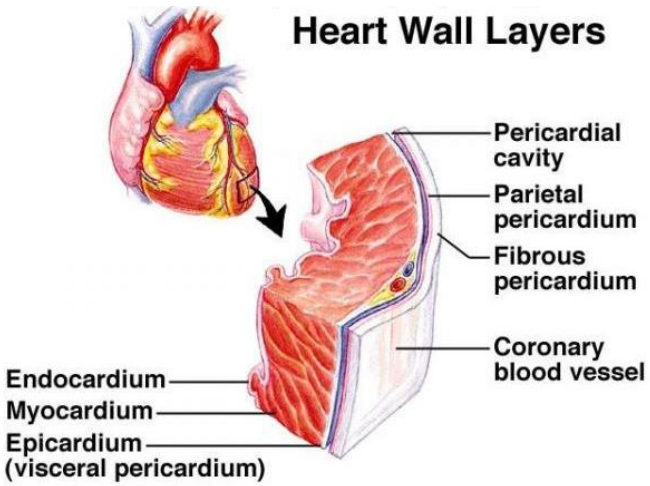

Figure 2.2: Four layers of the heart tissue [8].

2.2 Cardiac Electrophysiology

Every single cell including the cardiac cell, contains three main parts: cytoplasm, nucleus, and membrane. The cytoplasm is the semi-fluidic material filling the cell in which all organelles float. The nucleus is the control center of the cell, which controls all actions taken by the cell. The membrane is a protective wall of the cell,

holding the contents together, protecting the cell, communicating with extracellular environment, and controlling the entrance and exit of materials. The latter is done through the channels, some of which are used to pass specific ions between intracellular and extracellular environments. Because ions are charged particles, difference in their intracellular and extracellular concentrations causes an electrical potential across the membrane, which is called the transmembrane potential (TMP). TMP is a potential difference across the cell membrane, which can be defined as:

$$V_m = \varphi_i - \varphi_e, \tag{2.1}$$

where φ_i and φ_e are the intracellular and the extracellular potentials, respectively.

There are some types of cells called excitable cells, each of which response to stimulation in a nonlinear manner. This response causes amplification and propagation of electrical impulse, namely, action potentials.

The TMP in the heart cells is due to movement of calcium, potassium, sodium and few other ions across the cell membrane.

Action potential of a healthy cardiac cell is accompanied by contraction of the heart. The action potential of the cardiac cell contains five phases, which are shown in Figure 2.3, along with related ions and their movement directions [9, 10].

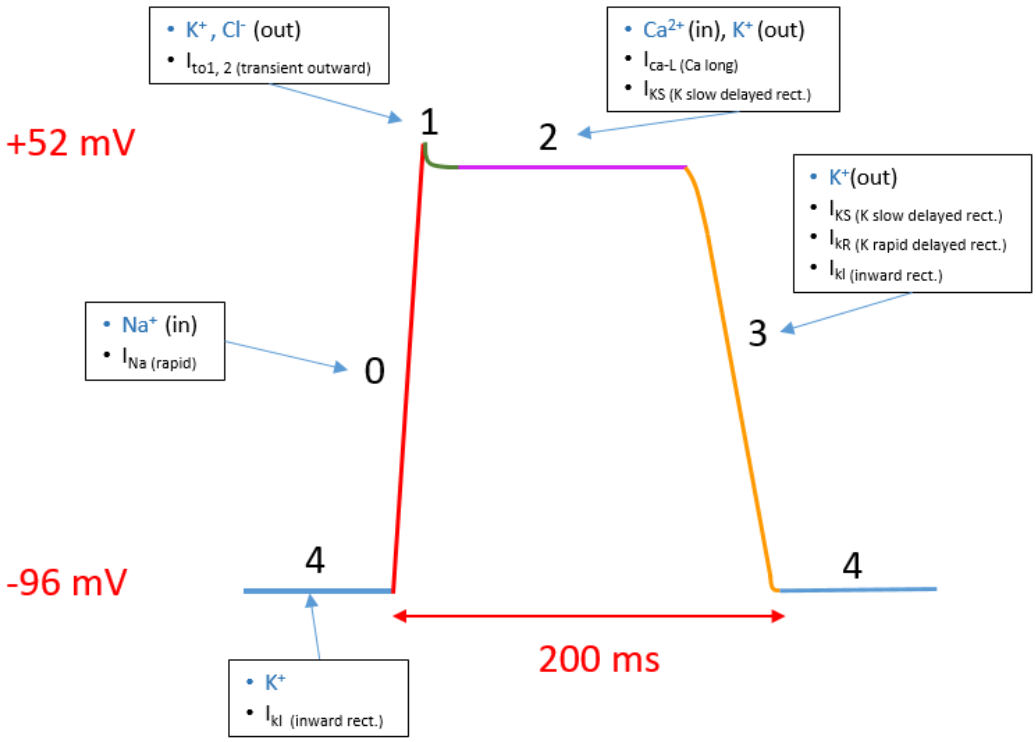

Figure 2.3: Action potential generated by a cardiac cell [11].

Phase 4 is a duration in which the cell is at resting potential. The heart is in diastole during this period. However, the resting period ends if an external electrical stimulus excites the cell. Some cells including some cardiac cells are able to depolarize continuously without any external stimuli. These cells are called the pacemaker cells that are located in a small pace generator region of the heart called the Sinoatrial (SA) node.

Phase 0 follows immediately after stimulation. This is the depolarization phase, during which the stimulus causes the TMP to go above the threshold value, i.e., the minimum necessary potential value to trigger the action potential. At once, fast sodium channels are opened and the sodium ions rush into the cell. Since sodium ions have positive charge, the inner potential of the cell gets a more positive value.

Phase 1 is a duration when fast sodium channels are closed and simultaneously the outflow of potassium and chlorine ions makes a tiny downward deflection in the waveform of the action potential.

Phase 2 is called the plateau phase where a balance between inflow of calcium ions and outflow of potassium ions is achieved.

Phase 3 is a very quick repolarization phase where calcium channels are closed and due to the movement of potassium ions there is an outward current, which leads to a negative membrane potential.

The above-mentioned action potential propagates through the specific path on the heart, meaning that after action potential generation, it is passed to neighboring cells, also stimulating them. In other words, the action potential moves from one cell to another. Each part of the heart has its specific action potential characteristic which is slightly different from each other. Figure 2.4 illustrates action potential waveforms related to different regions of the heart.

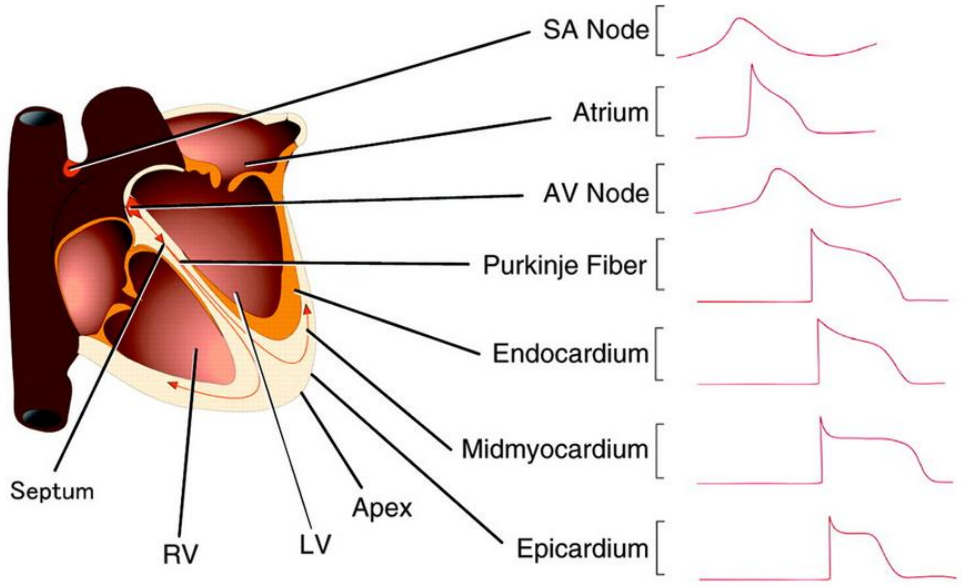

Figure 2.4: Different action potential wave forms related to different regions of the heart [12].

As it is mentioned, the action potential is generated by natural pacemaker of the heart called the Sinoatrial (SA) node, the point from which the heart beat starts. It means that without any external stimuli from other neighbor cells, the cells located in the SA node depolarize spontaneously. This spontaneous depolarization is due to phase 4 which is explained above. This action potential makes the atria contract, then it

follows its way to the AV node. After a small delay, it travels to Purkinji fibers through bundle of His, the fastest conduction network. The action potential finally reaches ventricular epicardium immediately after it has passed the endocardium and the myocardium.

2.3 Standard 12 – Lead Electrocardiography (ECG)

It is not easy to record the electrical activity from a single cell, especially in-vivo. The direct measurements from a tissue or an organ are often invasive, since in direct measurements direct contact electrodes are used to obtain the electrical signals from that tissue or organ. Therefore, noninvasive extracellular measurements, especially from outside of the body are of a great importance.

The well-known standard 12-lead ECG is a routine approach in clinical applications which records and amplifies the electrical changes on the body surface which are caused by depolarization of the myocardium. The objective of ECG is to reconstruct the information of spatio-temporal pattern of cardiac electrical activity [13, 14], in other words ECG translates the electrical impulses of the heart into a waveform. Several symptoms such as myocardial infarction, pulmonary embolism, abnormal cardiac murmurs, etc., are detectable from the ECG. The configuration of standard 12-lead ECG is illustrated in Figure 2.5.

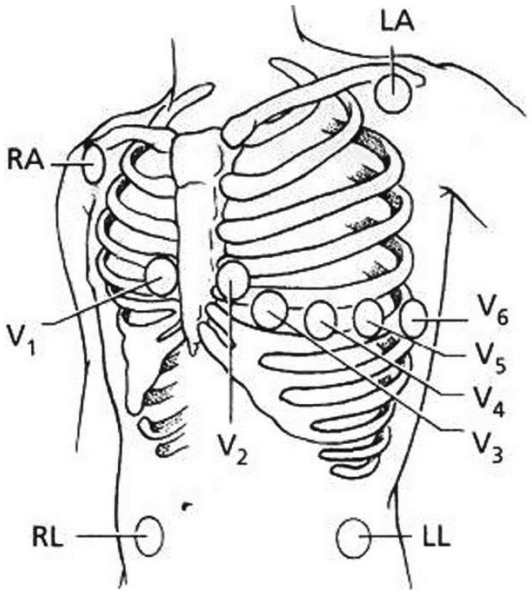

Figure 2.5: Standard configuration of 12-lead ECG [15].

As it is shown in the Figure 2.5, V_1-V_6 are precordial leads attached to the surface of the torso, RA and LA electrodes are attached to right and left arms, and RL and LL electrodes are attached to right and left legs, respectively.

The electrocardiogram consists of superposition of signals from all active heart cells shown in Figure 2.4., as they are reflected on the torso surface. A normal electrocardiogram consists of three major parts (Figure 2.6):

- P wave reflects the depolarization of the right and left atria, which starts from the SA node and as a result the atria contract. Any change in duration, amplitude, or frequency of the P wave can be interpreted as atrial abnormality. The duration between the initiation of P wave and the starting point of QRS complex is called the PR interval, in which the electric impulse is conducted to ventricles. The P wave duration is around 40-100ms [16].
- QRS complex is the most noticeable part of the electrocardiogram which reflects the repolarization of atria and depolarization of ventricles. The left ventricle has thicker myocardium, because it is responsible for sending the blood out of the heart into the whole body, therefore the majority of the QRS signal reflects the depolarization of muscle cells of the left ventricle. QRS complex is composed of Q wave, the first negative deflection, R wave, the first positive deflection and S wave, the second negative deflection. Since

bundle of His – Purkinji fibers network has a very fast conduction, the peak of QRS waveform is sharp rather than round. The duration change of this complex may be an indication of arrhythmias, ventricular hypertrophy, or myocardial infarction.

- T wave reflects the ventricular repolarization. The absolute refractory period is a duration which the cell does not respond to any stimuli. The duration between the beginning of the QRS complex and to the peak of the T wave is the refractory period. The second half of the T wave is the relative refractory period, where the initiation of action potential is probable.

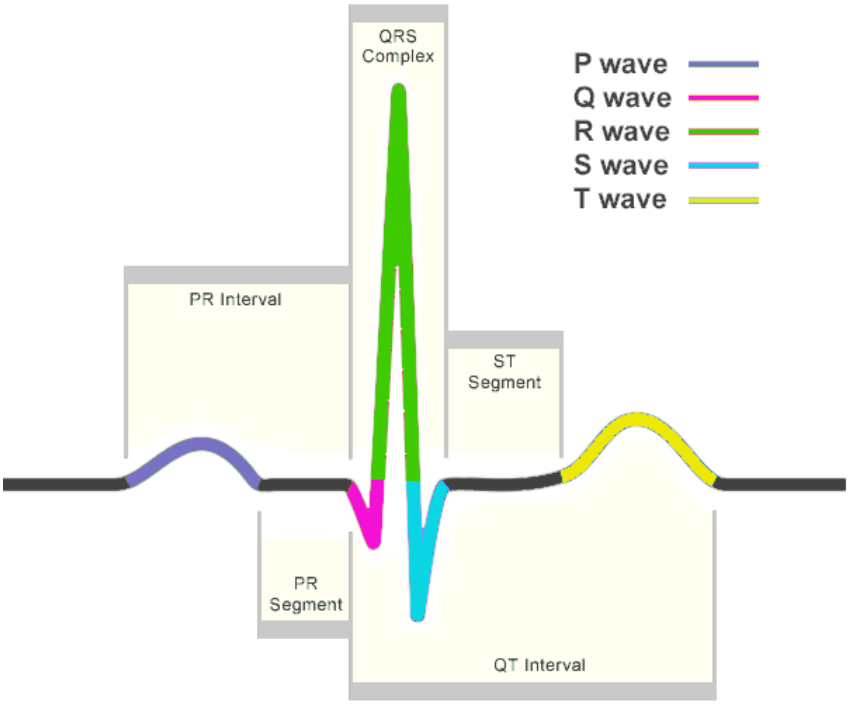

Figure 2.6: The normal electrocardiogram [17].

Although several cardiac abnormalities are diagnosable by standard 12-lead ECG, many others are *not* detectable by this fixed lead configuration. Since cardiac diseases are localized and ECG effect of those localized diseases are projected to other regions of the torso surface by different magnitudes, fixed lead measurements can lead to misinterpretation or misdetection in diagnosing and identifying the underlying disease [18].

One alternative to compensate the imperfection of standard 12-lead ECG in detection of many of the most informative signals from the torso surface is the Body Surface Potential Mapping (BSPM) method.

2.4. Body Surface Potential Mapping (BSPM) Method

Body surface potential mapping (BSPM) is an ECG technique that records the potentials from a wide region of the chest using 100-200 electrodes. Since the potentials are recorded from a broad area, this technique explores more information about the electrical activity of the heart than the standard 12-lead ECG [14] [19- 22]. The reason that the electrical activity of the heart can be interpreted less ambiguously by BSPM is its further sensitivity to the local electric fields than the conventional 12-lead ECG. Localized heart diseases or abnormal ECGs present specific ECG patterns on the body surface, these patterns play a significant role in diagnosing the problem. For instance, cardiac diseases such as myocardial infarction, transient myocardial ischemia, Wolf Parkinson White syndrome (WPW), etc., present detectable, characterized and special patterns on the body surface [18].

The prominent aspects of recording electrical activity from a broad area, which is not usually covered by conventional lead-systems, fall into three groups. First, clinically and diagnostically important information may be projected to the parts of the chest not usually sampled by the standard 12-lead system. Detection of such vital information is an important pre-requisite to investigate the disease. Second, extracted information from any sub-set of the complete lead set can be considered as adequate information only if they are considered as part of the total body surface lead-set. Last, the complete torso electric field sampling is a demanding part of the methods that require surface integration [23].

Despite standard 12-lead ECG, there is no standard configuration for the BSPM approach. Although this method has potential benefits in clinical applications, in fact it has not been used widely in practice since at least 100 electrodes should be attached to the torso for data acquisition. Additionally, complexity of processing of the acquired data, their analysis and display are other insufficiencies of the BSPM approach. There are a number of studies that have undertaken to reduce the number of leads used in BSPM approach, and at the same time maintaining the efficiency of

this method. In this study, to make BSPM more practical than its current state, a novel method is proposed and implemented to select optimal electrodes from a large number of BSPM electrodes.

2.5. Lead Selection for BSPM

As it is mentioned before, BSPM is an invaluable method in cardiac diagnostic approaches. For this method to also be clinically practical, the number of attached electrodes on the torso surface should be as small as possible considering their optimal configuration to acquire information as much as possible. Toward this end, numerous studies are conducted under "Lead Reduction" topic, each of which aims to reduce the number of attached electrodes to the body surface in a way that informative potential distribution on the torso surface would still be accurately detectable. The common aim of all these studies is to use less number of electrodes than the nodes in associated geometry model.

Barr *et al.*, [24, 25] were among pioneers in the context of lead reduction, who years ago intended to select the most signal information containing leads. Their work consists of locating the sites needed for proper recording the signals to precisely estimate the total QRS signals on the body surface as they change over time. In that study, 150 lead BSPM data were acquired from 45 subjects. The notation G_j is used to show the mathematical generator matrix, and the coefficient matrix, A, relates mathematical generators to surface recording positions. An approximation of experimentally measured surface potentials W_j can be calculated by Eqn. (2.2).

$$W_j = A.G_j, \tag{2.1}$$

where A is a matrix containing eigenvectors, and G_j are surface voltages that vary in time. The Principal Component Analysis (PCA) method is used to determine A and G_j. After A and G_j are determined, a group of experimentally measured surface voltages is used to estimate values of generators (G_j) now called as G_e. Then, the estimated G_e values are used along with previously calculated coefficient matrix A to obtain potential maps. An iterative method, which selects different individual leads each time, is then adopted to choose the best recording site. At last, the study has

concluded that minimum of 24 appropriately located leads are enough to get acceptable accuracy in body surface potential reconstruction.

In another set of invaluable studies undertaken by Lux *et al.*, [24, 26, 27], *Sequential Selection* method is proposed, which is the lead selection process that accounts for how well one individual recording site can contribute to estimate the potentials on other sites. In this method, a recording site which has the highest correlation with other recording sites can be a reasonable choice for being in the reduced lead-set. For a recording site to be in the reduced lead-set, only having the highest correlation with the unmeasured sites is not sufficient, since sites with high correlation but little signal variations most probably contain similar information. Therefore, they introduced a notion called "information index" which provides a qualifying measurement of how well one site correlates with other remaining sites considering the signal variation. The algorithm starts with calculating the information index for all recording sites to find the maximum value of information index. Then the corresponding lead that owns the highest information index value is removed from the data matrix and placed in reduced lead-set as the first lead. Then the process repeats itself to select the second lead of reduced lead-set. Again the information index value is calculated for each of the remaining recording sites in the data matrix, whose rank is now reduced by one. And the process continuous until a stopping criteria, for example the desired number of leads, is reached. For this study, data are obtained from 70 normal subjects with no cardiac disease and 62 subjects with old myocardial infarction. The data are acquired by 192 electrodes, which consists of uniformly spaced grid of 16 columns and 12 rows. To evaluate the performance of the Sequential Selection algorithm, the authors considered three criteria. The first one is the Correlation Coefficient (CC), second is the spatial root mean square (RMS), and the last one is ratio of error power to signal power. As the result of this study, it is claimed that 32 leads are significant to estimate the remaining sites with considerable accuracy, additionally, the configuration of the reduced lead-set is not unique since the distance between the source of the signals and recording sites causes blurring and smoothing effect on surface distribution. The Sequential Selection method is then suggested as a "clinically practical lead system" [27], in which it is concluded that applying this method with no constraint, which means setting no limit for the location of candidate leads, gives better results than solving the problem by

constraint, which means limiting the solution to precordial leads. Additionally, according to the results, they claimed that using 20-35 leads out of 192 leads can reconstruct nearly all of the information content of the 192 lead-system.

In another lead reduction algorithm called *Sequential Forward Selection* (SFS) proposed by the same authors [28], *data mining* methodology is employed. This algorithm starts with a set of BSPM recording site, 192 recording sites, and tries to find out how well one individual recording site is able to estimate the remaining unmeasured sites. The site that best estimates the unmeasured sites becomes first selected lead in the reduced lead-set. Then, in the second iteration, each of the remaining 191 sites are individually employed to estimate the remaining unseen sites in conjugate with the previously selected site. The algorithm goes on until a stopping criteria, for example desired number of leads is reached. To compare the quality of the reconstructed BSPM with the original data, two criteria are considered, one is spatial root mean square (RMS) voltage error, between estimated and measured sites, and the other is CC between estimated and original data. According to the results, performance of 32 leads chosen by this method have nearly the same accuracy as 32 leads chosen by Sequential Selection method.

In another study conducted by Kors *et al.*, [22], the authors used already available 12-lead ECG device to reconstruct BSPM. Due to impracticality of the several proposed lead configurations which use more than 10 electrodes, the available electrodes for measurement in ECG device, the proposed method seeks one or more electrodes in standard 12-lead configuration whose information can be reconstructed by other remaining leads. In other words, this method aims to increase the information content of standard 12-lead ECG, by repositioning one or more electrodes. The process of selecting the best position for the electrode/electrodes starts with analyzing recorded data from 746 subjects with healthy hearts together with patients with various cardiac abnormalities. Data are recorded by 120 non-equally spaced electrodes that cover the torso surface. The exact configuration for this system is available in Appendix A. Then the recorded data are randomly divided into training set and learning set. Using the linear regression on training data, the general coefficient is obtained to reconstruct the BSPM. This study was successful since information captured by 12-lead ECG contains redundant information and information content of missing electrode/electrodes can be reconstructed by adjacent

electrodes. The study concluded that the absent information in standard 12-lead ECG can be captured by repositioning V_4 and V_6 to a different position than standard 12-lead configuration. The positions of the leads in the proposed lead configuration are so specific that they are hardly misplaced. The resultant lead configuration is presented in Appendix A.

Lux *et al*., in [29] have tried to extract optimal *diagnostic* information from torso surface by using new electrodes in addition to 12 leads and estimation of unmeasured leads. Considering that the best signal leads do not necessarily contain the best diagnostic information, the process of selecting the position of the new electrodes starts with selecting the best classifier for the given pairs of electrodes. Data for this study are collected from a population of 841 patients: 159 subjects with normal heart, 233 patients with myocardial infarction, and 189 patients with left ventricular hypertrophy. The complete lead system in this study contains 120 electrodes, which simultaneously record electrical activity of the heart from the body surface. In this study the investigators compared 3 different strategies of classifying ECG data in order to attain an improvement over the diagnostic performance of the standard 12-lead ECG. In the first strategy, it is tried to select the electrodes from 120 leads, which are optimal in the sense of discrimination. In the second, few optimal electrodes in terms of best signal and best diagnostic leads are selected from leads for discrimination, and added to the 12-lead ECG. The third strategy is based on estimating the 120 BSPM leads using the 12-leads augmented by a few optimal signal leads and then selecting those leads which are best for discrimination. This study concluded that using 4 additional leads along with 8 independent leads of 12-lead ECG can compromise between the best signal leads and the best diagnostic leads. After applying the resultant configuration, it is revealed that this system is capable of reconstructing BSPM in acceptable extent. They refer to this lead system as "8+4" lead-system. The complete lead system used in this study (120 lead system) and the resultant 8+4 lead system configuration is shown in Appendix A.

In another study conducted by the same authors [30], Principal Component Analysis (PCA) is applied to the BSPM to identify eigenvectors. The process of selecting the electrodes starts with representing the original data as the product of PCs and eigenvectors for the 117 complete lead set. Considering isopotential map

frame which consists of the potential at each recording site, the total map frame can be represented:

$$P = (p_1, p_2, \dots, p_{117}). \tag{2.2}$$

After applying PCA, each spatial map can be shown:

$$P = \sum_{i=1}^{117} \alpha_i \varphi_i, \tag{2.3}$$

where φ_i is the i[th] eigenvector and α_i is the i[th] PC that weights that eigenvector. Then three bipolar leads called "eigenleads" are identified using extrema on the resultant eigenvectors. Not surprisingly, the main location for these eigenleads is on precordial region. It is reported that the signal strength of the proposed lead system is higher than other lead systems. Although the proposed lead-configuration using eigenleads is *not* able to reconstruct the whole BSPM, it can estimate the information content of the standard 12-lead ECG comparable with other limited lead-sets. As it is concluded in this study, the proposed lead system is better than EASI lead system in reconstructing the information of precordial leads. The lead configuration of EASI can be found in Appendix A.

2.6 Forward Problem of Electrocardiography

In order to locate the sources of electrical activity recorded from the body surface, inverse problem of electrocardiography should be solved, as it will be discussed in the next section in detail. For inverse electrocardiography problem to be solved, forward problem of electrocardiography should be solved in advance. In this section, we briefly discuss forward problem of electrocardiography in terms of cardiac electrical source distribution.

To get forward solution for epicardial potential source model, the Laplace's equation should be solved in source free volume, Ω, limited between two closed surfaces, Γ_T and Γ_E, representing the torso and epicardium surfaces, respectively:

$$\nabla.(\sigma.\nabla\Phi) = 0 \quad \text{in} \quad \Omega \tag{2.4}$$

by employing the proper boundary conditions [31- 35]. In the above equation, σ is the conductivity of the medium, and Φ is the scalar electrostatic potential at any point within the volume. In order to define analytical forward problem, considering

Φ_E as potential distribution on the epicardium surface and Φ_T as potential distribution on torso surface, by defining boundary conditions we have:

$$\Phi = \Phi_E \text{ on } \Gamma_E, \qquad \text{Dirichlet} \tag{2.5}$$

$$\Phi = \Phi_T \text{ on } \Gamma_T, \tag{2.7}$$

$$(\sigma . \nabla \Phi) . n = 0 \text{ on } \Gamma_T, \qquad \text{Neumann} \tag{2.8}$$

where n is the outward surface normal vector.

Several elements are needed for solving the forward problem, such as geometric model which includes both heart and torso surfaces, intermediate surfaces or intervening volume, and assumptions of σ, inside of the volume conductor.

As it is mentioned, realistic heart-torso geometry is complex, so the related geometry can be obtained by imaging modalities such as Computerized Tomography (CT), or Magnetic Resonance Imaging (MRI). Then the resulting images should be discretized and segmented, and electrode locations should be mapped to the torso and heart surfaces in the geometry, then both heart and torso should be represented by a group of nodes in space in a way that they form polygons in order to form a mesh (triangle for surface based methods, and tetrahedra or hexahedra for volume based methods) [36].

In simulation studies for ECG, analytic solutions are only available for the simple surfaces as spheres, while the realistic surface of the heart is much more irregular and complex than that of the sphere. Thus numerical methods are employed to calculate the forward problem [37, 38]. Two major groups of methods to solve electromagnetic problems are volume methods and surface methods. While volume methods are based on differential equations such as Finite Element Method (FEM) [39- 41], surface methods are based on integral equations such as Boundary Element Method (BEM) [42- 50]. Both of these methods require node choice and construction of meshes.

In this thesis, a BEM formulation based on what proposed by Barr *et al.*, in [34] is employed. The calculation of the solution related to Eqn. (2.5) using boundary conditions from Eqn. (2.6-2.8), results in the forward transfer matrix A. This matrix calculates a set of discrete torso potentials from a set of discrete epicardial potential distributions. The related numerical solution can be displayed as:

$$\Phi_T = A\Phi_E, \tag{2.9}$$

where A is the forward transfer matrix, Φ_E and Φ_T are the matrices including potentials on the epicardium and the torso surface nodes, respectively. Thus the rows of A can be interpreted as weights of the linear combination of the epicardial potentials which yield the potentials on each node of the torso surface. Then, by using a forward model, having epicardial potential distribution, Φ_E , the torso surface potential distribution, Φ_T, can be calculated.

The inverse problem of electrocardiography, as it will be discussed more in the next section, includes determination of the potential distribution on epicardium, Φ_E, on the epicardial surface, Γ_E.

2.7 Inverse Problem of Electrocardiography

The objective of inverse problem of electrocardiography is to reconstruct electrical activity of the heart using noninvasive potential measurements from body surface along with a geometric model of the conducting volume between desired sources and sites of measurements.

Gulrajani *et al.,* in [51] gave a detailed review of equivalent intracardiac dipole, and multipole models. In other methods such as epicardial potential-based models the sources for forward and inverse problems are considered as potentials on the outer surface of the heart [34, 52, 53].

The epicardial potential-based inverse solution has several advantages over equivalent source solutions:

1. The solution of potential-based models, at least theoretically, is unique [31].
2. The underlying physiological processes are more feasible in potential-based solutions than equivalent solutions [31].
3. Unlike equivalent source model, there is no need to make prior assumptions about nature of the sources, for instance number of dipoles [31].

4. In potential-based formulation the most important inhomogeneity, intra-cavity blood inhomogeneity, is implicitly taken into account [31, 51, 54].
5. The direct comparison of the potential-based solution with epicardial measurements obtained in parallel with BSPM in animal experiments [52], or with an electrolyte filled tank model of heart-torso model is possible [31].

More detailed information about potential-based solutions can be found in [54-57]. Another potential-based method acquires information invasively from inner surface of the heart, *i.e.*, from the endocardial surface. This method measures potentials inside of the chambers of the heart employing noncontact electrodes [58-60]. This method is extremely invasive so it is impractical in clinical applications.

In this thesis, heart surface potentials are used as equivalent sources, resulting in a linear forward model. In the following part, we briefly discuss the methods to treat inverse problems in order to obtain reliable solutions.

Inverse problem of electrocardiography is ill-posed, or in other words the forward matrix is ill-conditioned, due to attenuation and smoothing effect of the intermediate volume between electrical sources located on the surface of the heart and the measurement points on the body surface [61]. This means that small perturbation, caused by noise, error in the forward model, attenuation, discretization effects *etc*., can result in an unbounded error in the solution of the inverse problem. In order to overcome the mentioned ill-posedness, various regularization methods are used imposing constraints derived from prior information. In what follows, several regularization methods are explained, including the well-known Tikhonov regularization, Truncated Singular Value Decomposition (TSVD), Truncated Generalized Singular Value Decomposition (TGSVD), Total Truncated Least Squares (TTLS) method, Lanczos Bidiagonalization Total Truncated Least Squares (LTTLS) method, Least Squares QR factorization (LSQR), Lanczos Bidiagonalization Least Square QR factorization (LLSQR) method, L_1-norm based solutions, Generalized global Arnoldi method, and combination of self-organizing feature maps and support vector.

Almost all of above-mentioned regularization algorithms need a regularization parameter, which is selected by the regularization parameter selection method. The parameter selection methods will be discussed in the next section in detail.

Tikhonov regularization is a well-known method to regularize ill-posed inverse problems. In terms of inverse problem of ECG, Tikhonov regularization method aims to minimize the cost function, which is least square minimization, by imposing constraints on magnitude or derivatives of epicardial potentials. Although Tikhonov regularization can effectively deal with measurement errors in torso measurements, it fails to handle geometric errors. Tikhonov regularization in its standard form is shown below,

$$\Phi_{E\lambda} = \text{argmin} \, \|A\Phi_E - \Phi_T\|_2^2 + \lambda^2 \, \| R\Phi_E \|_2^2, \tag{2.10}$$

where $A \in \mathbb{R}^{m \times n}$ is the forward transfer matrix, λ is a scalar regularization parameter, and $R \in \mathbb{R}^{n \times n}$ is the regularization matrix, Φ_E and Φ_T are epicardial potentials and torso measurements, respectively.

There are many studies on selecting the optimal regularization parameter, λ, for Tikhonov regularization method. Johnson *et al.*, in [62] compared three parameter selection methods, L-curve, Composite Residual and Smoothing Operator (CRESO), and zero crossing method which they proposed in their article. According to their reported results, similar results are obtained for all three methods, however, selecting the regularization parameter by zero crossing method is simpler than the other two. In another study conducted by Shou *et al.* [63] the performance of Generalized Cross Validation (GCV), L-curve and Discrepancy Principle (DP) are compared. According to the reported results, although DP obtains better results, L-curve and GCV methods are more useful than DP, since the latter needs prior information about noise.

There is a modified version of Tikhonov regularization called Twomey regularization which is not as practical as Tikhonov regularization, as it needs prior information about the desired epicardial potential [64].

In [65], Liu introduced a new dynamical Tikhonov regularization method and called it Optimal Vector Method (OVM) for solving ill-posed linear algebraic systems. Besides allowing stability, on a proper invariant manifold, this method

computes the approximate linear solution for the system. The selection of regularization parameter, the central issue of Tikhonov like methods, is adaptively and optimally embedded in the main algorithm. By examining several ill-posed numerical examples, the author showed that this method works better than classical methods like Steepest Descent Method (SDM) and Conjugate Gradient method (CGM).

In [66], Reichel *et al.,* have considered Tikhonov regularization with regularization operator in a general scheme and present an iterative approach to solve linear ill-posed problems based on generalized Krylov subspace method. In this method, both matrix of a linear discrete ill-posed problem and the regularization operator are reduced simultaneously. Then the reduced-sized problem is solved by an ordinary method, e.g., Singular Value Decomposition (SVD).

Another well-known regularization method is TSVD, which is based on eliminating very small singular values. For ill-conditioned matrices, many of the eigenvalues, while non-zero, can become too small leading to matrix inversions to become extremely large if there is any error in the measurements. By truncating these very small singular values, high frequency components are ignored, and this leads to a smooth solution. Similar to other least square based methods for ill-posed problems, TSVD, which is also a least square based method, is affected by geometrical error. Most frequently both Tikhonov regularization and TSVD are used as reference methods to evaluate the performances of other regularization methods.

In a study conducted by Shou *et al*., [67], TSVD method is compared with Tikhonov regularization and Truncated Total Least Squares (TTLS) method. According to the results reported by these authors, although when only a measurement error is considered all methods give similar results, by increasing the measurement noise Tikhonov regularization and TTLS give better results. Furthermore, in the case of both measurement error and geometry error, TTLS performs better than the other two.

TTLS method is very similar to TSVD method. The significant difference is that in TTLS method unlike TSVD, the singular values of conjugate matrix ($A\ \Phi_T$) are computed and small singular values are neglected in the reconstruction process [68].

TTLS method performs notably well in presence of both measurement errors and geometry errors.

Shou *et al.,* [69] employed a new TTLS-based method to solve ECG inverse problem, to obtain epicardial potentials. In this study, the error is considered on both sides of the equation, $\Phi_E = \Phi_T$. This newly proposed method treats geometrical error in a new manner. To test the proposed algorithm, a realistic heart-lung-torso model with inhomogeneous conductivities is used. To solve the related forward problem *h*-adaptive boundary element method (*h*-BEM) is used and the performance of the proposed algorithm is compared with conventional Tikhonov regularization and TSVD with zeroth-, first-, and second-order. The simulation results revealed that, in the presence of only measurement noise TTLS performs very similar to Tikhonov regularization and TSVD, but it performs better than the other two when geometry error is involved. In this study, it is reported that it is better to use *zero-order* regularization in order to solve ECG inverse problem to find the epicardial potentials.

LTTLS algorithm is a modified version of TTLS method. Due to the complexity of SVD algorithm, $O(mn^2)$, the problems with large dimensions are computationally expensive, since it is difficult to calculate SVD of a large transfer matrix. Although, there are partial singular value decomposition algorithms to calculate SVD of conjugate matrix ($A \ \ \Phi_T$), for a considerably large truncation parameter, by applying these methods the structure and sparsity of the transfer matrix is lost. To compensate for this shortcoming, iterative methods based on Lanczos- bidiagonalization, which leaves the transfer matrix unchanged, are used [68]. Therefore, the computational cost of the Lanczos TTLS is less than TTLS, subsequently, the runtime of the Lanczos TTLS method is shorter than that of TTLS algorithm. LTTLS method has been used to solve discretization of Phillip's problem [70] and in image reconstruction problems [71]. But, for the first time, Güçlü has used this method to solve inverse problem of ECG [72].

LLSQR method is based on Lanczos bidiagonalization and at the same time QR factorization. LLSQR method performs well when the transfer matrix is large and sparse. Jiang *et al*., in [73] compared the performances of conventional regularization methods, Tikhonov regularization and TSVD, with LLSQR method. In this study, in

order to improve the performance of LLSQR method, Genetic Algorithm (GA) is used. During the study, a realistic heart-torso model is used. A single dipole is used to model epicardial potentials and different Gaussian noise levels are added to measured torso potentials. During the process of solving the ECG inverse problem in this study, the iteration number of LLSQR method, the regularization parameter of Tikhonov method and the truncation level of TSVD method are selected by L-curve method. According to the results reported by this study, LLSQR method gives better results than Tikhonov regularization and TSVD method in different measurement and geometry noise levels. Additionally, the superiority of LLSQR method becomes clearer when the noise levels go further. It is also reported that the combination of LLSQR method and genetic algorithm (GA) gives better results than using only LLSQR in regularizing inverse problem of ECG.

Many proposed regularization methods employ L_2-norm based approaches, both in data term and penalty term, to deal with the ill-posed nature of the inverse problems. But, the use of L_2-norm in the penalty function leads to considerable smoothing of the solution and generates sensitive solutions to the measurement noise. This affects distinguishing abnormal activities of the heart and makes it difficult to locate the diseased region [14]. To overcome this defect, L_1-norm based solutions are used to handle ill-posedness of the inverse problem. In [14], Wang *et al.*, proposed a kind of L_1-norm based method to solve the inverse problem in the form:

$$\Phi_{E_\lambda} = \min \|A\Phi_E - \Phi_T\|_2 + \lambda \| R\Phi_E \|_1 \quad (2.11)$$

where $A \in \mathbb{R}^{m\times n}$ is the forward transfer matrix, λ is a scalar regularization parameter, and $R \in \mathbb{R}^{n\times n}$ is the regularization matrix, Φ_E and Φ_T are epicardial potentials and torso measurements respectively.

To solve Eqn. (2.11), the method starts with variable splitting, since many L_1-norm based approaches operate better on sparse data than the dense data. After transforming the data to sparse form, the problem is reformulated as a quadratic problem. Then, it is solved by Gradient Projection (GP) in an iterative manner, which is based on successive projections on the feasible region. At this step, Barzilai and Borwein (BB) method [74], as the line search parameter method, is used to find optimal parameters. As it is reported in this study, the results of the proposed method

are more accurate than the methods which use other combinations of L_2- norm and L_1-norm, i.e., the methods that employ L_2-norm minimization on data term and L_1-norm minimization on penalty term. In addition to the efficient results, this method can significantly handle both geometry and measurement errors. Besides, non-expensive operations, low memory requirements, and simplicity of the algorithm are further advantages of this method.

In another study conducted by Shou *et al.*, [75] L_1-norm minimization is applied on data term to solve the inverse problem of ECG. To solve the minimization problem Iterative Reweighted Norm (IRN) algorithm is applied to the L_1-norm-related part along with both L_1 and L_2 penalty terms of normal derivative constraint. The results of this study demonstrate that the solutions obtained by this method have less relative error than other L_2-norm based solutions. Additionally, when large noise occurs in the data received from some electrodes, L_1L_2 approach can obtain more robust results than other methods.

In the next chapter, few of the above-mentioned regularization methods that are used in this thesis work will be discussed and explained, thoroughly.

CHAPTER 3

METHODS

The inverse problem of electrocardiography (ECG) is the determination of electrical sources on the heart surface having the measured body surface potentials. As previously mentioned in Chapter 2, inverse problem of ECG is ill-conditioned [57], hence in order to solve it regularization methods should be applied. In this chapter, the problem definition of inverse ECG in terms of epicardial potentials and different regularization methods that are used to solve it are discussed. In this study, among various regularization methods, the well-known Tikhonov regularization, Lanczos Least Squares QR factorization (LLSQR), Lanczos bidiagonalization Truncated Total Leads Squares (LTTLS), and Truncated Total Least Squares (TTLS) methods are selected to solve the inverse ECG problem, since these regularization methods are widely used in the context of inverse problems. For all of the employed regularization methods, Maximum Correlation Coefficient (MCC) regularization parameter selection method is used, which will also be discussed in this chapter.

As explained before, to obtain Body Surface Potential Maps (BSPM), one needs to attach a large number of electrodes to the torso in order to detect the electrical activity of the heart. BSPM provides a denser spatial sampling over the torso surface, which provides more detailed information about the electrical activity of the heart than the traditional 12-lead ECG system. However, an increased number of electrodes in BSPM approach makes it less practical to use in clinical applications than the 12-lead ECG system. In this chapter, we propose a novel lead reduction algorithm to reduce the number of leads in BSPM approach with the goal of making this method more practical in clinical applications with little or no loss of information.

3.1 Problem Definition

In the forward problem of ECG, the epicardial potentials are related to body surface potentials by the following linear equation:

$$\Phi_T = A\,\Phi_E + N, \tag{3.1}$$

where $\Phi_T \in \mathbb{R}^{m\times t}$ and $\Phi_E \in \mathbb{R}^{n\times t}$ are the matrices that contain body surface potentials and epicardial potentials, respectively. The matrix $A \in \mathbb{R}^{m\times n}$ is the forward transfer matrix, which is the result of the solution of the forward problem of ECG, and the matrix $N \in \mathbb{R}^{m\times t}$ is used to model measurement errors. Here, it is assumed that, there are m measurement leads on the torso and n nodes on the epicardial surface, and the signals are measured on body surface at t different time instances in terms of milliseconds. Therefore, the matrix Φ_T is composed of m rows representing m number of measurement leads, and t columns each representing one time instant. For example, $\Phi_{T\,12}$ means the measured potential from lead number *1* in time instant *2*. Similarly, the matrix Φ_E is composed of n rows representing n number of nodes on the epicardial surface, and t columns each representing one time instant. For example, $\Phi_{E\,12}$, means the potential obtained at node 1 in time instant 2. An example of the lead locations on the torso and the node locations on the epicardial surface is shown in the Figure 3.1. There are 771 leads on the torso surface and 490 nodes on the epicardial surface. As it can be seen in the Figure 3.1, 771 torso leads are distributed equidistantly on the surface on the body surface. Similarly, 490 measuring points on the surface of the heart are distributed in order.

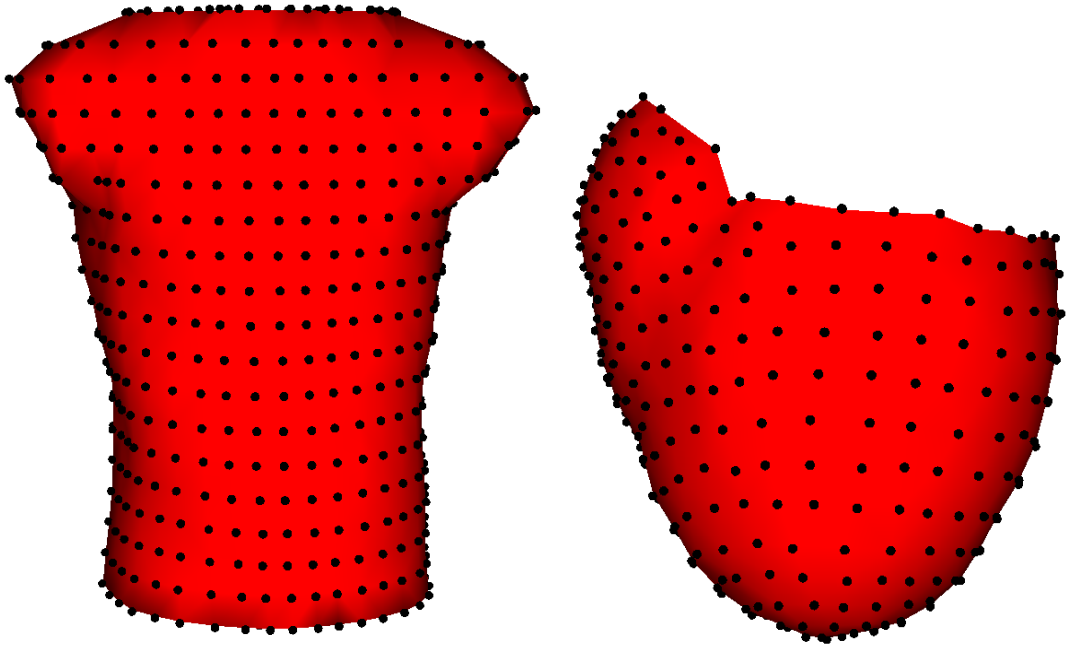

(a) (b)

Figure 3.1: (a) The locations of 771 leads on torso surface, and (b) the location of 490 nodes on epicardial surface.

For every time instant, Eqn. (3.1) can also be stated by vector notation as follows:

$$\Phi_T(k) = A\,\Phi_E(k) + N(k) \qquad (k = 1,2,\dots,t), \tag{3.2}$$

where k represents each time instant. So one can solve the problem by using the forward transfer matrix, A, and vectors $\Phi_T(k)$ and $\Phi_E(k)$ representing measured torso surface and epicardial surface potentials at time instant k, respectively. The notation used in this study is the matrix form of the equation as in Eqn. (3.1).

3.2 Properties of the Forward Transfer Matrix (A)

The transfer matrix A is the result of the solution of the forward problem of ECG. In order to calculate the forward matrix, Boundary Element Method (BEM) is used [76].

In our case, the forward transfer matrix A is not a square matrix so that its direct inversion cannot be calculated. For a full rank non-square matrix $A \in \mathbb{R}^{m\times n}$, the left inverse of matrix , A, is calculated as follows:

$$A^{-1} = (A^T A)^{-1} A^T \tag{3.3}$$

where A^T represents the transpose of the matrix A. But here in our case, the matrix A is not full rank either, therefore Eqn. (3.3) is not applicable. Hence, the pseudo inverse of the matrix A is calculated; however, using this pseudo inverse matrix may not give good results. This is related to an attribute of a matrix called the condition number or singular values of the matrix. The condition number can be used to consider a matrix as ill or well-conditioned.

One way to calculate the condition number of a matrix is to divide the largest singular value by the smallest singular value of the matrix. If the answer of division is closed to 1, then the matrix can be called well-conditioned, which means that the inverse of the matrix can be calculated accurately. Conversely, matrices with large condition numbers are called ill-conditioned, so their inverse cannot be calculated correctly. If the condition number of a matrix is infinity, then it is not invertible at all [77].

The Singular Value Decomposition (SVD) is one on the effective methods to solve ill-posed problems. The singular value decomposition is defined for a matrix $A \in \mathbb{R}^{\mathrm{m}\times\mathrm{n}}$, where $m \geq n$ as:

$$A = USV^T, \tag{3.4}$$

where U and V are:

$U = \{u_1, u_2, \dots, u_m \in \mathbb{R}^{\mathrm{m}\times\mathrm{m}}\}$ and $UU^T = I^{\mathrm{m}\times\mathrm{m}}$,

$V = \{v_1, v_2, \dots, v_n\} \in \mathbb{R}^{\mathrm{n}\times\mathrm{n}}$ and $VV^T = I^{\mathrm{n}\times\mathrm{n}}$.

The columns of U and V are left and right singular matrices, respectively. Furthermore, S is a diagonal matrix consisting of singular values $(s_1, s_2, \dots, s_3)$ of matrix A where $s_1 \geq s_2 \geq \cdots \geq s_m$. Additionally, the off-diagonal elements of S are zero.

The aim of SVD method is to calculate the eigenvectors and eigenvalues of the matrix A^TA and AA^T. The eigenvectors of A^TA are the columns of the matrix U, and the eigenvalues of the matrix AA^T are the columns of the matrix V.

The singular values of matrix A corresponding to the complete lead-set containing 771 leads, is presented in the Figure 3.2. As it is displayed in the figure, the largest singular value of the matrix A is 2.39 and the smallest singular value is

something near to 0. Therefore, the condition number of the matrix A is very large so that it can be called an ill-conditioned matrix.

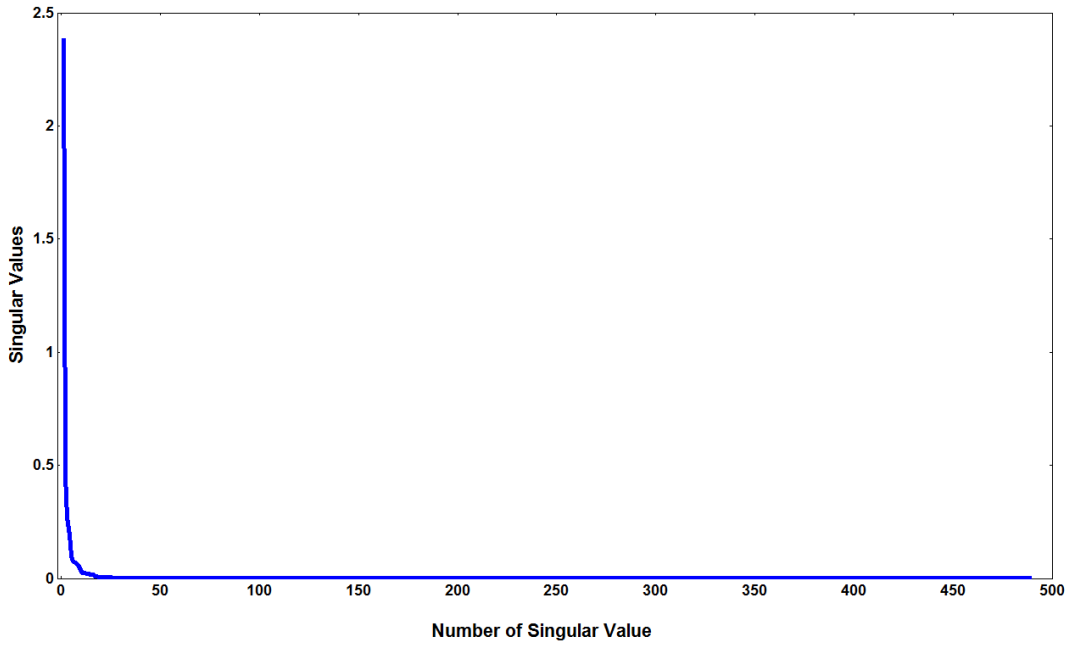

Figure 3.2: The singular values vs. the number of singular values of the coefficient matrix A.

3.3 Regularization Methods

As it was mentioned in the previous section, the forward transfer matrix A is ill-conditioned causing the inverse problem to be ill-posed, which means any small amount of noise in the measurements leads to large perturbations in the solution. This means that even a small amount of noise can lead in meaningless solutions. To overcome this problem many regularization methods are proposed and implemented in literature. In this section four different regularization methods, which are employed to estimate epicardial potentials Φ_E in this study, are presented. These methods are Tikhonov regularization, Truncated Total Least Square (TTLS) method, Lanczos Truncated Total Least Squares (LTTLS) method, and Lanczos Least Squares QR (LLSQR) method, all of which are explained thoroughly in the next sections.

3.3.1 Tikhonov Regularization

Tikhonov regularization method is one of the most well-known and popular regularization methods to deal with the ill-posed nature of the inverse ECG problem [78]. In this method a cost function consisting of the residual norm and the constraint norm is defined, and the solution is chosen to such minimize the cost function. The cost function defined for Tikhonov regularization is as follows:

$$\Phi_{E_\lambda} = \min \|A\Phi_E - \Phi_T\|_2^2 + \lambda^2 \| R\Phi_E \|_2^2, \tag{3.5}$$

where λ is the regularization parameter balancing the relative weights of the residual and constraint norms, Φ_{E_λ} is the solution according to a specific regularization parameter λ, and R is the regularization matrix which defines regularization constraint. In the "zero order" Tikhonov regularization, the identity matrix, I, is used as the regularization matrix ($R = I$). In the "first-order" Tikhonov regularization, R is chosen to be surface gradient matrix ($G = R$), and for "second-order" Tikhonov regularization R is defined as the surface Laplacian operator ($R = L$). In this study, zero-order Tikhonov regularization method is used, since it is more suitable for solving the inverse ECG problem [79].

Two alternative representations of Tikhonov regularization is presented below:

$$(A^TA + \lambda^2 R^TR)\Phi_E = A^T\Phi_T, \tag{3.6}$$

$$\min \left\| \begin{pmatrix} A \\ \lambda R \end{pmatrix} \Phi_E - \begin{pmatrix} \Phi_T \\ 0 \end{pmatrix} \right\|_2. \tag{3.7}$$

Considering the above two equations, it can be inferred that if the null space of A intersects with the null space of R (i.e., $N(A) \cap N(R) = \{0\}$), then there would be a unique solution, $\Phi_{E_{est}}$, then the coefficient matrix, $(A^TA + \lambda^2 R^TR)$, has full rank, and the solution is calculated as:

$$\Phi_{E_{est}} = A_\lambda \Phi_T \ , \tag{3.8}$$

where

$$A_\lambda = (A^TA + \lambda^2 R^TR)^{-1} A^T. \tag{3.9}$$

Tikhonov regularization is equivalent to applying filter factors on singular value decomposition (SVD) representation of Φ_E:

$$\Phi_{E\,est} = \sum_{i=1}^{n} \frac{s_i^2}{s_i^2+\lambda^2} \frac{u_i^T \Phi_T}{s_i} V_i, \tag{3.10}$$

where V is the same V matrix in the SVD decomposition of A. The term , $f_i(\lambda) = \frac{s_i^2}{s_i^2+\lambda^2}$, in the above equation is called the filter factor since it filters the amplification of small singular values. By using this filter factor Eqn. (3.8) can be re-written as:

$$\Phi_{E\,est} = \sum_{i=1}^{n} f_i \frac{u_i^T \Phi_T}{s_i} V_i \tag{3.11}$$

It can be inferred from the above equation that the larger a singular value, the larger the effect it has on the solution. Additionally, the effect of the regularization parameter on the solution is very important. Here, MCC is used as the regularization parameter selection method, which will be explained later on in this chapter.

3.3.2 Lanczos Least Squares QR Factorization (LLSQR) Method

Lanczos Least Squares QR Factorization (LLSQR) is an iterative method to solve linear systems. When the coefficient matrix is large, iterative methods are more preferable than the direct solutions. LLSQR method iteratively produces solution matrices in each iteration. After k iterations, the solution will approach to the optimal solution. However, this method suffers from a phenomena of "semi-convergence". If the number of iterations are not limited, the solution may converge to a worse solution with higher relative error [69]. To avoid obtaining a noise contaminated solution, a reasonable stopping criteria should be defined for k. One of the most important steps of this algorithm is to determine the regularization parameter, k [65]. The general theme of LLSQR method is explained below.

LLSQR method starts with finding the sequence of Lanczos vectors using Lanczos Bidiagonalization method. Lanczos Bidiagonalization computes $u_j \in \mathbb{R}^m$, $v_j \in \mathbb{R}^n$ and scalars α_j and β_j, such that $B_k = U^T A V$ is met. B_k is lower bidiagonal matrix:

$$B_k = \begin{bmatrix} \alpha_1 & & & \\ \beta_1 & \alpha_2 & & \\ & \beta_2 & \ddots & \\ & & \ddots & \alpha_k \\ & & & \beta_{k+1} \end{bmatrix} \tag{3.12}$$

Lanczos vectors are orthonormal such that:

$U_{k+1} = (u_1, u_2, \dots, u_{k+1}) \in \mathbb{R}^{m\times(k+1)}$, $U_{k+1}^T U_{k+1} = I_{k+1}$

and,

$V_k = (v_1, v_2, \dots, v_k) \in \mathbb{R}^{m\times k}$, $V_k^T V_k = I_k$.

The Lanczos Bidiagonalization algorithm is given below [83]:

Lanczos Bidiagonalization

1. Choose a starting vector $\Phi_T \in IR^m$ and $\beta_1 = \|\Phi_T\|_2$, $u_1 = \frac{\Phi_T}{\beta_1}$, $v_0 = 0$ and α_1
2. For $k = 1, 2, \dots, k$ do
3. $r_i = A^T u_i - \beta_i v_{i-1}$
4. $\alpha_i = \|r_i\|_2$
5. $v_i = \frac{r_i}{\alpha_i}$
6. $P_i = A v_i - \alpha_i u_i$
7. $\beta_{i+1} = \|P_i\|_2$
8. $u_{i+1} = \frac{P_i}{\beta_{i+1}}$
9. End

After k iterations, three matrices will have been computed, a lower bidiagonal matrix B_k and two matrices U_{k+1} and V_k. These matrices are related by the following relationships:

$$\begin{aligned} \Phi_T &= \beta_1 u_1 = \beta_1 U_{k+1} e_1, \\ A V_k &= U_{k+1} B_k, \\ A^T U_{k+1} &= V_k B_k^T + \alpha_{k+1} v_{k+1} e_{k+1}^T, \end{aligned} \tag{3.13}$$

where e_i represents the i[th] unit vector. Now, the calculated quantities by Lanczos Bidiagonalization algorithm can be used to solve the least squares problem:

$$\min \|A\Phi_E - \Phi_T\|_2. \tag{3.14}$$

Here, the solution has the form:

$$\Phi_E^{(k)} = v_k y^{(k)}, \tag{3.15}$$

where the length of the vector $y^{(k)}$ is k. Then, $r^{(k)} = \Phi_T - A\Phi_E$ is defined and by substituting we have:

$$r^{(k)} = \beta_1 u_1 - AV_k y^{(k)} = U_{k+1}\left(\beta_1 e_1 - B_k y^{(k)}\right). \tag{3.16}$$

Let us define $t_{k+1} = \beta_1 u_1 - B_k y^{(k)}$. Since U_{k+1} has orthonormal columns this can be concluded that $y^{(k)}$ should be chosen in a way that it minimizes $\| t_{k+1}\|$. So the least square problem changes to:

$$\min \left\|\beta_1 e_1 - B_k y^{(k)}\right\|_2. \tag{3.17}$$

By standard QR factorization of Eqn. (3.17) we have:

$$Q_k[B_k \quad \beta_1 e_1] = \begin{bmatrix} R_k & f_k \\ & \tilde{\varphi}_{k+1} \end{bmatrix} = \begin{bmatrix} \rho_1 & \theta_1 & & & & & & \vdots & \varphi_1 \\ & \rho_2 & \theta_2 & & & & & \vdots & \varphi_2 \\ & & \cdot & \cdot & & & & \vdots & \cdot \\ & & & \cdot & \cdot & & & \vdots & \cdot \\ & & & & \cdot & \cdot & & \vdots & \cdot \\ & & & & & \cdot & \theta_k & \vdots & \varphi_{k-1} \\ & & & & & & \rho_k & \vdots & \varphi_k \\ \cdots & \cdots & \cdots & \cdots & \cdots & \cdots & \cdots & \vdots & \cdots \\ & & & & & & & \vdots & \tilde{\varphi}_{k+1} \end{bmatrix} \tag{3.18}$$

Then, by Eqn. (3.19) $y^{(k)}$ and t_{k+1} can be found:

$$f_k = R_k y^{(k)}, \; t_{k+1} = Q_k^T \begin{bmatrix} 0 \\ \tilde{\varphi}_{k+1} \end{bmatrix}. \tag{3.19}$$

Finally, by combining Eqn. (3.15) and (3.19) we have:

$$\Phi_E^{(k)} = v_k R_k^{-1} f_k = D_k f_k. \tag{3.20}$$

As it was stated before LLSQR is semi-convergence method, which by further iteration may diverge from optimal solution. Therefore, defining a limit for k, number of iterations, can solve the semi-convergence phenomena problem.

3.3.3 Truncated Total Least Square (TTLS) Method

The total least squares method (TLS) is based on the least squares approximation. This method is used when the coefficient matrix A and the left hand side matrix Φ_T contain errors. Truncated Total Least Square (TTLS) method is modified version of TLS method. This method filters the effect of the very small *singular values* on the solution [68, 81, 82], in other words this method discards the redundant information from both A and Φ_T matrices. The most important stage of the TTLS method is the truncation level.

The steps of TTLS algorithm is given below:

1. The Singular Value Decomposition (SVD) of the augmented matrix $(A\ \Phi_T)$ is calculated as:

$$(A\ \Phi_T) = USV^T = \sum_{i=1}^{n+1} u_i s_i v_i^T, \tag{3.21}$$

where $s_1 \geq s_2 \geq \cdots \geq s_{n+1}$.

2. A truncation parameter $k \leq \min(n, rank(A\ \Phi_T))$ is selected such that: $s_k \geq s_{k+1}$ and $v_{22} = (v_{n+1,k+1}, \ldots, v_{n+1,n+1}) \neq 0$. The selection of the regularization parameter is accomplished by using different regularization parameter selection methods.
3. The V matrix should be partitioned as:

$$\bar{V} = \begin{pmatrix} \bar{V}_{11} & \bar{V}_{12} \\ \bar{V}_{21} & \bar{V}_{22} \end{pmatrix}, \tag{3.22}$$

where $\bar{V}_{11} \in \mathbb{R}^{n\times k}$, $\bar{V}_{12} \in \mathbb{R}^{n\times(n-k+1)}$, $\bar{V}_{21} \in \mathbb{R}^{1\times k}$ and $\bar{V}_{22} \in \mathbb{R}^{1\times(n-k+1)}$.

4. Then the TTLS solution can be calculated by:

$$\Phi_{E_k} = -\bar{V}_{12}\bar{V}_{22}^{+} = -\frac{\bar{V}_{12}\bar{V}_{22}^T}{\|\bar{V}_{22}\|_2^2} \tag{3.23}$$

In (3.23) the pseudo inverse of $\bar{V}_{22}$ exists, because $\|\bar{V}_{22}\|_2 \neq 0$.

The norm of the solution is calculated as:

$$\left\|\Phi_{E_k}\right\| = \sqrt{\|\bar{V}_{22}\|^{-2} - 1}. \tag{3.24}$$

And TLS residual matrix is calculated as:

$$\|(A - \Phi_T) - (\tilde{A} - \widetilde{\Phi_T})\|_F = \sqrt{s_{k+1}^2 + \cdots + s_{n+1}^2}, \tag{3.25}$$

where $\| \ \|_F$ is Frobenius norm and A, Φ_T are error containing versions of A and Φ_T, respectively. We see that the norm of Φ_{E_k} increases with k, while the residual norm decreases with k. When the sub-matrix $\bar{V}_{22}$ is zero or something near zero x_k grows very large, therefore it is beneficial to define a threshold for this sub-matrix in order to limit the solution norm $\left\|\Phi_{E_k}\right\|_2$.

3.3.4 Lanczos Truncated Total Least Square (LTTLS) Method

Although Singular Value Decomposition (SVD) method itself and the methods which use this process as a part of their regularization approaches are efficient, they become inapplicable when the size of coefficient matrix is large. Since the complexity of SVD method is O (mn^2), it is time consuming and impractical to employ this method to solve inverse problems with large coefficient matrices. Instead, a method called "Lanczos Bidiagonalization" which minimizes the size of coefficient matrix without losing the large and efficient singular values is used to solve large discrete ill-posed inverse problems. The Lanczos Bidiagonalization method is able to be combined and used along with other regularization methods like TTLS. In this case, it is called Lanczos TTLS (LTTLS).

In LTTLS algorithm [80], by starting vector, $u_1 = b/\|b\|_2$, after k iterations the two sets of vectors V_k and U_k , and $(k + 1) \times k$ bidiagonal matrix, B_k, are produced such that:

$V_k = \{v_1, v_2, \dots, v_k\}$, and $U_k = \{u_1, u_2, \dots, u_{k+1}\}$,

where these matrices are related to each other by the equations:

$$AV_k = U_k B_k \text{ and } \Phi_T = \beta_1 u_1. \tag{3.26}$$

After k iterations, if k is large enough to include all singular values of the matrix A, the TLS problem can be projected into subspaces spanned by V_k and U_k.

The final form of the problem will be:

$$\min \ \left\|(B_k, \beta_1 e_1) - \hat{B}_k, \hat{e}_k\right\|_F, \text{ subject to } \hat{B}_k y = \hat{e}_k. \tag{3.27}$$

Then the TLS method is applied on small sized matrix, which is the result of Lanczos Bidiagonalization process, in order to create the truncated TLS solution, namely, the

TTLS solution. To calculate TTLS solution, SVD is applied on the matrix ($B_k = \beta_1 u_1$):

$$(B_k \ \beta_1 u_1) = \bar{\bar{U}}^{(k)} \bar{\bar{\Sigma}}^{(k)} \left(\bar{\bar{V}}^{(k)}\right)^T. \tag{3.28}$$

The matrix $\bar{\bar{V}}^{(k)}$ is partitioned as noted below:

$$\bar{\bar{V}} = \begin{pmatrix} \bar{\bar{V}}_{11} & \bar{\bar{V}}_{12} \\ \bar{\bar{V}}_{21} & \bar{\bar{V}}_{22} \end{pmatrix}, \tag{3.29}$$

where $\bar{\bar{V}}_{11} \epsilon \mathbb{R}^{(k-1)\times(k-1)}$,$\bar{\bar{V}}_{12} \epsilon \mathbb{R}^{(k-1)\times 1}$, $\bar{V}_{21} \epsilon \mathbb{R}^{1\times(k-1)}$, and $\bar{\bar{V}}_{22} \epsilon \mathbb{R}^{1\times 1}$.

Then the standars TLS solutiona can be defined as:

$$\bar{y}_k = -\bar{\bar{V}}_{12}^{(k)} (\bar{\bar{v}}_{22}^{(k)})^{-1}, \tag{3.30}$$

Finally, the solution is calculated as:

$$\widetilde{\Phi_E} = V_k \bar{\bar{V}}_{12}^{(k)} (\bar{\bar{v}}_{22}^{(k)})^{-1}, \tag{3.31}$$

3.4 Regularization Parameter Selection Method

The regularization parameter is a positive scalar used to find the balance point when it is to minimize the residual norm and the solution norm simultaneously. This parameter is symbolized as λ, a very small positive scalar, or k, truncation level, according to the regularization method. When a regularization parameter is selected to be small, the effect of high frequency elements of a signal increases. This case is called *under-regularization*, no meaningful information about ECG signal is obtained in this way. Conversely, when the regularization parameter is selected to be large, the effect of high frequency signal elements is eliminated and this causes smoothing effect on the signal. This case is called *over-regularization*.

Therefore, selecting a correct and effective regularization parameter is one of the most important stages of regularization procedure. As it was stated before, in this study, Maximum Correlation Coefficient (MCC) method is used as regularization parameter selection method.

Although, MCC method is neither practical nor suitable for clinical usage, since it uses real epicardial potentials to determine regularization parameter, it

provides significant information about the effectiveness of the regularization parameter during the regularization process.

In the MCC method, first the number of regularization parameters to be tested are decided, then upper and lower limits are also decided. Finally, for each single parameter the corresponding inverse solution is calculated. These calculated results are compared with the real values of the epicardial potentials and the solution that gives the maximum Correlation Coefficient (CC) is selected to be regularization parameter. MCC method is invaluable when the aim is to assess the performance of the regularization methods independent from regularization parameter selection method.

3.5 Lead Reduction Algorithm

As it is stated before, to obtain BSPM, a large number of leads are attached to the body surface to detect the informative heart signals. The attachment of large number of leads makes the BSPM approach hard to apply in practice. There are several lead selection methods to choose a subset of leads that provides significant information about the heart signals. In the lead reduction algorithm, proposed in this study, this goal is accomplished by choosing the leads whose acquired signals are informative and eliminating those whose signals have small or no contribution to understand the electrical activity of the heart.

In this section, the lead reduction algorithm is explained completely. During the lead selection process, Tikhonov regularization along with Maximum Correlation Coefficient method are used, which are described in the previous sections of this chapter.

In this study, the lead reduction algorithm is applied on a 192 lead-set, whose configuration is the same as the one used by Lux *et al.* [27] to select 64 and 32 optimal and reduced lead-sets. The lead reduction algorithm is an iterative algorithm and to make it easier to understand, the algorithm is divided into 4 main steps. Starting from the first iteration, in the first step of the algorithm, Tikhonov regularization is applied on every single row of the data matrix. In the second step, the mean of Correlation Coefficient (CC) values are calculated for the obtained

solutions. In the third step, maximum value of mean CC is selected and the corresponding rows are extracted from data and the forward transfer matrices. In the fourth step, the selected rows are deleted from data and forward transfer matrices, and are kept to be used in further iterations. In the next iterations, the algorithm looks for the lead whose performance is the best when combined with the previously selected lead(s), by going through steps one to four. The algorithm repeats itself until the desired number of leads is reached. The four main steps of the algorithm are explained below along with their illustrations, comprehensively.

In step one, the lead reduction algorithm starts with selecting a single lead that gives the best solution in terms of CC when it is employed to solve the inverse ECG problem through Tikhonov regularization. In other words, Tikhonov regularization is applied on every single row of the data matrix, Φ_T, and forward transfer matrix A. As it was explained before, each row in the data matrix is a signal received from a specific lead. In this step, all epicardial potentials are estimated using the signal from only one electrode. At the end of this step, the number of computed inverse solutions equals to the number of rows of the data matrix; here, 192. The schematic explanation of this step is illustrated in the Figure 3.3.

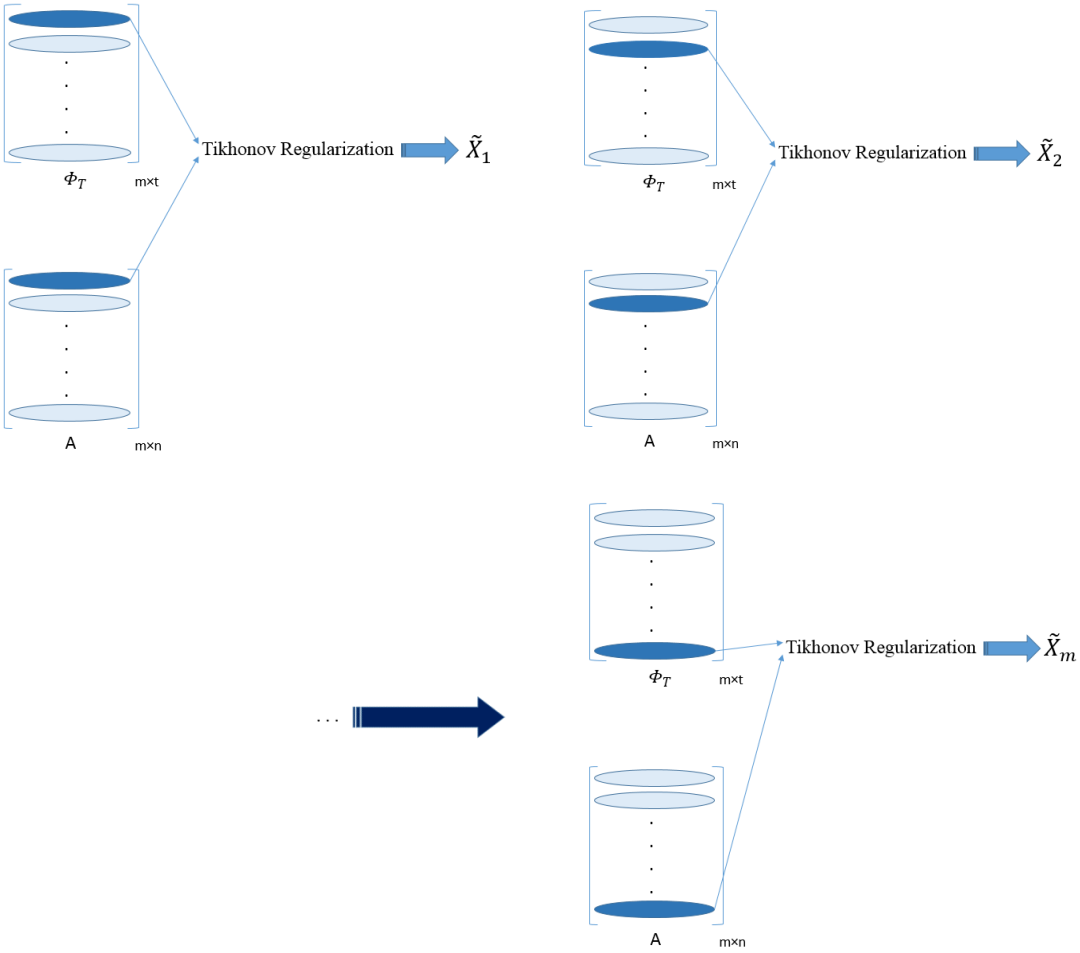

Figure 3.3: The illustration of the first step of the lead reduction algorithm.

In the second step, for each of these 192 solutions, mean of Correlation Coefficient values are calculated. Figure 3.4 shows the second step of the algorithm.

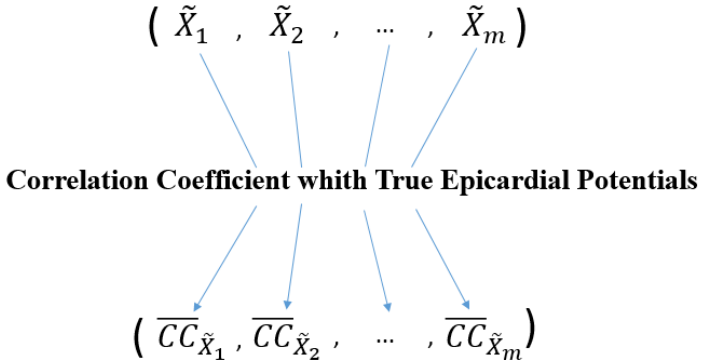

Figure 3.4: The illustration of the second step of the lead reduction algorithm.

In the third step, the largest mean Correlation Coefficient value, among calculated values in the previous step, is selected and its corresponding rows from data matrix and forward transfer matrix are retrieved. In Figure 3.5, this selection is illustrated with the assumption that the maximum mean CC value, $\overline{CC}_{\tilde{X}_i}$, belongs to the i[th] row.

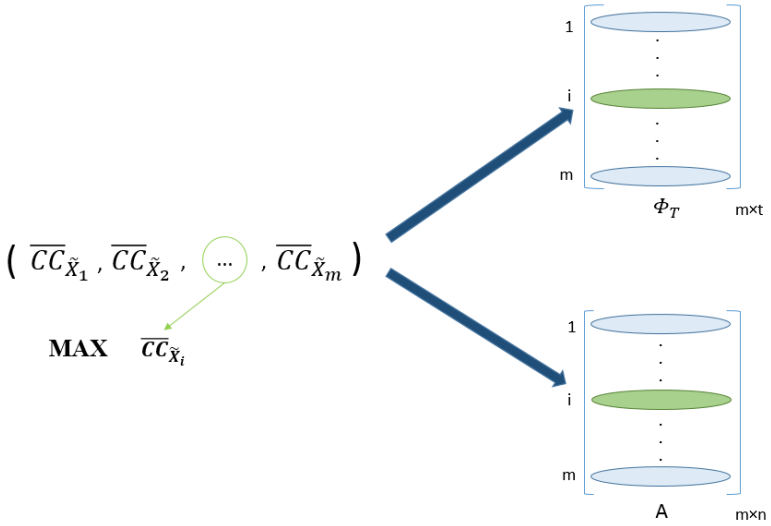

Figure 3.5: The illustration of the third step of the Lead Reduction Algorithm.

In the fourth step, selected rows from the previous step are deleted from data and forward transfer matrices and kept in temporary matrices $\phi_{T_{Temp}}$ and A_{Temp} to be used in the next iterations. Figure 3.6 illustrates this step.

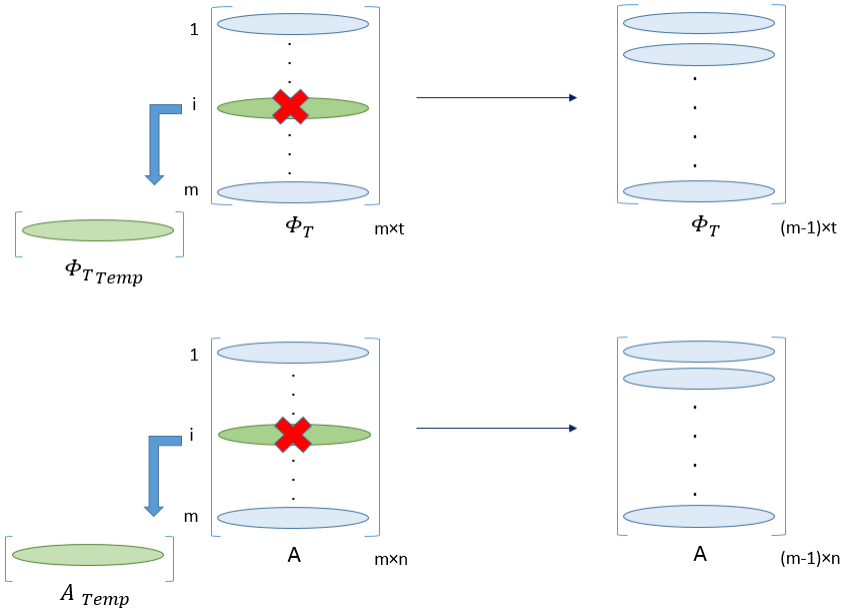

Figure 3.6: The illustration of the fourth step of the lead reduction algorithm.

In the next iteration, again the algorithm looks for the next optimal lead by going through steps one to four. From second iteration on, as it is shown in the Figure 3.7, the previously selected rows from data and forward transfer matrices are conjugated with each row of remaining data and forward transfer matrices, respectively. Again the algorithm looks for the answer that gives the best mean Correlation Coefficient value by applying Tikhonov regularization on each of augmented matrices. It is obvious that at the end of each iteration, the size of the data matrix and forward transfer matrix reduces by one, and the size of $\phi_{T_{Temp}}$ and the forward matrix corresponding to these data increase by one. The algorithm proceeds untill the number of desired leads in $\phi_{T_{Temp}}$ is reached.

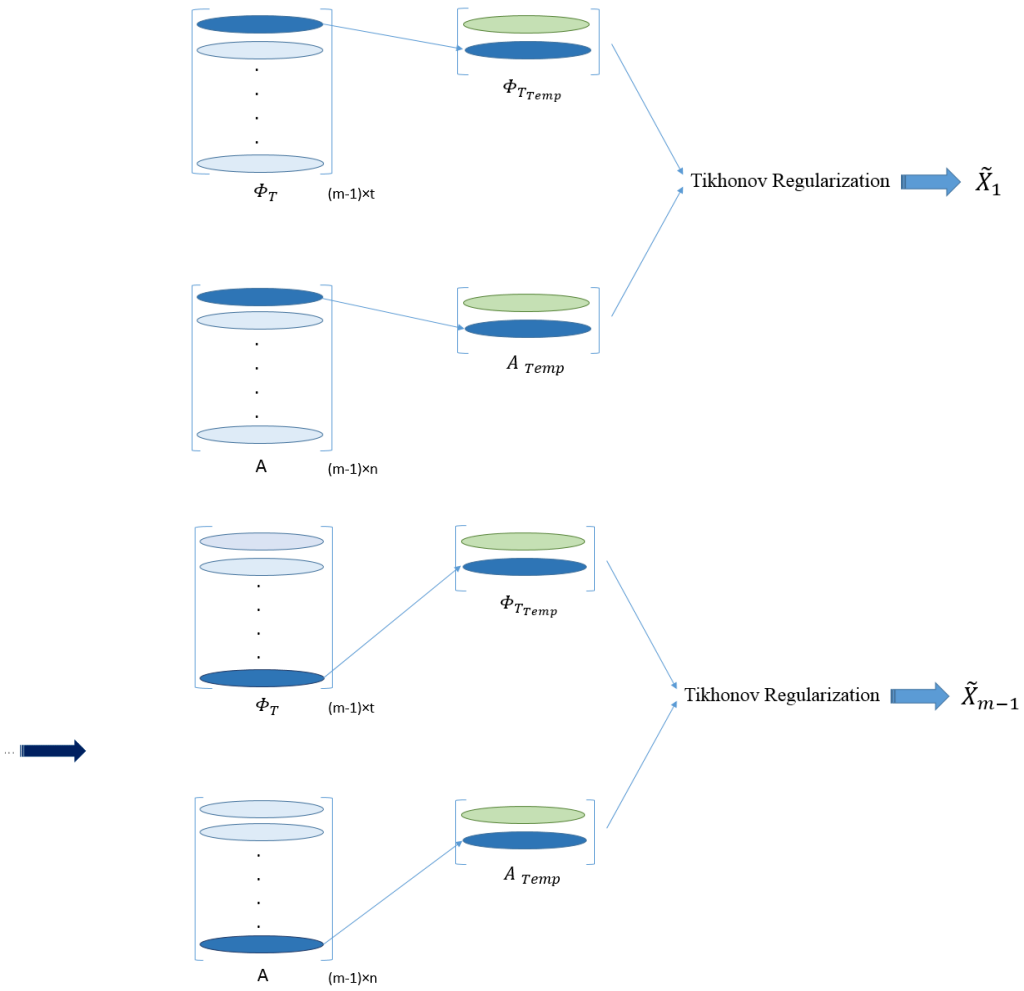

Figure 3.7: The illustration of the lead reduction algorithm at each iteration.

Finally, at the end of iterations, all of the selected rows from data and forward transfer matrices are stored and their corresponding electrodes on the surface of the torso are specified.

In this study, the lead reduction algorithm is applied on different data-sets to obtain data-set dependent lead-set configurations for a number of 64 and 32 leads, respectively. These data-sets, their configuration, and their quantitative and qualitative comparisons will be discussed in the next chapter.

CHAPTER 4

RESULTS

In this chapter, first, the properties of the data used in the lead selection process are explained, and for few samples, the resulted lead-set configurations are shown. Then, a single lead-set is proposed that works for all data-sets. Finally, different regularization methods are applied on data-sets and the results are compared.

4.1 Test Data

The epicardial potentials used for this study were measured at University of Utah Nora Eccles Harrison Cardiovascular Research and Training Institute (CVRTI) [84]. The epicardial measurements were taken from a dog's heart, perfused from another dog's circulatory system and suspended in an electrolytic filled (500 Ω.cm) adolescence human thorax shaped fiberglass tank. To measure the epicardial potentials, a nylon sock electrode with silver wires was slipped over the ventricles. During measurements the heart is stimulated from the ventricles to simulate ventricular arrhythmias. The epicardial measurements are taken from 490 points with sampling rate 1000 samples per second. Figure 4.1 shows the illustration of the data acquisition setup.

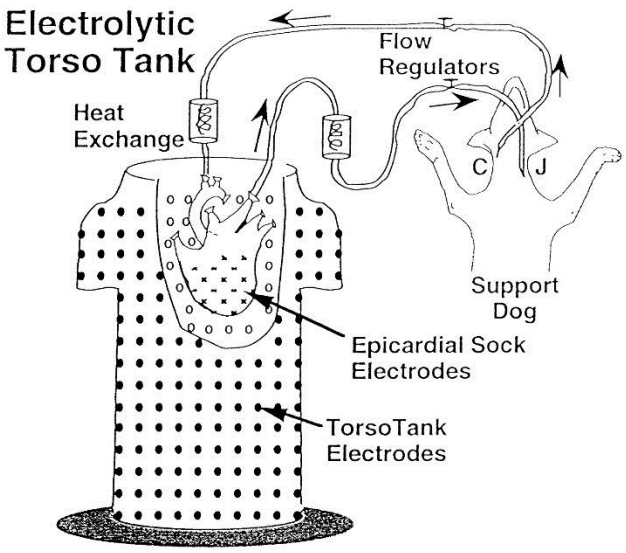

Figure 4.1: Perfused dog heart suspended in the electrolytic tank. Recording electrodes consist of 490 lead epicardial sock array [23].

To calculate the forward matrix, Boundary Element Method (BEM) is used. The geometric model consists heart, torso, and lungs. This forward model along with the epicardial potential measurements from 490 leads were used to simulate torso potentials at 771 points on the body surface. In this study, the actual size of the forward matrix is 771-by-490. The body surface potentials are obtained by multiplying the forward matrix with epicardial potentials and adding independent and identically distributed Gaussian noise (Figure 4.2).

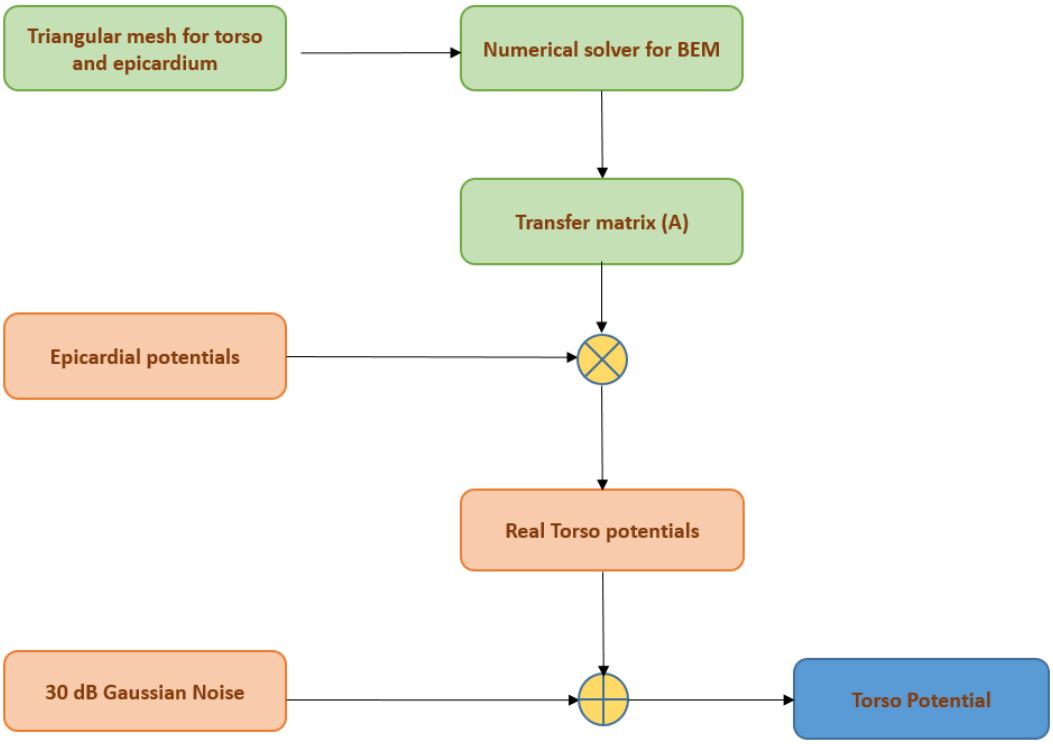

Figure 4.2: Calculation of torso potentials.

To assess the efficiency of the lead reduction algorithm proposed in this study, several data-sets are used. In order to achieve a maximum diversity from data-set standpoint, we utilize 23 data-sets related to 23 different stimulation sites on the epicardium surface. Figure 4.3 shows the heart geometry that is divided into 23 different regions. Because of 3-dimensional geometry of the heart, the whole surface of the heart is shown in three connected planes, frontal plane (panel (a)), backplane (panel (b)), and side plane (panel (c)). For each of the 23 regions, we pick one epicardial potential data-set stimulated from a site that falls within that region.

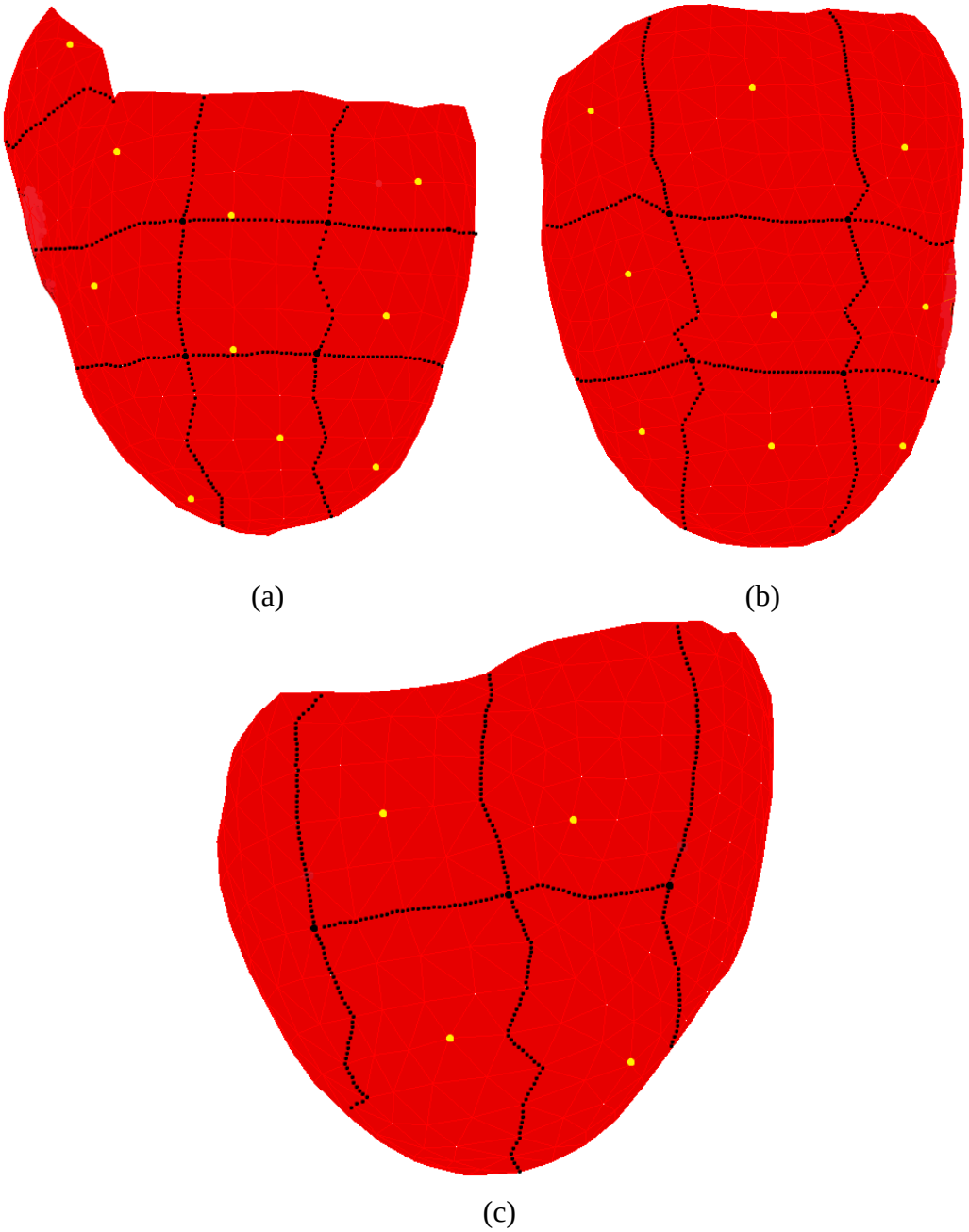

(a) (b)

(c)

Figure 4.3: Regions on the surface of the heart are divided by dotted line and stimulation sites are marked by yellow dots, (a) 10 frontal regions, (b) 9 back regions, (c) 4 side regions.

Due to stimulation sites other than the natural pace maker, *i.e.*, the SA node, the QRS waves have different durations and propagation paths, meaning that every individual pacing site results in a different data-set.

Here, instead of applying lead reduction algorithm on the complete lead-set consisting of 771 torso surface leads, the 192 lead-set configuration (12-by-16 equidistant electrode arrays), proposed by Lux *et al.*, [23- 24] is used. Figure 4.4

shows this 192 lead-set configuration on the body surface. As it is seen in this figure, a large number of leads have to be attached to the surface of the torso to obtain BSPM. Not only attaching a large number of electrodes to the body surface of patients is impractical, but also it takes a long time to process the acquired data. Additionally, these acquired data should be stored which is space consuming process. Therefore, the motivation here is to reduce the number of electrodes and receiving an informative signals at the same time.

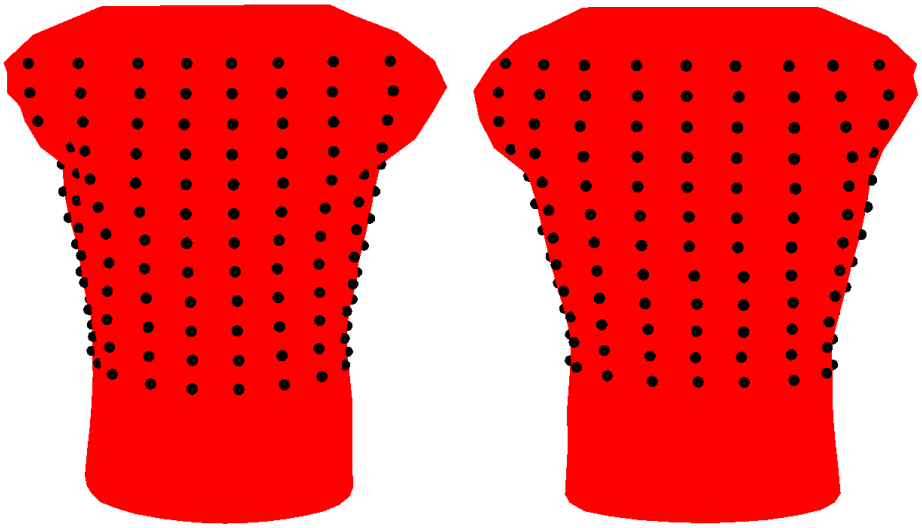

(a) (b)

Figure 4.4: 192 lead-set configuration, (a) Frontal view, (b) back view.

4.2 Quantitative Comparisons

To compare the quality of the inverse solutions related to each different data-set, Correlation Coefficient (CC) and Relative Difference Measurement Star (RDMS) are used.

$$CC(i) = \frac{\sum_{i=1}^{t}[(\phi_C)_i - \bar{\phi}_C].[(\phi_E)_i - \bar{\phi}_E]}{\|\phi_C - \bar{\phi}_C\|_2 . \|\phi_E - \phi_E\|_2}, \tag{4.1}$$

$$RDMS(i) = \left\| \frac{(\phi_C)_i}{\|(\phi_C)_i\|_2} - \frac{(\phi_E)_i}{\|(\phi_E)_i\|_2} \right\|_2, \tag{4.2}$$

where ϕ_E and ϕ_C represent known epicardial potentials and computed epicardial potentials, respectively. The quantities $\bar{\phi}_E$ and $\bar{\phi}_C$ are mean values of ϕ_E and ϕ_C, respectively. If the value of CC increases or the value of RDMS decreases, it can be

interpreted that the solution has improved. These measures give quantitative comparisons between true epicardial potentials and the reconstructed ones, however, it is beneficial to compare the true epicardial potentials and the reconstructions visually, in other words, qualitatively. Another reason to use visual comparison is to assess the ability of the method to reconstruct the activation wave front correctly. The latter is one of the most important aims of inverse electrocardiography. In this study, MAP3D software is used to visualize the reconstructed epicardial potentials. This software is a part of Scientific Computing and Imaging (SCI) software developed by University of Utah researchers. With this software, displaying and editing three-dimensional geometric models and time-based data associated with those models are possible. The results are displayed as isopotential surfaces of epicardial potential distribution on the 3D heart geometry.

Through comparing the results visually, two important characteristics are taken into account:

1. The ability of the solution to reconstruct the wave front without dispersion. The reason of the dispersion of the solution is the smoothing effect of the regularization method.
2. The ability of the solution to estimate the potential contours as correct as possible, and to approximate activated or inactivated regions appropriately.

4.3 Results of Lead-Set Reduction

In this section, first the effect of the reduction in the number of used leads in the signal acquisition is studied to see how the quality of the acquired data changes when the number of the leads is reduced. Then, a single common 64 and 32 lead-set is proposed. These reduced lead-sets are then assessed in terms of their signal information, whether their acquired signals are qualified enough to be used in the reconstruction of epicardial potentials.

4.3.1 Reduced Lead-set Effects

In this section, we study the effects of reduced lead-sets on the quality of the reconstructed epicardial potentials by both quantitative and qualitative approaches.

To have a clear understanding about the resultant lead-sets of lead reduction algorithm, here, 3 samples out of 23 different pacing sites, on the epicardium surface are selected and the lead reduction algorithm is applied on their corresponding data. These three activation sites are chosen from three different regions of the heart, one from frontal region (data-set-*I*), one from back region (data-set-*II*), and one from side region (data-set-*III*). The selected 3 pacing sites are shown in Figure 4.5 These pacing sites are marked in blue in the Figure 4.5.

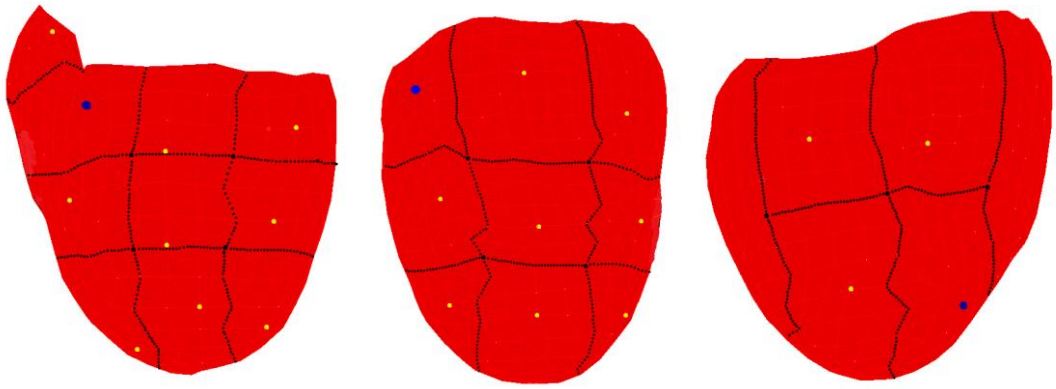

(a) (b) (c)

Figure 4.5: Three selected pacing sites are marked with blue color (a) a pacing site from frontal region of the heart, (b) a pacing site from back region of the heart, (c) a pacing site from side region of the heart.

As it is stated before, the primary complete lead-set which is used in this study, is the configuration that is proposed by Lux *et al.*, [23, 24] as shown in Figure 4.4. Applying the lead reduction algorithm on these 3 data-sets related to 3 different activation sites results in three different reduced 64 and 32 lead-sets optimal for these three specific data. The reduced 64 and 32 lead-set configurations are shown in Figure 4.6. In this figure two left columns are frontal and back view of the reduced 64 lead-set, and two right columns are frontal and back view of the reduced 32 lead-set, respectively, related to each of the mentioned data-sets.

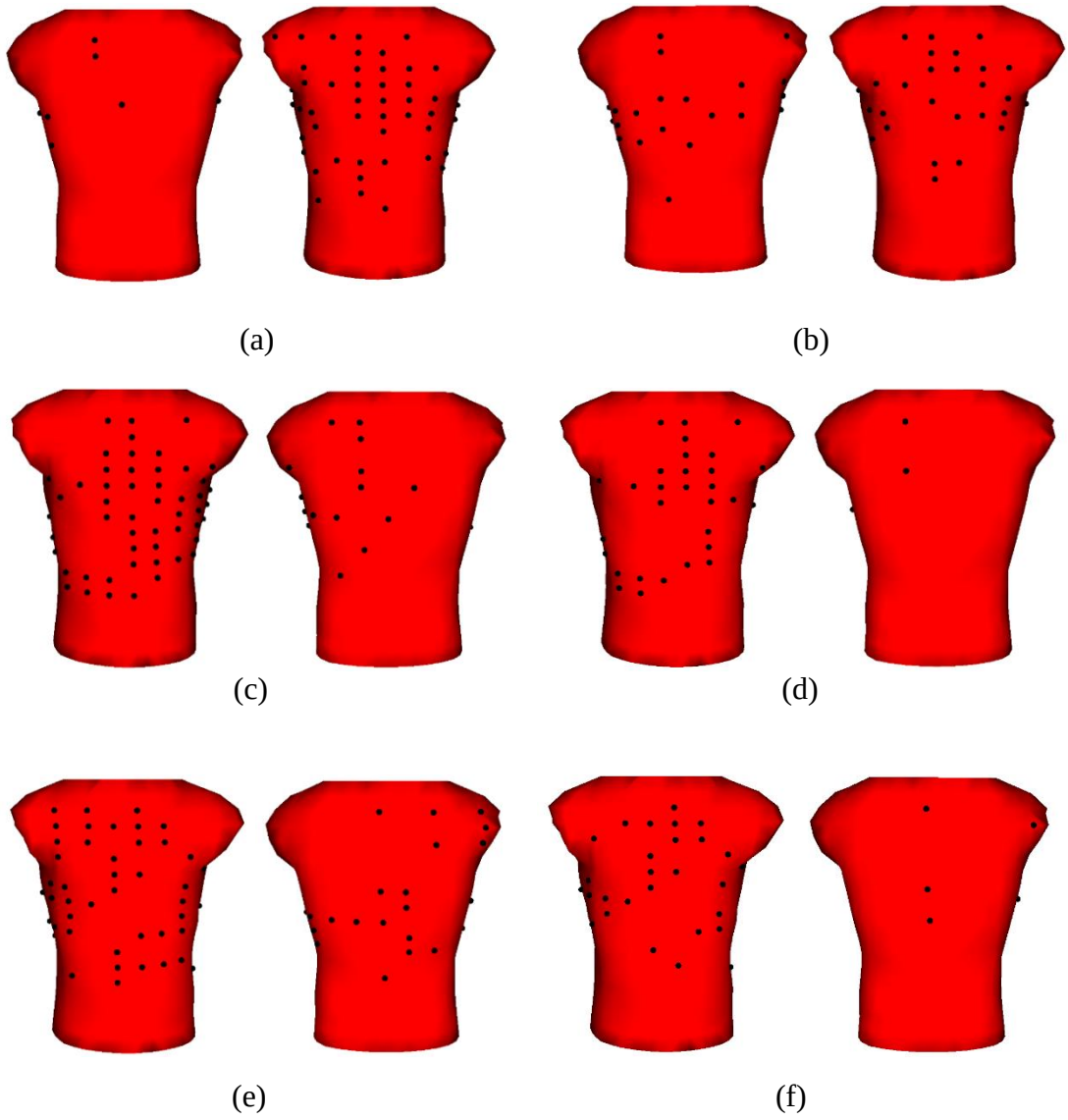

Figure 4.6: (a) reduced 64 lead-set related to data-set-*I*, (b) reduced 32 lead-set related to data-set-*I*, (c) reduced 64 lead-set related to data-set-*II*, (d) reduced 32 lead-set related to data-set-*II*, (e) reduced 64 lead-set related to data-set-*III*, and (f) reduced 32 lead-set related to data-set-*III*.

Not surprisingly, each data-set results in a specific optimal lead-set configuration which is arranged exclusively for that data-set. Depending on the specific activation site, the distribution of the selected leads differs such that useful information is obtained as much as possible. Since every data-set has a specific lead-set configuration, applying lead reduction algorithm on 23 different data-sets results in to 23 different lead-set configurations.

The main motivation here is to find one common lead-set configuration for all of the data-sets whose acquired signals are qualified and informative in an acceptable extent. If such a lead-set configuration is found it can be used instead of all other exclusive configurations.

The remaining part of the section is organized as following steps:

1. The lead reduction algorithm is applied on each of 23 data-sets, and 64 and 32 reduced lead-sets tuned to each inidividual recording sites are obtained, separately.
2. For each reduced lead-set (64 and 32 lead-sets) according to each of 23 data-sets, related rows and columns are extracted from data-matrix, Φ_T , and forward transfer matrix, A. Then, these reduced-sized data and forward transfer matrices are used to solve inverse problem of ECG. To solve the inverse problem related to each data-set, Tikhonov regularization is employed and as a regularization parameter selection approach Maximum Correlation Coefficient (MCC) method is used. For each 23 data-set, Tikhonov regularization is applied on the complete 771 lead-set, 192 lead-set, reduced 64-lead-set, and reduced optimal 32 lead-set related to that data set. In this study, a fixed 30 SNR dB Gaussian noise is added to all data-sets in advance.
3. The results of regularization, reconstructed epicardial potentials, are then compared quantitatively by the means of calculating the average and the standard deviation values of Correlation Coefficient (CC) values, and similarly for Relative Difference Measurement Star (RDMS) values. The higher values of CC, as values approach to 1, indicate inverse problem solutions with high quality. So, higher values of CC are preferable. The smaller values of RDMS indicate that less error exists in the solution, so that the smaller values of RDMS are preferable.

The results of calculation of CC and RDMS of the inverse problem solution of each 23 data-set are presented in Table 4.1 and Table 4.2, respectively.

Table 4.1: Mean (avg) and standard deviation (std) of Correlation Coefficient (CC) values for complete 771 lead-set, 192 lead-set, reduced 64-lead-set, and reduced optimal 32 lead-set for each of the 23 different data-sets.

# of Leads / Data Sets	771 (avg±std)	192 (avg±std)	64 (avg±std)	32 (avg±std)
Data-1	0.79±0.20	0.78±0.20	0.74±0.22	0.73±0.22
Data-2	0.72±0.22	0.70±0.23	0.68±0.25	0.67±0.25
Data-3	0.78±0.20	0.75±0.20	0.75±0.21	0.74±0.21
Data-4	0.74±0.18	0.72±0.19	0.72±0.20	0.70±0.20
Data-5	0.79±0.17	0.77±0.18	0.76±0.19	0.72±0.17
Data-6	0.79±0.17	0.77±0.18	0.77±0.18	0.76±0.19
Data-7	0.79±0.15	0.77±0.16	0.77±0.17	0.76±0.18
Data-8	0.73±0.16	0.71±0.17	0.71±0.17	0.70±0.18
Data-9	0.79±0.16	0.76±0.17	0.75±0.19	0.74±0.19
Data-10	0.77±0.19	0.75±0.20	0.75±0.20	0.73±0.21
Data-11	0.67±0.27	0.64±0.27	0.60±0.29	0.60±0.30
Data-12	0.70±0.28	0.68±0.29	0.67±0.30	0.65±0.30
Data-13	0.77±0.19	0.76±0.19	0.76±0.19	0.75±0.19
Data-14	0.70±0.23	0.68±0.23	0.67±0.25	0.65±0.25
Data-15	0.78±0.17	0.76±0.18	0.75±0.18	0.74±0.18
Data-16	0.79±0.15	0.77±0.17	0.77±0.16	0.77±0.16
Data-17	0.66±0.22	0.64±0.22	0.64±0.23	0.62±0.23
Data-18	0.66±0.20	0.64±0.21	0.63±0.20	0.62±0.21
Data-19	0.74±0.15	0.71±0.16	0.71±0.16	0.70±0.15
Data-20	0.74±0.17	0.72±0.19	0.71±0.19	0.70±0.20
Data-21	0.66±0.25	0.63±0.26	0.61±0.28	0.59±0.28
Data-22	0.80±0.13	0.78±0.14	0.77±0.16	0.75±0.17
Data-23	0.68±0.18	0.66±0.19	0.66±0.18	0.65±0.18

Table 4.2: Mean (avg) and standard deviation (std) of Relative Difference Measurement Star (RDMS) value for complete 771 lead-set, 192 lead-set, reduced 64-lead-set, and reduced optimal 32 lead-set for different 23 data-sets.

# of Leads / Data Sets	771 (avg±std)	192 (avg±std)	64 (avg±std)	32 (avg±std)
Data-1	0.55±0.23	0.58±0.24	0.63±0.26	0.64±0.26
Data-2	0.68±0.25	0.71±0.26	0.73±0.28	0.75±0.27
Data-3	0.60±0.25	0.65±0.25	0.65±0.25	0.67±0.25
Data-4	0.67±0.23	0.70±0.23	0.67±0.23	0.72±0.24
Data-5	0.59±0.23	0.64±0.23	0.65±0.24	0.71±0.21
Data-6	0.59±0.21	0.62±0.22	0.62±0.22	0.64±0.23
Data-7	0.60±0.20	0.62±0.21	0.62±0.21	0.64±0.21
Data-8	0.65±0.16	0.68±0.17	0.68±0.17	0.69±0.17
Data-9	0.60±0.20	0.64±0.21	0.65±0.22	0.67±0.22
Data-10	0.63±0.22	0.66±0.23	0.67±0.23	0.69±0.24
Data-11	0.74±0.30	0.78±0.30	0.81±0.31	0.82±0.31

(Table 4.2 continued)

Data-12	0.67±0.32	0.70±0.32	0.72±0.32	0.74±0.32
Data-13	0.61±0.20	0.63±0.20	0.64±0.20	0.65±0.20
Data-14	0.70±0.26	0.73±0.27	0.73±0.26	0.76±0.26
Data-15	0.61±0.20	0.65±0.20	0.65±0.20	0.67±0.20
Data-16	0.60±0.18	0.64±0.19	0.63±0.19	0.64±0.19
Data-17	0.73±0.26	0.76±0.26	0.76±0.26	0.78±0.27
Data-18	0.73±0.20	0.75±0.24	0.76±0.23	0.77±0.23
Data-19	0.65±0.19	0.68±0.19	0.69±0.19	0.70±0.19
Data-20	0.68±0.20	0.70±0.20	0.71±0.21	0.73±0.21
Data-21	0.75±0.29	0.78±0.28	0.79±0.29	0.81±0.29
Data-22	0.59±0.17	0.62±0.18	0.63±0.19	0.65±0.20
Data-23	0.71±0.22	0.73±0.22	0.73±0.22	0.75±0.21

Considering the results shown in Table 4.1 it can be concluded that, while the number of involved leads in solving the inverse problem of ECG decreases, the mean of CC values of the inverse solution, which is a numerical indicator of the quality of the solution, shows a small decrease. While comparing mean of CC values of 771 complete lead-sets and reduced 32 lead-sets the largest variation in mean of CC values is about 0.07 is related to data-sets 11 and 21, the smallest variation in mean CC value is about 0.02 which is related to data-sets 13 and 16. The mean variation between all mean CC values of all 771 data-sets and all reduced 32 lead-sets is about 0.042. This means that decreased number of measurement leads does not have a considerable effect on the final inverse solution. In other words, solving the inverse problem of ECG using smaller number of leads instead of the complete lead-set provides approximately similar results to that of the complete lead-set. Therefore, by using small number of leads configured optimally to acquire informative signals from body surface, the need of using large number of leads will be eliminated.

In the case of RDMS, as it is shown in Table 4.2, while the number of measurement leads decrease, the mean of RDMS values show small increase. This again validates that instead of complete lead-set, which uses large number of leads, a small number of optimally placed leads can be used to reconstruct epicardial potentials, since the results of the latter have a negligible difference with the former.

To have an overview about the difference between the mean of Correlation Coefficient (CC) values of 23 different lead-sets, we present two different plots in Figures 4.7 and 4.8. These plots are different presentations of Table 4.1. Each

column group in the Figure 4.7, presents average CC values related to 23 data-sets for 771 lead-set, 192 lead-set, reduced 64 and 32 lead-sets, respectively.

Figure 4.7 represents the bar plot of average CC values of each individual lead-set, for 23 different lead-sets.

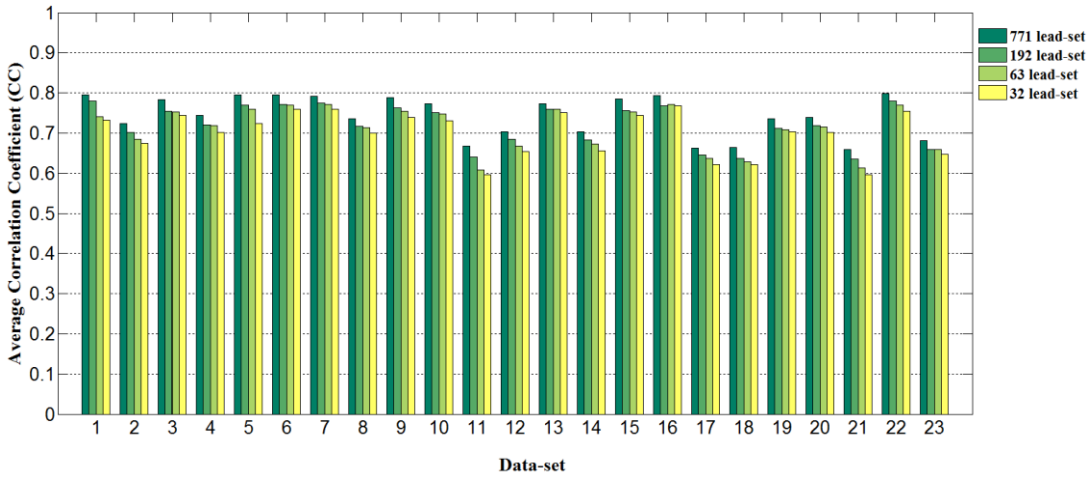

Figure 4.7: Bar plot of average Correlation Coefficient (CC) value.

As it can be inferred from Figure 4.7 there is not a considerable difference between the average CC values of complete 771 lead-sets and reduced 32 lead-sets.

Figure 4.8 shows average over average of CC values for all data-sets together, along with average over standard deviation of their CC values. Each bar of this plot represents average over columns of Table 4.1 related to 771, 192, 64, and 32 lead-sets, respectively. The average over standard deviation of CC values are shown by pins in the plot.

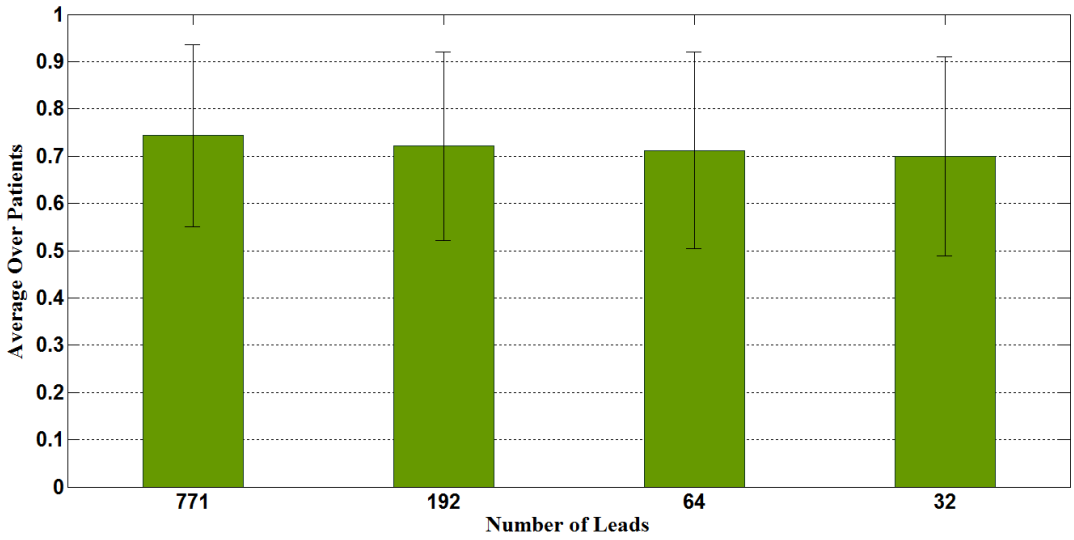

Figure 4.8: Average over average of CC values for all data-sets along with average over standard deviation of all data-sets.

From Figure 4.8 again it can be concluded that there is not a considerable difference between the left most bar, related to average CC over all 771 lead-sets, and the right most bar, related to average CC over all 32 lead-sets. To mention the difference between these two plots by percentage, there is 5% difference between mentioned two bars, which is very small and negligible.

4.3.2 Common Lead-set for All Data-sets

In the previous section, reduced 64 lead-sets and reduced 32- lead-sets optimal for each of the 23 data-sets, related to 23 different pacing sites on epicardium, are investigated. Therefore, as a result, 23 different configurations for 64 lead-sets and similarly, 23 different configurations for 32 lead-sets were obtained.

In this section, it will be shown that a common reduced 64 and 32 lead-set optimal for all of the data-sets can be obtained using the results of the previous section. To achieve such a common lead-set, the position of the most repeated leads and the number of their repetition have to be known. Therefore, first we should determine how many times a specific lead is repeated in the all of the reduced 64 lead-sets related to 23 different data-sets. The same procedure should be done to determine the common reduced 32 lead-set which is optimal for all data-sets.

4.3.2.1 Common 64 Lead-set for All Data-sets

To tackle the question “Is there any single common lead-set whose acquired data can be used to reconstruct the epicardial potentials?” one needs to know the number of times that any individual lead from 192 lead-set configuration is selected in 23 reduced lead-sets. To accomplish this mission, Figure 4.9 is shown to display the location of leads on the torso and the number of times that they have been repeated for 64 lead-sets obtained from each of 23 data-sets. In other words, this figure represents all 192 leads in terms of the number of times that they have been repeated when the lead reduction algorithm is applied on 23 data-sets individually to select 64 leads optimally configured for that individual data-set.

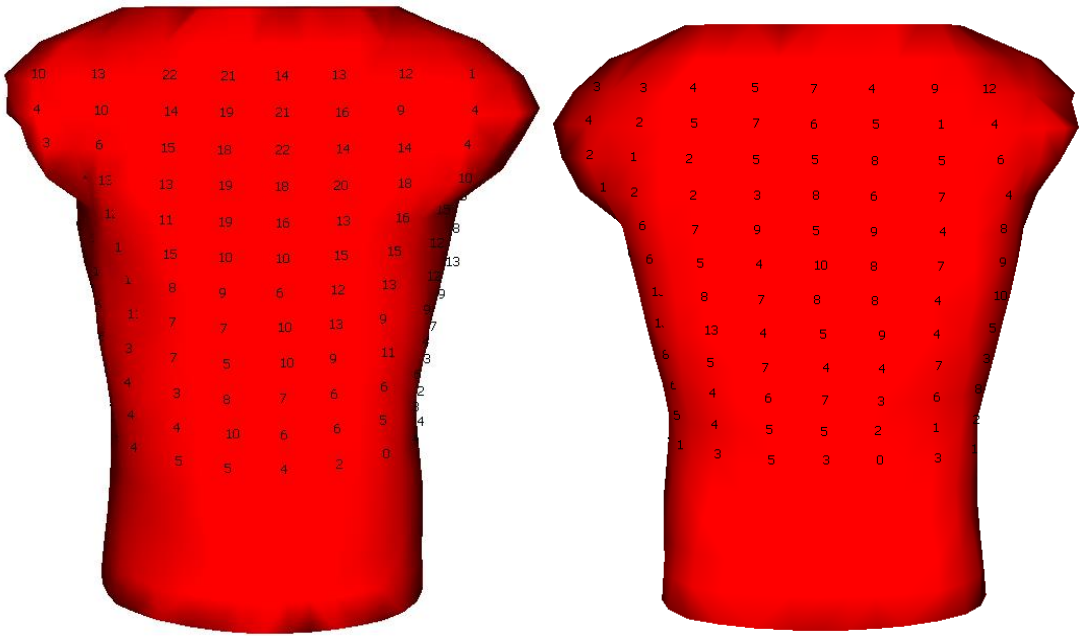

(a) (b)

Figure 4.9: 192 leads and the number of their repetition in the case of selecting 64 leads from 192 leads. (a) Frontal view and (b) back view.

As it was expected, the quantity of leads and their number of repetitions are more in the frontal region of the torso, where the electrical activity of the heart is more detectable. Now the aim is to select the most repeated 64 leads to form a common optimal lead-set for which acquired data is consistent enough to reconstruct the epicardial potentials in an acceptable quality. To facilitate the selection process a histogram plot is obtained by applying the steps below:

1. Finding the reduced lead set for each of the 23 data-set by applying lead reduction algorithm (see section 4.3.1).
2. Finding the number of repetition for each lead in 192 lead-set, e.g., Figure 4.9.
3. Finally, picking 64 leads (depending on desired number of leads in final configuration this can be 32 leads too) that have been selected the most by the algorithm in each data-set.

Figure 4.10 displays the histogram plot which shows lead numbers (indices) versus the number of times that they have been repeated in every 64 lead-set selected for each of the 23 single data-sets.

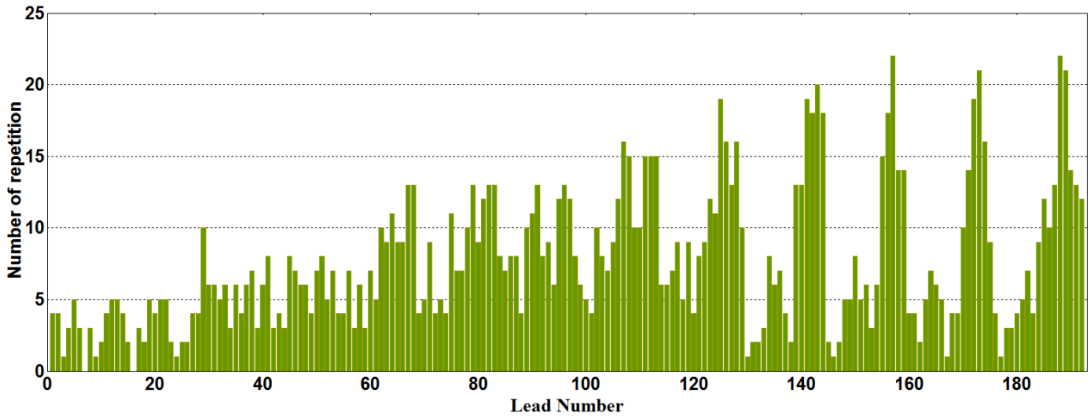

Figure 4.10: Histogram plot for 64 lead-set.

To have a better view of the above plot, Figure 4.11 is presented, in which the number of leads are sorted according to their number of times that they have been repeated. Note that the indices in the x-axis are no longer displayed from the 1st lead to the last (192nd) lead, but displayed from the most selected lead to the least selected lead.

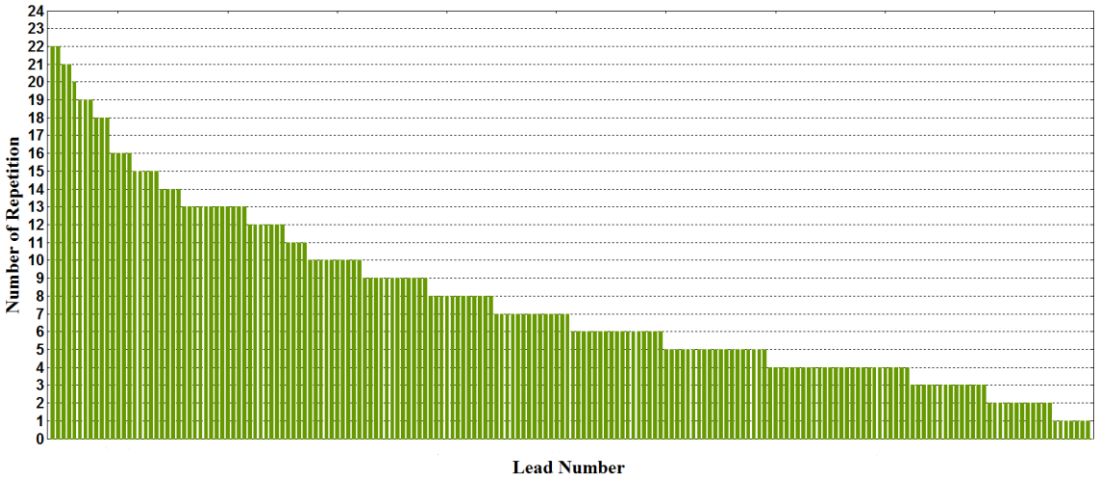

Figure 4.11: Bar graph of sorted leads according to their number of repetition, *x*-axis is lead number and *y*-axis is repetition time.

As it is shown in the Figure 4.11, several leads are selected by the algorithm (when applied on 23 different data-sets) more than 20 times. As is can be seen in the Figure 4.11 only 4 leads are selected more than 20 times, leads 157, 173, 188, and 189. By looking to Figure 4.11, it is obvious that lead number 128 is repeated 16 times, lead number 82 is repeated 13 times, and lead number 102 is repeated 10 times.

To form the common reduced 64 lead-set, which is aimed to be optimal for all 23 data-sets, all the lead numbers that are repeated more than 10 times are selected. This selection results in a lead-set with 57 leads. It left 7 leads to be selected from the leads which are repeated 9 times, but there are 12 leads with 9 repetitions. Figure 4.12 shows these 12 leads.

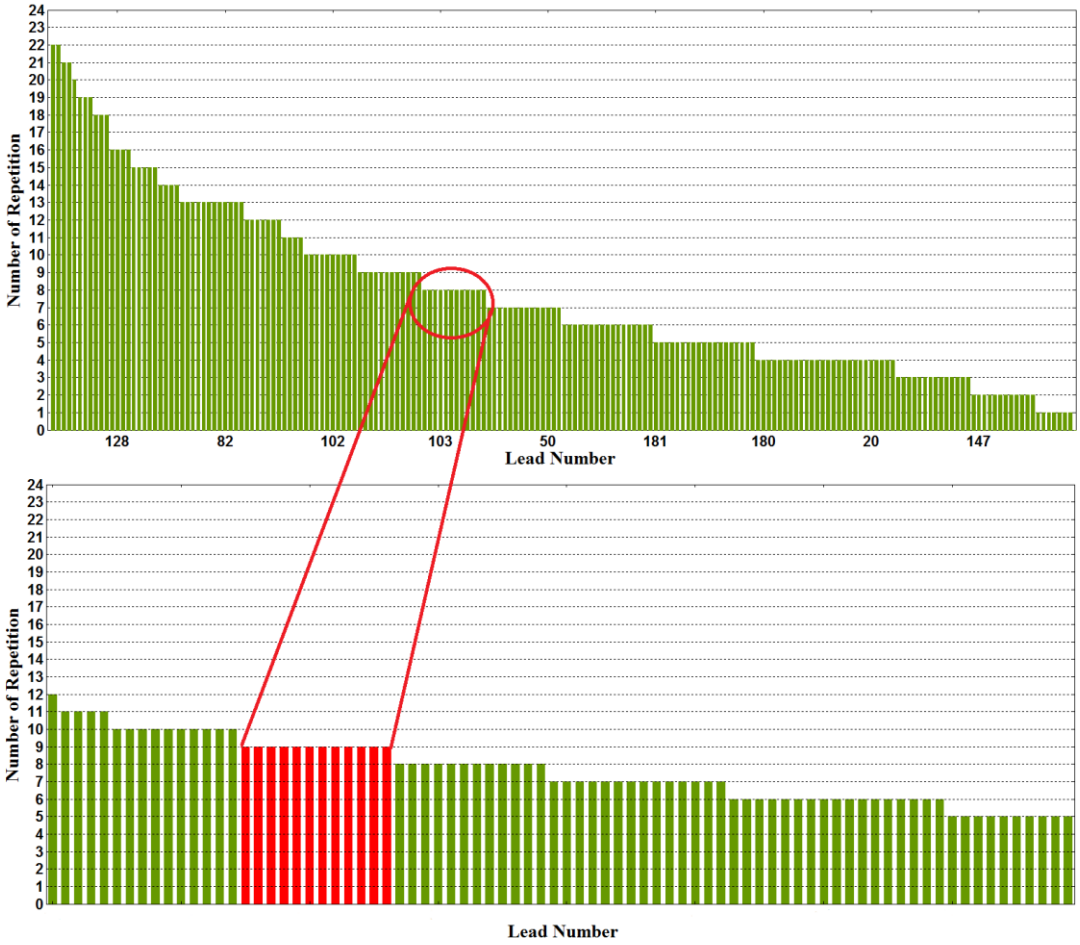

Figure 4.12: 9 times repeated leads shown by red bars.

In order to select 7 leads out of these 12 leads, the positions of all 12 leads are examined on the torso surface, and then the leads that ensure the most attainable sparse configuration is obtained (by following the idea that any selected pair should have the largest possible distance in between). The main reason to select these 7 leads in this way is to obtain the heart signals from wider region, consequently getting samples from widely distributed lead-set configuration. Figure 4.13: shows 57 selected leads (black dots) together with these 12 candidate leads for selection (blue and yellow). In these images, 7 out of 12 leads which are selected are shown in blue and rejected ones are in yellow.

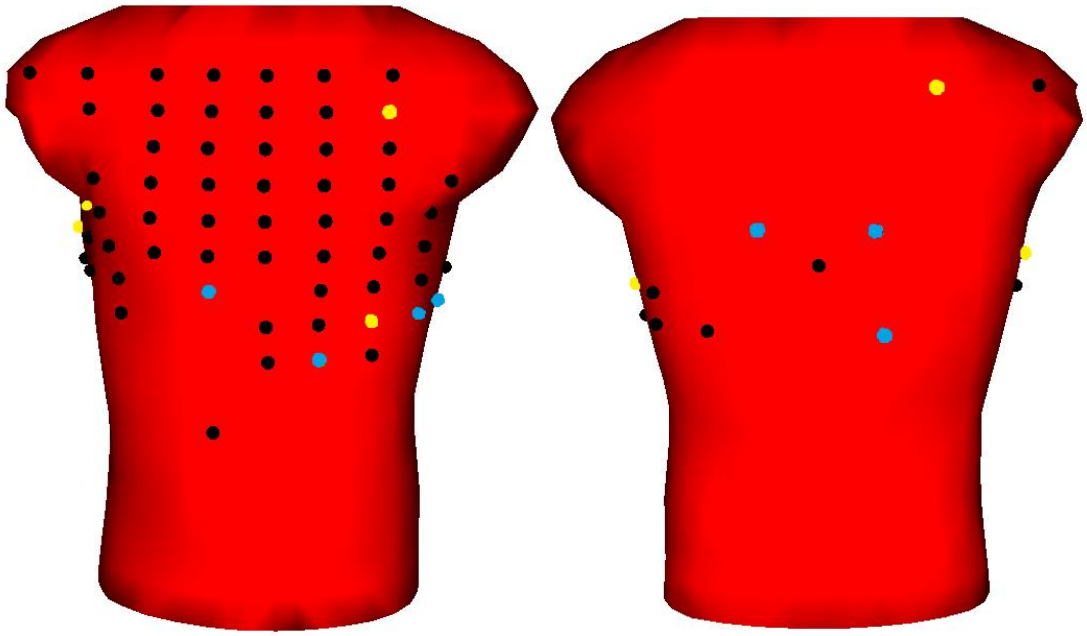

(a) (b)

Figure 4.13: position of 57 selected are shown by black mark. 7 out of 12 leads which are selected are shown in blue and rejected ones are in yellow. (a) Frontal view of lead-set configuration on the torso surface and (b) back view of lead-set configuration on the torso surface.

Finally, after considering all criteria above, 64 lead-set optimal for all data-sets, namely *common 64 lead-set*, is obtained. Figure 4.14 shows the position of these 64 leads on the torso surface.

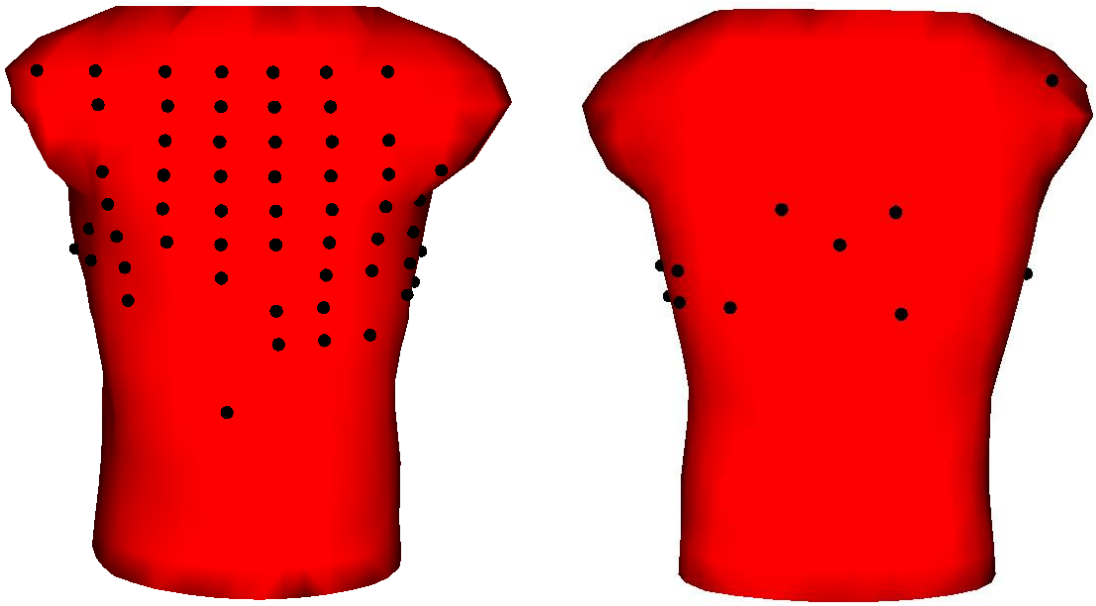

(a) (b)

Figure 4.14: The lead-set configuration for common 64 lead-set, (a) frontal view of lead-set configuration on the torso surface and (b) back view of lead-set configuration on the torso surface.

Considering Figure 4.14, as it was expected, the leads are denser in the frontal part of the torso leaving the small number of leads for the back region of the torso. This indicates that the method used to select common 64 lead-set is wise enough to select the leads from the regions in which the electrical activity of the hart is more detectable by electrodes.

The resultant configuration for 64 lead-set would be an efficient arrangement of leads to reconstruct the epicardial potentials. The ability of this common 64 lead-set to reconstruct the epicardial potentials will be assessed by comparing the results of the reconstructed epicardial potentials using the individual optimal 64 lead-sets and the results of reconstructed epicardial potentials using the common 64 lead-set. To this end, the epicardial potentials related to all 23 data-sets are reconstructed by by Tikhonov regularization and Maximum Correlation Coefficient (MCC) as the regularization parameter selection method. Then, the average of CC and standard deviation values of every single result are calculated. Table 4.3 displays these results together with the average and standard deviation values of the results obtained using individual optimal lead-sets for all 23 data-sets the second column (including the data-set label column) of this table is equal to the forth column of Table 4.1).

Table 4.3: Mean (avg) and standard deviation (std) of Correlation Coefficient (CC) values for optimal individual 64 lead-sets and common 64 lead-set for different 23 data-sets.

Lead-set / Data-set	64 Optimal Lead-set CC(avg±std)	Common 64 Lead-set CC(avg±std)
Data-1	0.74±0.22	0.77±0.20
Data-2	0.68±0.25	0.69±0.23
Data-3	0.75±0.21	0.75±0.20
Data-4	0.72±0.12	0.69±0.20
Data-5	0.76±0.18	0.76±0.19
Data-6	0.77±0.18	0.77±0.18
Data-7	0.77±0.17	0.76±0.17
Data-8	0.71±0.17	0.71±0.18
Data-9	0.75±0.19	0.75±0.17
Data-10	0.75±0.20	0.74±0.20
Data-11	0.61±0.29	0.62±0.28
Data-12	0.67±0.30	0.67±0.30
Data-13	0.76±0.19	0.75±0.19
Data-14	0.68±0.25	0.67±0.23
Data-15	0.75±0.18	0.75±0.18
Data-16	0.77±0.16	0.76±0.16
Data-17	0.64±0.23	0.63±0.23
Data-18	0.63±0.20	0.63±0.21
Data-19	0.71±0.16	0.71±0.15
Data-20	0.71±0.19	0.67±0.21
Data-21	0.61±0.28	0.61±0.27
Data-22	0.77±0.16	0.75±0.18
Data-23	0.66±0.18	0.64±0.19

To better understand the results presented in Table 4.3, they are displayed in two ways in the Figure 4.15. The mean of Correlation Coefficient values presented in the above table are shown by bars in the up panel of the Figure 4.15 and by dots in the bottom panel.

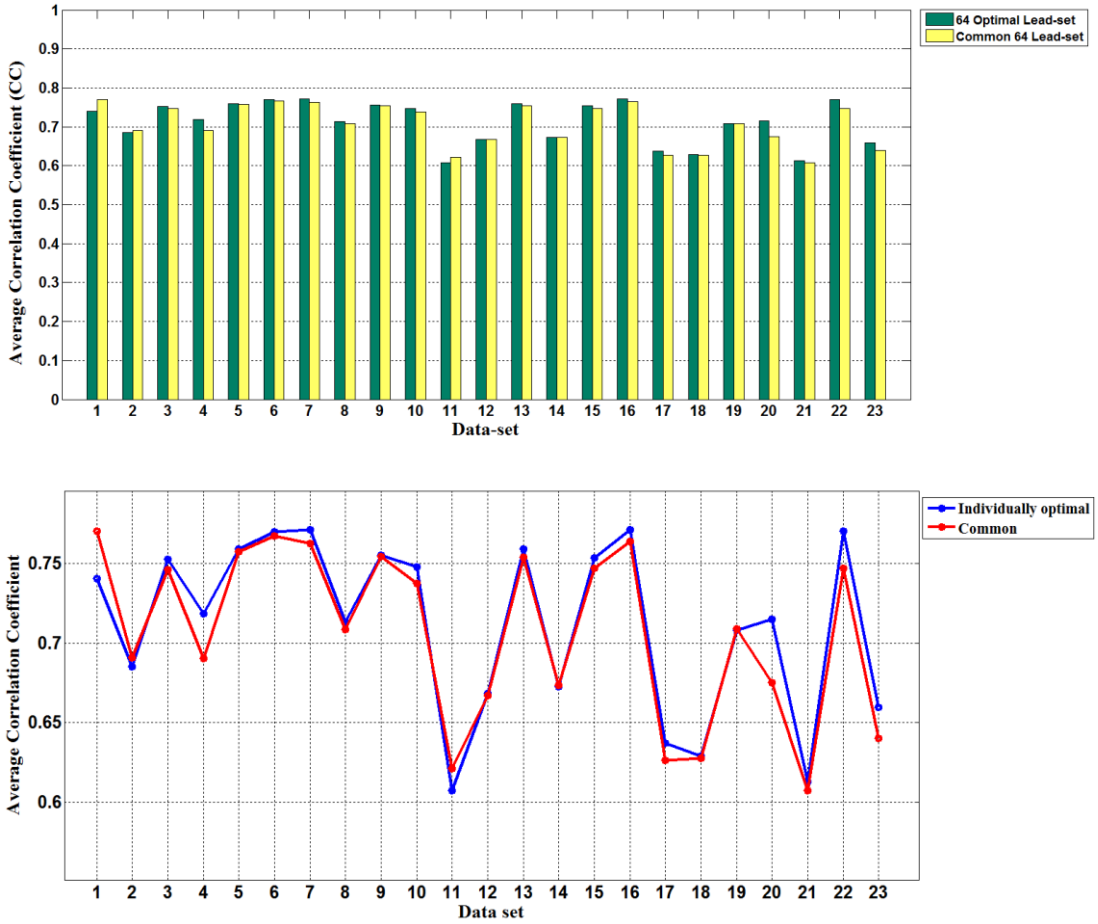

Figure 4.15: Mean (avg) of Correlation Coefficient (CC) values for optimal individual 64 lead-sets and common 64 lead-set for different 23 data-sets.

As it is displayed in Table 4.3. and Figure 4.15 there are some data-sets whose individually optimal 64 lead-set give better results than common 64 lead-set, as well as data-sets whose individual optimal lead-sets give equal or worse results than common 64 lead-set. This behavior can be explained by the nature of the lead reduction algorithm which stands on the conditional selection of the candidate leads in conjugate with the previously selected leads such that the selected set gives the best result in each step (see Chapter 3).

Obviously, it is not feasible to examine all possible number of 64 combinations from the complete primary 771 lead-set (or the 192 lead-set), since the related *binomial coefficient* (see Appendix A) approximately equals to $3.1619e+94$. This amount of combination is impossible to test in MATLAB to select the best configuration. Therefore, by applying the lead reduction algorithm on each data-set, we tried to estimate a *nearly* optimal configuration for each of the data-sets.

4.3.2.2 Common 32 Lead-set for All Data-sets

All of the above-mentioned procedure is again repeated to select common 32 lead-set out if the optimal individual 32 lead-sets related to 23 data-sets. Here, the results are presented exactly in the same order as they have been presented for the common 64 Lead-set.

Same as common 64 lead-set, the figure that displays the number of lead repetition along with their locations should be obtained. Figure 4.16 displays the mentioned property for every individual optimal 32 lead-set for 23 different data-sets.

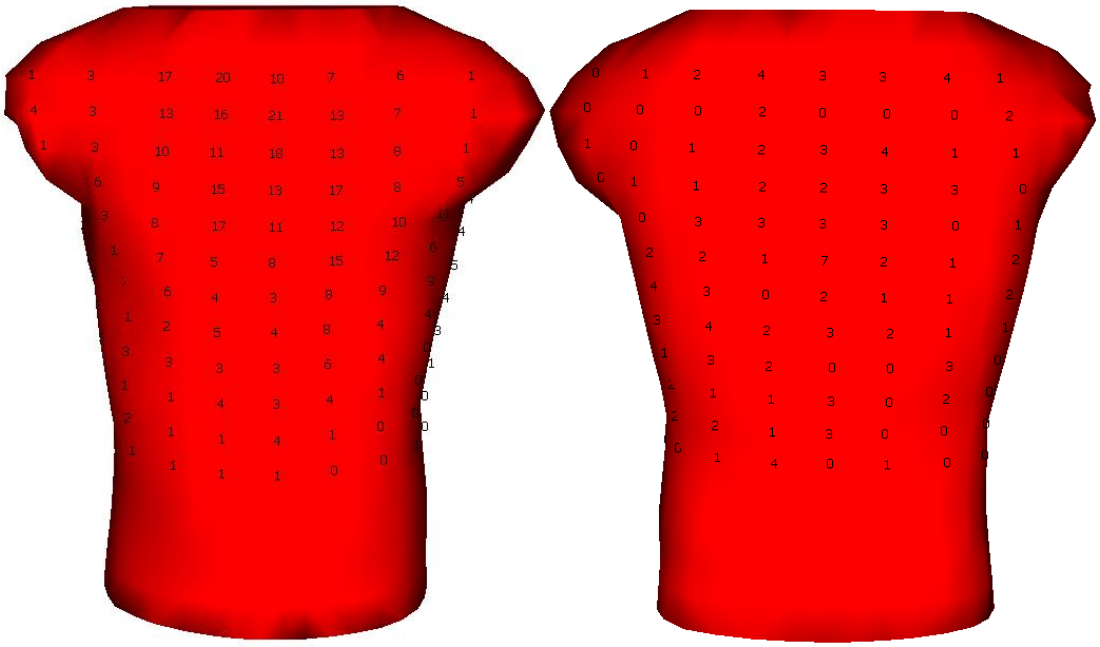

(a) (b)

Figure 4.16: 192 leads and their repetition times in the case of selecting 32 leads from 192 leads. (a) Frontal view and (b) back view.

Similar to what we have done to form common 64 lead-set, a histogram plot should be obtained to facilitate the selection process following the steps mentioned in the previous section. Figure 4.17 displays the histogram plot which shows lead numbers (indices) versus the number of times that they have been repeated in the case of selecting 32 lead-set for every one of 23 data-set.

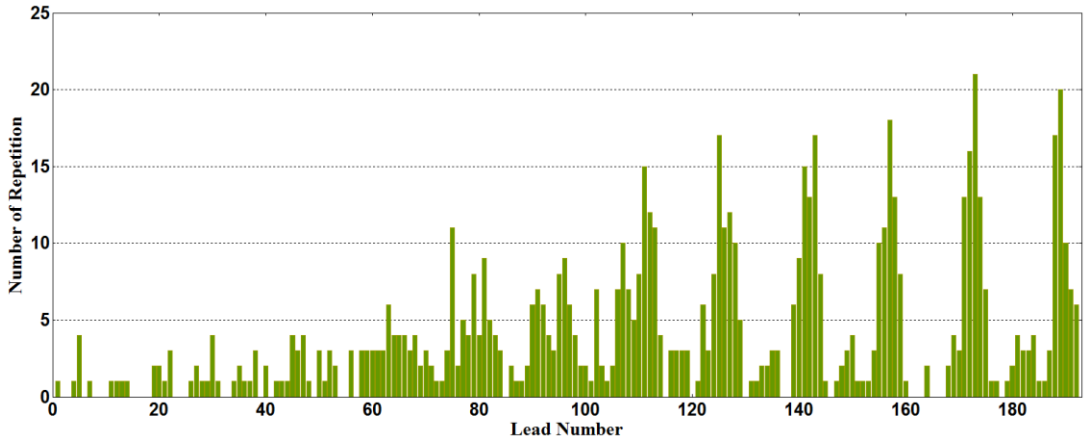

Figure 4.17: Histogram plot for 32 lead-set.

To have better view of the plot in Figure 4.17, first the number of leads are sorted according to the number of times that they have been repeated, then the most repeated leads are selected to be insert in common 32 lead-set. This sorted histogram is displayed in Figure 4.18. As it is shown in this figure, all of the leads with repetitions times 21 to 8 are selected to form common 32 lead-set.

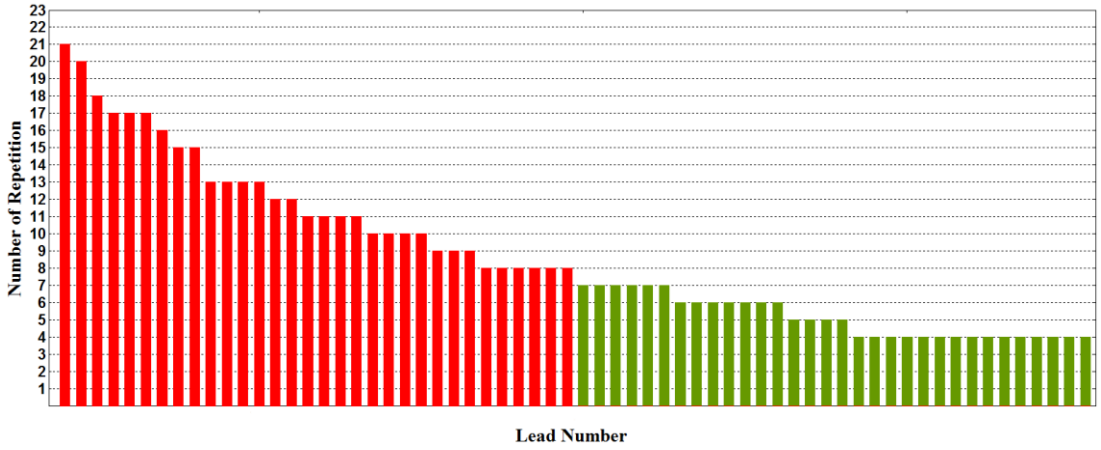

Figure 4.18: 32 leads that are selected to form common lead-set 32 are shown by the red bars.

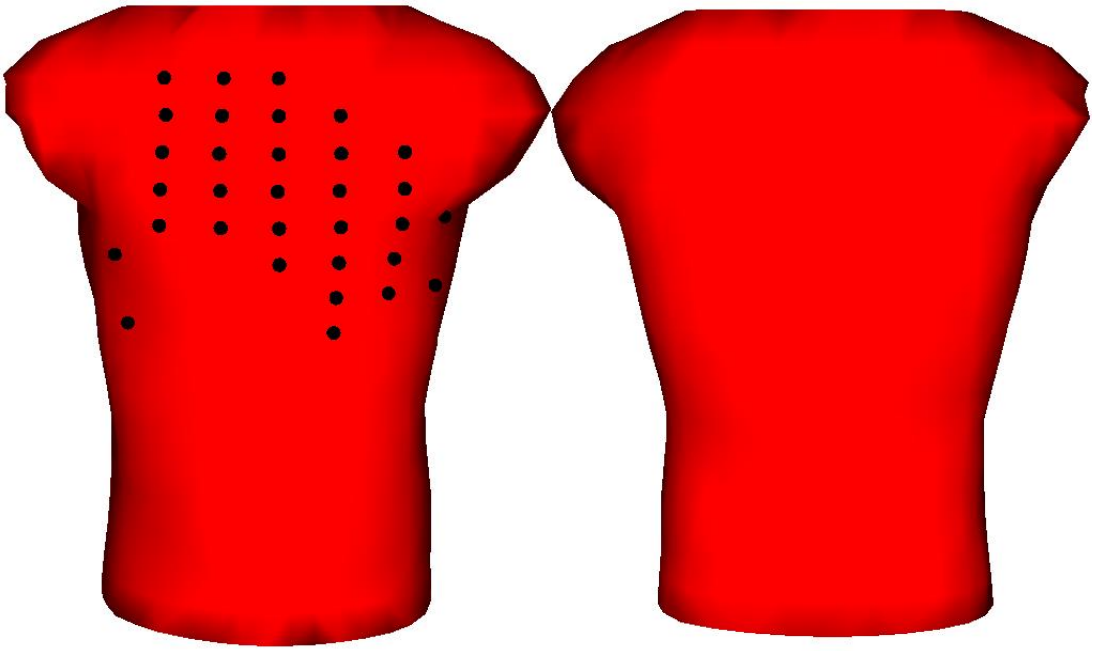

(a) (b)

Figure 4.19: Common 32 lead-set configuration. (a) Frontal view and (b) back view.

Figure 4.19 shows the location of common 32 lead-set on the torso surface. As it is seen in the figure, there is no lead in the back part of the torso. The reason for this is that when a limited number of leads is desired, it is more beneficial to select the leads from the frontal part of the torso surface, where the electrical signals of the heart are more significant, informative, and powerful [26]. Therefore, the epicardial potentials are expected to be reconstructed efficiently using this common lead-set.

Same as what was done for common 64 lead-set, in order to assess the ability of the acquired data using common 32 lead-set to reconstruct the epicardial potentials, inverse problem of ECG is solved. The epicardial potentials related to 23 data-sets are reconstructed using Tikhonov regularization along with Maximum Correlation Coefficient (MCC) as the regularization parameter selection method. Then, the average and standard deviation of CC values for each one of the 23 data-sets are calculated using the common 32-lead data and compared with the average and standard deviation of CC values related to every single 23 individual optimal lead-sets (the second column of this table is equal to the last column of Table 4.1). Table 4.4 displays these results.

Table 4.4: Mean (avg) and standard deviation (std) of Correlation Coefficient (CC) values for optimal individual 64 lead-sets and common 32 lead-set for different 23 data-sets.

Lead-set / Data-set	32 Optimal Lead-set CC(avg±std)	Common 32 Lead-set CC(avg±std)
Data-1	0.73±0.22	0.74±0.20
Data-2	0.67±0.25	0.66±0.23
Data-3	0.74±0.21	0.73±0.21
Data-4	0.70±0.20	0.65±0.22
Data-5	0.72±0.17	0.73±0.20
Data-6	0.76±0.19	0.76±0.18
Data-7	0.76±0.18	0.73±0.18
Data-8	0.70±0.18	0.69±0.18
Data-9	0.74±0.19	0.74±0.17
Data-10	0.73±0.21	0.71±0.22
Data-11	0.60±0.30	0.58±0.30
Data-12	0.65±0.30	0.63±0.30
Data-13	0.75±0.19	0.74±0.19
Data-14	0.65±0.25	0.63±0.25
Data-15	0.74±0.18	0.72±0.18
Data-16	0.77±0.16	0.74±0.16
Data-17	0.62±0.23	0.59±0.23
Data-18	0.62±0.21	0.58±0.21
Data-19	0.70±0.15	0.69±0.15
Data-20	0.70±0.20	0.56±0.27
Data-21	0.59±0.28	0.56±0.28
Data-22	0.75±0.17	0.71±0.20
Data-23	0.65±0.18	0.60±0.20

Generally, as it is expected that the CC values of individually optimal 32 lead-sets are better than CC values of common 32 lead-set. Only a few data-sets show different behaviors.

Considering the values presented in the Table 4.4, it can be seen that there are some data-sets whose common 32 lead-set gives better results than their individually optimal 32 lead-set. The same thing is observed in the previous section for 64 lead-sets. Here, again the nature of the lead reduction algorithm, which selects the next lead depending on the previously selected leads, namely conditional selection of leads, could be the reason for such difference.

To better understand the results presented in Table 4.4, they are displayed in two different plots in the figure below. The mean of Correlation Coefficient values presented in the above table are shown by bars in the upper panel of Figure 4.20 and by dots in the bottom panel.

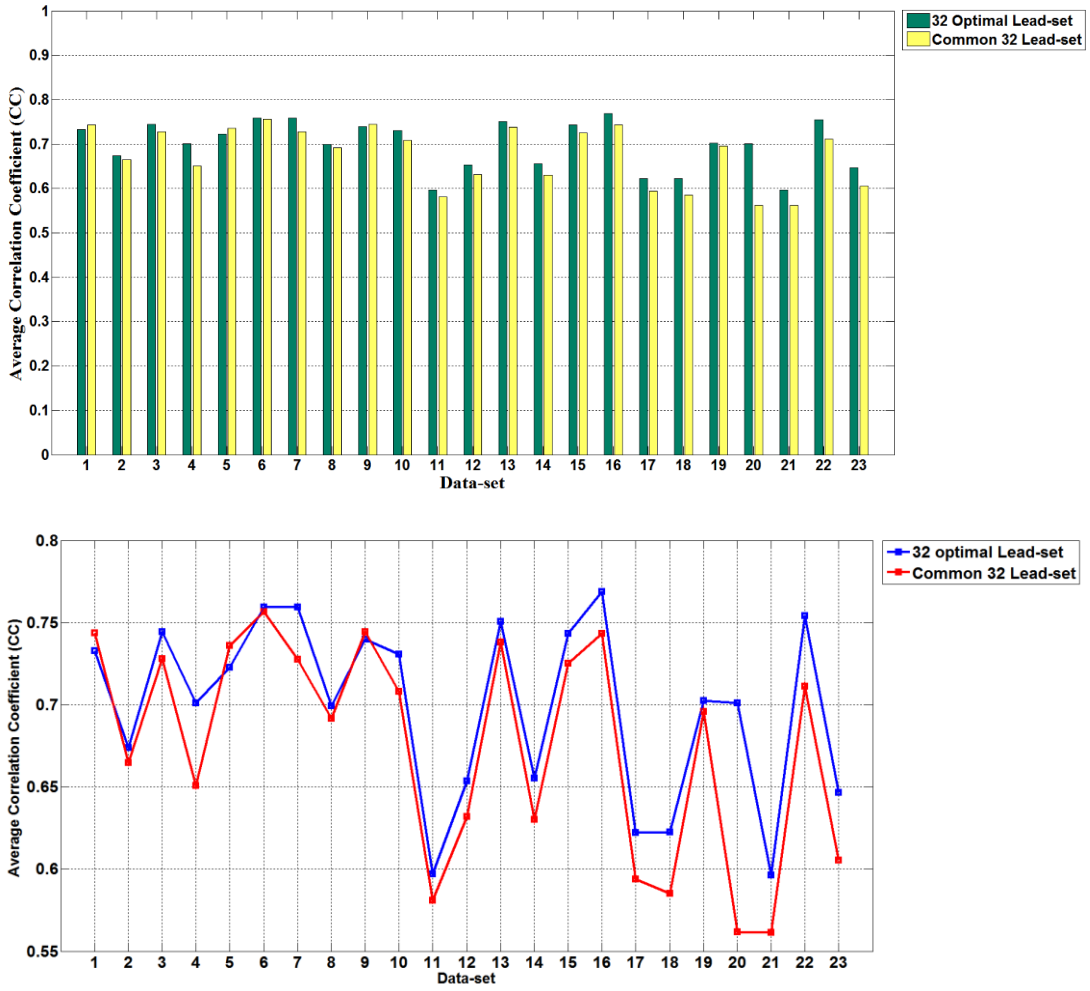

Figure 4.20: Mean (avg) values of Correlation Coefficient (CC) for optimal individual 64 lead-sets and common 32 lead-set for different 23 data-sets.

As it can be inferred from the Figure 4.20, average of CC values do not show significant changes when they are compared to individually optimal 32 lead-set, exclusive for each of the 23 data-sets.

To further demonstrate that reducing the lead number and solving the inverse problem of ECG using the related data to those reduced-sized lead-sets does not significantly affect the solution of inverse problem, MAP3D visualization software is

used to present the reconstructed epicardial potentials. MAP3D visualization software is developed at University of Utah, Nora Eccles Harrison Cardiovascular Research and Training Institute (CVRTI) for the purpose of displaying and editing three-dimensional geometric models and time-based data associated with those models. Another reason to visualize the reconstructed epicardial potentials by MAP3D software is to observe the reconstruction of activation wave front, which is one of the most important features of the inverse electrocardiography problem. Towards this end, three data-sets are selected out of 23 data-sets and displayed in two time instances. The next three figures show MAP3D results for data-sets 2, 11, and 23 at two different time instants. Figure 4.21 displays MAP3D images of reconstructed potentials of data-set 2, using Tikhonov regularization with Maximum Correlation Coefficient as the regularization parameter selection method. To recognize the quality of different solutions using different number of leads, the true potential distribution on the epicardial surface is also presented. Panel (a) and (b) in the Figure 4.21, display related solutions for data-set 2 in time t=32 *ms* and t=69 *ms*, respectively. The top maps in both panels are true potential distribution on epicardial surface along with color-bar related to those specific time instances.

In the figures, 4.21-4.23, the reconstructed potentials on epicardial surface using three data-sets, 2, 11, and 23 are displayed, respectively. Each figure contains the MAP3D results in 2 different time instances. As it can be inferred from the set of figures in one time instant, although, the wave-front is widened in all of the results related to different lead-sets (Figure 4.21 (b-g)), the reduced common lead-sets can estimate the active regions on the epicardial surface Figure 4.21 (e, g).

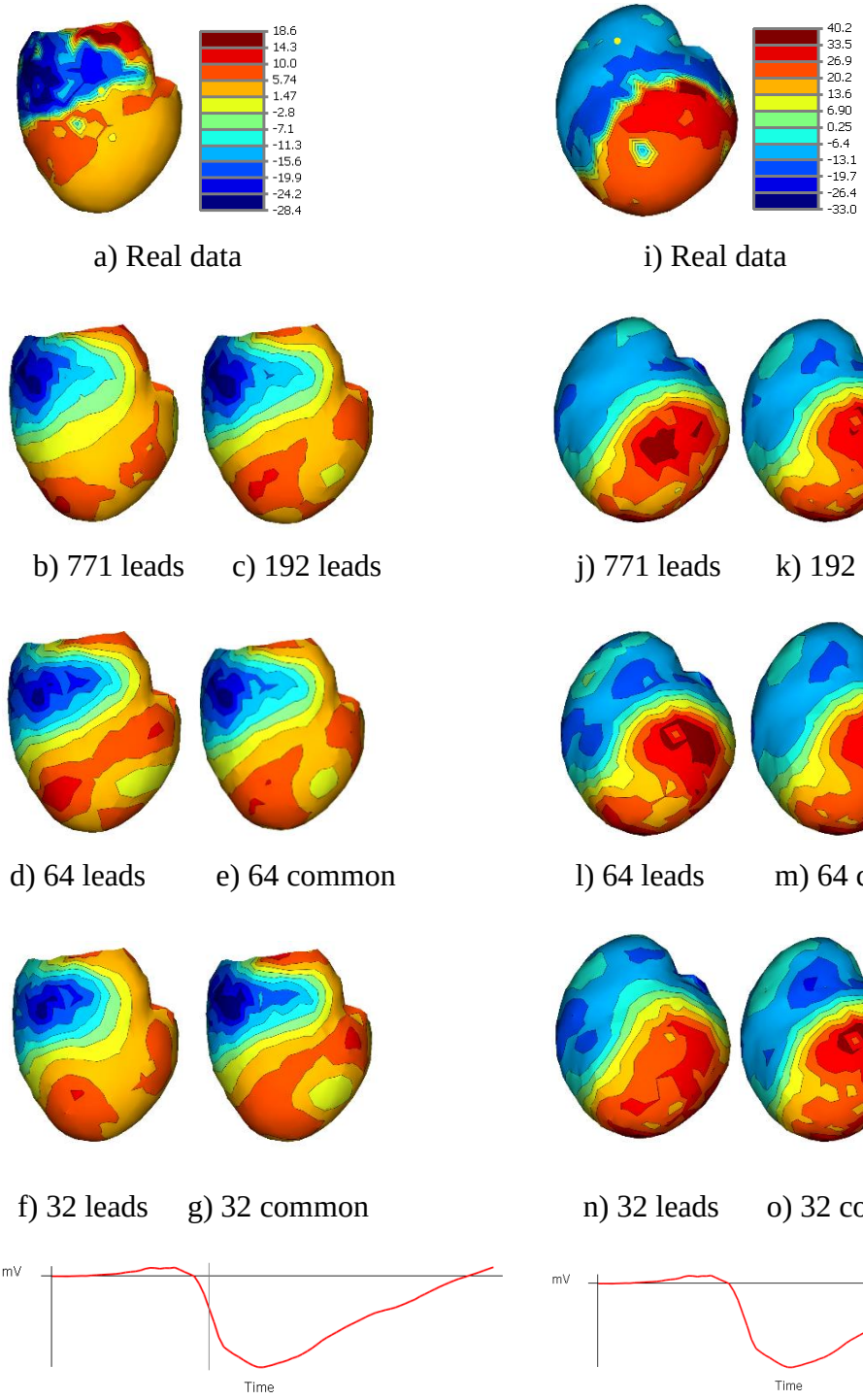

a) Real data i) Real data

b) 771 leads c) 192 leads j) 771 leads k) 192 leads

d) 64 leads e) 64 common l) 64 leads m) 64 common

f) 32 leads g) 32 common n) 32 leads o) 32 common

(h) (p)

Figure 4.21: Epicardial potential map for data-set 2 at *t*=32 ms in the left panels and *t*=69 ms in the right panels. (a) and (i) are the real epicardial potentials, (b) and (j) are the reconstructed epicardial potentials using the 771 lead-set, (c) and (k) are the reconstructed epicardial potentials using the 192 lead-set, (d) and (l) are the reconstructed epicardial potentials using individually optimal 64 lead-set, (e) and (m) are the reconstructed epicardial potentials using common 64 lead-set, (f) and (n) are the reconstructed epicardial potentials using individually optimal 32 lead-set, (g) and (o) are the reconstructed epicardial potentials using common 32 lead-set.

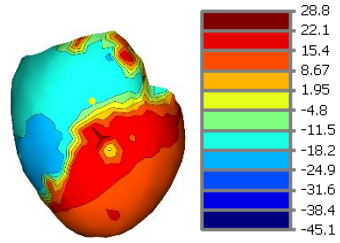

a) Real data

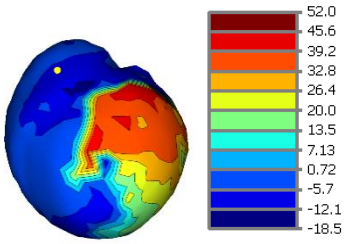

i) Real data

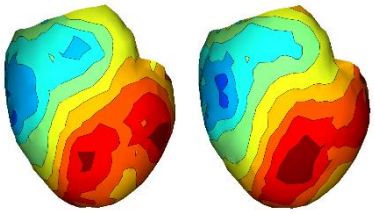

b) 771 leads c) 192 leads

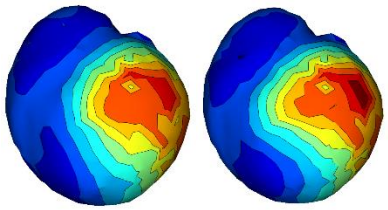

j) 771 leads k) 192 leads

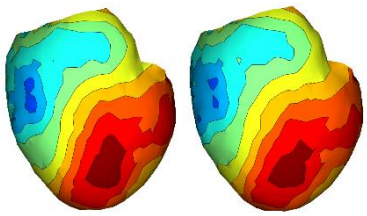

d) 64 leads e) 64 common

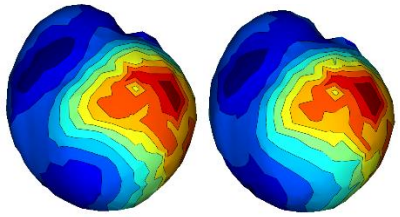

l) 64 leads m) 64 common

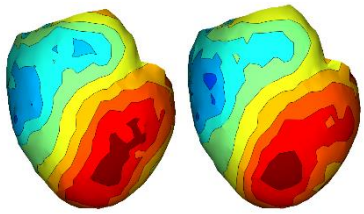

f) 32 lead (g) 32 common

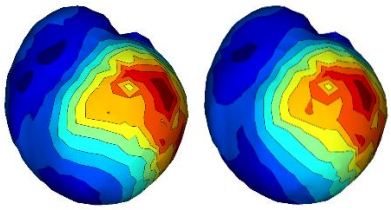

n) 32 leads o) 32common

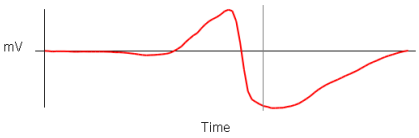

(h)

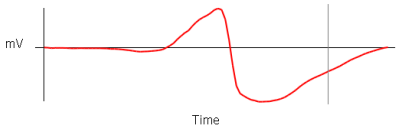

(p)

Figure 4.22: Epicardial potential map for data-set 11 at *t*=56 ms in the left panels and *t*=78 ms in the right panels. (a) and (i) are the real epicardial potentials, (b) and (j) are the reconstructed epicardial potentials using the 771 lead-set, (c) and (k) are the reconstructed epicardial potentials using the 192 lead-set, (d) and (l) are the reconstructed epicardial potentials using individually optimal 64 lead-set, (e) and (m) are the reconstructed epicardial potentials using common 64 lead-set, (f) and (n) are the reconstructed epicardial potentials using individually optimal 32 lead-set, (g) and (o) are the reconstructed epicardial potentials using common 32 lead-set.

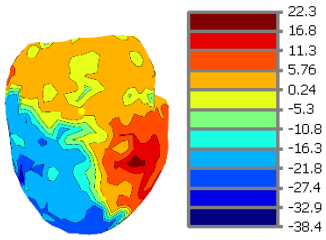

a) Real data

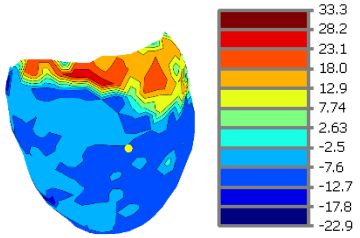

i) Real data

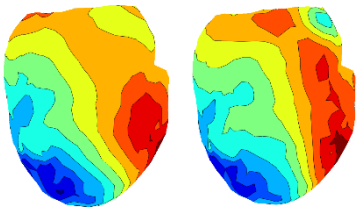

b) 771 leads c) 192 leads

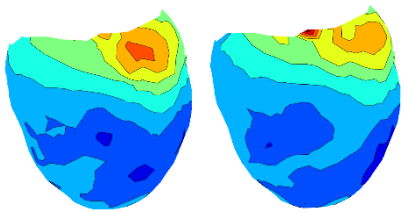

j) 771 leads k) 192 leads

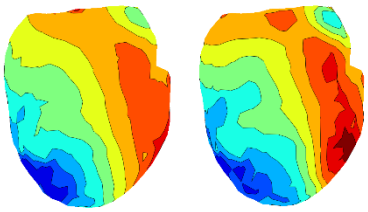

d) 64 leads e) 64 common

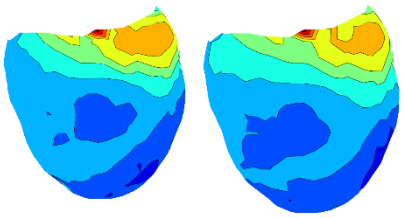

l) 64 leads m) 64 common

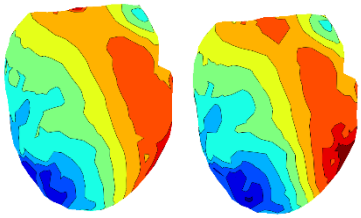

f) 32 leads g) 32 common

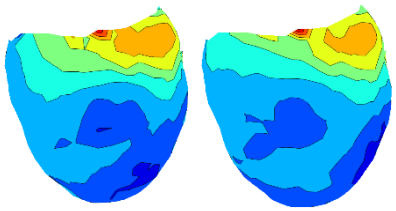

n) 32 leads o) 32 common

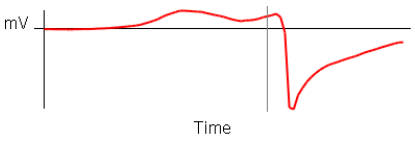

(h)

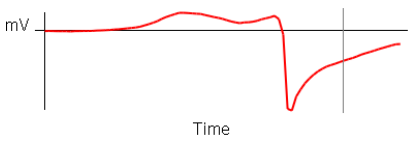

(p)

Figure 4.23: Epicardial potential map for data-set 23 at *t*=51 ms in the left panels and *t*=70 ms in the right panels. (a) and (i) are the real epicardial potentials, (b) and (j) are the reconstructed epicardial potentials using the 771 lead-set, (c) and (k) are the reconstructed epicardial potentials using the 192 lead-set, (d) and (l) are the reconstructed epicardial potentials using individually optimal 64 lead-set, (e) and (m) are the reconstructed epicardial potentials using common 64 lead-set, (f) and (n) are the reconstructed epicardial potentials using individually optimal 32 lead-set, (g) and (o) are the reconstructed epicardial potentials using common 32 lead-set.

4.3.3 Comparison of Different Methods

In this section, four different regularization methods, described in Chapter 3, are applied to 3 data-sets out of the 23 data-sets in order to compare the ability of these regularization methods to reconstruct the epicardial potentials with reduced number of leads. The regularization methods compared here are Tikhonov regularization, Truncated Total Least Square (TTLS), Lanczos Truncated Total Least Square (LTTLS), and Lanczos Least Square QR factorization (LLSQR) methods. For all of these regularization methods, MCC method is used as the regularization parameter selection method.

The results for each data-set are presented in separate tables in order to give a clear view about the performances of the applied regularization methods.

In Tables 4.5, 4.6, and 4.7 mean and standard deviation of of Correlation Coefficient (CC) values corresponding to inverse solutions using the 771 and 192 lead-sets, along with 64 and 32 lead-sets selected exclusively for that data-set only and common 64 and 32 lead-sets are presented, respectively.

Table 4.5: The results of mean (avg) and standard deviation (std) of Correlation Coefficient (CC) values calculated for different lead-sets for data-set 2.

Data-set 2 / **Method**	**771 Complete Lead-set CC (avg±std)**	**192 Lux Configur. CC (avg±std)**	**64 Optimal Lead-set CC (avg±std)**	**Common 64 Lead-set CC (avg±std)**	**32 Optimal Lead-set CC (avg±std)**	**Common 32 Lead-set CC (avg±std)**
Tikhonov	0.72±0.22	0.70±0.23	0.68±0.25	0.69±0.23	0.67±0.25	0.66±0.23
TTLS	0.65±0.23	0.65±0.24	0.66±0.25	0.66±0.24	0.66±0.25	0.65±0.24
LTTLS	0.69±0.23	0.68±0.24	0.67±0.25	0.68±0.24	0.67±0.25	0.66±0.24
LLSQR	0.64±0.23	0.64±0.23	0.64±0.24	0.65±0.23	0.65±0.24	0.64±0.24

Table 4.6: The results of mean (avg) and standard deviation (std) of Correlation Coefficient (CC) values calculated for different lead-sets for data-set 11.

Data-set 11 / Method	771 Complete Lead-set CC (avg±std)	192 Lux Configur. CC (avg±std)	64 Optimal Lead-set CC (avg±std)	Common 64 Lead-set CC (avg±std)	32 Optimal Lead-set CC (avg±std)	Common 32 Lead-set CC (avg±std)
Tikhonov	0.67±0.27	0.64±0.27	0.61±0.29	0.62±0.28	0.60±0.30	0.58±0.30
TTLS	0.59±0.27	0.59±0.28	0.59±0.29	0.60±0.28	0.60±0.29	0.58±0.29
LTTLS	0.62±0.28	0.62±0.28	0.60±0.30	0.61±0.29	0.60±0.29	0.58±0.30
LLSQR	0.58±0.26	0.58±0.27	0.58±0.29	0.59±0.28	0.59±0.29	0.57±0.29

Table 4.7: The results of mean (avg) and standard deviation (std) of Correlation Coefficient (CC) values calculated for different lead-sets for data-set 23.

Data-set 23 / Method	771 Complete Lead-set CC (avg±std)	192 Lux Configur. CC (avg±std)	64 Optimal Lead-set CC (avg±std)	Common 64 Lead-set CC (avg±std)	32 Optimal Lead-set CC (avg±std)	Common 32 Lead-set CC (avg±std)
Tikhonov	0.68±0.18	0.66±0.19	0.66±0.18	0.64±0.19	0.65±0.18	0.60±0.20
TTLS	0.58±0.20	0.59±0.20	0.62±0.20	0.61±0.20	0.63±0.19	0.60±0.21
LTTLS	0.63±0.19	0.63±0.20	0.64±0.19	0.63±0.20	0.64±0.19	0.61±0.21
LLSQR	0.57±0.20	0.58±0.19	0.60±0.18	0.60±0.20	0.62±0.19	0.59±0.21

As it can be inferred from these results, Tikhonov regularization yields better mean CC values than other regularization methods. Methods like LTTLS yield approximately similar results to that of Tikhonov regularization with shorter runtime. The runtime issue may seem unimportant when the size of the problem is medium or small. But when the problem has a large size, runtime issue gains further importance. For instance, when the inverse problem of ECG is solved in terms of Transmembrane Potentials (TMP) the size of the problem becomes very large, therefore it would be beneficial to use methods with short runtime.

To compare runtime duration for the above-mentioned regularization methods, namely Tikhonov, TTLS, LTTLS, and LLSQR, the execution time is calculated for several test-data. Since the sizes of the 23 used data-sets in this thesis are approximately similar, the runtimes are also approximately similar. The runtime is calculated for solving the inverse problem of ECG using 771 complete lead-set by 1.74 GHz Core i7 processor with 8 GB RAM. For Tikhonov, TTLS, LTTLS, and

LLSQR regularization methods the runtimes are 60, 100, 41, and 40 seconds, respectively. As it was mentioned before, although the difference between different runtimes is not eye-catching in our particular data-sets, in the case of dealing with large data-sets, it would be beneficial to use methods for which run times are short and are able to produce accurate results.

CHAPTER 5

CONCLUSIONS

In this study, a new method is proposed and implemented to reduce the number of leads attached to the body surface. The aim of this study is to propose a lead-set configuration whose acquired data from the surface of the torso is informative enough to reconstruct the epicardial potentials through solving the inverse problem of electrocardiography. In order to achieve such a lead-set, 23 different data-sets are used. In these data-sets, the heart is stimulated from 23 different sites and epicardial potentials are obtained from 490 electrodes. Then, these epicardial potentials are used to simulate body surface potentials at 192 equally spaced electrodes, which is the electrode configuration that Lux *et al.* used in [27]. Then the lead reduction algorithm is applied on each of these 23 data-sets. The algorithm terminated when the desired number of leads is reached. In this study, first the desired number of leads are set to 64 and then to 32 leads. Since 23 different data-sets are used, 23 different lead configurations consisting of 64 leads and 23 different lead configurations consisting of 32 leads are obtained. The performance of each of these lead-sets are assessed by solving the inverse problem of ECG, reconstructing epicardial potentials, using the data obtained by these lead-set configurations. In order to reconstruct epicardial potentials, in this study, Tikhonov regularization is used, and Maximum Correlation Coefficient (MCC) is employed as the regularization parameter selection method. To assess the performance of different lead-sets, Correlation Coefficient (CC) values between the reconstructed potentials using data obtained by reduced lead-sets and real potentials on the surface of the epicedium are calculated and compared. As it is reported in the result chapter of this thesis, there are not any significant difference between the performances of complete lead-sets and reduced ones.

However, a reduced lead-set obtained for one data-set may not be appropriate for another data-set. Therefore, there is need to obtain a lead-set configuration that works accurate enough for all 23 data-sets. To achieve one common 64 or 32 lead-set, whose obtained data performs with an acceptable accuracy when employed to reconstruct epicardial surface potentials, the most repeated leads in 23 different lead-set configurations are chosen. Then the performances of previously obtained 23 lead-sets related to 23 data-sets are compared calculating CC values between reconstructed epicardial potentials using data, obtained by common lead-set and, and real epicardial potential values. It has been revealed that no significant difference exists between the reconstructed epicardial potentials using large number of leads and the reconstructed epicardial potentials using common reduced lead-set.

To evaluate the performance of the reduced common lead-set, in addition to Tikhonov regularization, Lanczos Least Squares QR (LLSQR), Truncated Total Least Squares (TTLS), and Lanczos Truncated Total Least Squares (LTTLS) regularization methods are employed to reconstruct the epicardial potentials using the data acquired by this lead-set. As it is reported in the Results chapter, the reconstructed epicardial potentials using these regularization methods give reasonable answers. By further examining the performance tables related to these four regularization methods, it can be inferred that the LTTLS method, which employs Lanczos bidiagonalization algorithm as part of its regularization scheme, performs better than the TTLS method. Additionally, the runtime related to LTTLS regularization method is shorter than that of TTLS. It can be concluded that it would be better to use LTTLS method instead of TTLS method when dealing with large data matrices. For example, to solve inverse problem of ECG using Transmembrane Potentials (TMP), one has to deal with really large matrices and it would be beneficial to use LTTLS to reduce time cost of the operation.

5.1 Future Work

- Making the lead reduction algorithm independent of using the real values of epicardial potentials.
- Reducing the runtime of lead reduction algorithm.

REFERENCES

[1] World Health Organization, 2014. [Online]. Available: http://www.who.int/cardiovascular_diseases/resources/atlas/en. [Accessed 30 12 2014].

[2] "Hürriyet," 08 04 2009. [Online]. Available: http://www.hurriyet.com.tr/yasasinhayat/11372004.asp. [Accessed 05 01 2015].

[3] R.S. MacLeod and C.R. Johnson, "Map3d: interactive scientific visualization for bioengineering data," in Proceedings of *The Annual Conference on Engineering in Medicine and Biology*, 1993.

[4] P.C. Hansen, Regularization Tools: A MATLAB package for Analysis and Solution of Discrete Ill-Posed Problems. Version 4.1. 16 Apr 1998 (Updated 18 Mar 2008)

[5] A.C. Guyton and J. E. Hall, in *Textbook of medical Physiology*, Elsevier Saunders, 2006.

[6] H.D. Arnold, "Weight of a Normal Heart in Human Adult," J Boston Soc Med Sci, vol. 3, no. 6, pp. 174-184, Feb 7, 1899.

[7] Anatomical heart image," www.thaidentist.org, 2015. [Online]. Available: http://www.thaidentist.org/anatomical-heart-image/. [Accessed 03 02 2015]

[8] D. A. Tamarkin, "Heart Information," 2011. [Online]. Available: http://faculty.stcc.edu/AandP/AP/AP2pages/Units18to20/heart/heart.htm. [Accessed 13 01 2015].

[9] Wikipedia, "Wikipedia," 19 12 2014. [Online]. Available: http://en.wikipedia.org/wiki/Cardiac_action_potential#cite_note-FOOTNOTESherwood2012310-1-7. [Accessed 30 12 2014].

[10] S. Sherwood, "Wikipedia," 05 2012. [Online]. Available: http://en.wikipedia.org/wiki/Cardiac_action_potential. [Accessed 30 12 2014].

[11] Cildren's Hospital of Philadelphia, "Long QT Syndrome Knowledge Base," 2015. [Online]. Available: http://www.research.chop.edu/programs/lqts/causes.php. [Accessed 13 01 2015].

[12] J. Nerbonne and R. S. Kass, "Physiological Reviews," 2005. [Online]. Available: http://physrev.physiology.org/content/85/4/1205. [Accessed 30 12 2014].

[13] H.S. Oster, B. Taccardi, R.L. Lux, P.R. Ershler and Y. Rudy, "Electrocardiographic Imaging: Noninvasive Characterization of Intramural Myocardial Activation from Inverse-Reconstructed Epicardial Potentials and Electrograms," *Circulation*, pp. 1496-1507, 1997.

[14] L. Wang, J. Qin, , T.T. Wong and P.A. Heng, "Application of L1-norm Regularization to Epicardial Potential Reconstruction Based on Gradient Projection," *Physics in Medicine and Biology*, vol. 56, no. 19, pp. 6291-6310, 2011.

[15] "Practice Standards for Electrocardiographic Monitoring in Hospital Settings," [Online]. Available: http://circ.ahajournals.org/content/110/17/2721/F5.expansion.html.. [Accessed 30 12 2014].

[16] S. Silbernagl, in *Color Atlas of Pathophysiology*, Stuttgart • New York, Thieme, 2000, pp. 182-183.

[17] "Small animal Cardiology, ECG Tutotial," 2015. [Online]. Available: http://research.vet.upenn.edu/smallanimalcardiology/ECGTutorial/tabid/4930/Default.aspx. [Accessed 13 01 2015].

[18] R.L. Lux, R.S. MacLeod, M. Fuller, L.S. Green, F. Kornreich, "Estimating ECG distributions from small numbers of leads," *Journal of Electrocardiology*, vol. 28(SUPPL), pp. 92-97, 1995.

[19] S. Ghosh and Y. Rudy, "Application of L1-Norm Regularization to Epicardial Potential Solution of the Inverse Electrocardiography Problem," *Annals of Biomedical Engineering*, vol. 37, no. 5, pp. 902-912, 05 2009.

[20] F. Kornreich and P.M. Rautaharju, "The missing waveform and diagnostic information in the standard 12 lead electrocardiogram," *Journal of Electrocardiology*, vol. 14, no. 4, pp. 341-350, 1981.

[21] F. Kornreich, R.L. Lux, R.S. MacLeod, "Map representation and diagnostic performance of the standard 12-lead ECG," *Journal of Electrocardiology*, vol. 28(SUPPL), pp. 121-123, 1995.

[22] Kors, J.A., Van Herpen, G., "How Many Electrodes and Where? A "Poldermodel" for Electrocardiography," *Journal of Electrocardiology*, vol. 35(SUPPL), pp. 7-12, 2002.

[23] L.I. Horwitz, "Current Clinical Utility of Body Surface Mapping.," *The Journal of invasive cardiology*, vol. 7, no. 9, pp. 265-274, 1995.

[24] M.P. Donnelly, D.D. Finlay, C.D. Nugent and N.D. Black "Lead selection: old and new methods for locating the most electrocardiogram information," *Journal of Electrocardiology*, vol. 41, no. 3, p. 257–263, 06 2008.

[25] R.C. Barr, M.S. Spach and G. Herman, "Selection of the number and position of measuring locations for electrocardiography," *IEEE Transactions on Biomedical Engineering*, Vols. BME-18, no. 2, pp. 125-138, 03 1971.

[26] R.L. Lux, R. F. Wyatt, J.A. Abildskov and C. R. Smith, "Limited Lead Selection For Estimation Of Body Surface Potential Maps In Electrocardiography," *IEEE Transactions on Biomedical Engineering*, Vols. BME-25, no. 3, pp. 270-276, 1978.

[27] R.L. Lux, M.J. Burgess, R. F. Wyatt, A.K. Evans, G.M.Vincent and J.A.Abildskov, "Clinically practical lead systems for improved electrocardiography: comparison with precordial grids and conventional lead systems," *Circulation*, vol. 59, no. 2, pp. 356-363, 1979.

[28] D.D. Finlay, Nugent, C.D., Donnelly, M.P., Lux, R.L., McCullagh, P.J., Black, N.D., "Selection of optimal recording sites for limited lead body surface potential mapping: A sequential selection based approach," *BMC Medical Informatics and Decision Making*, vol. 6, no. 9, p. 9, 17 02 2006.

[29] F. Kornreich, R.S. MacLeod, R.L. Lux, "Supplemented standard 12-lead electrocardiogram for optimal diagnosis and reconstruction of significant body surface map patterns," *Journal of Electrocardiology*, pp. 251-256, 11 02 2008.

[30] D.D. Finlay, C.D. Nugent, M.P. Donnelly, R.L. Lux, "Eigenleads: ECG leads for maximizing information capture and improving SNR," 2010.

[31] Y. Serinağaoğlu Doğrusöz, "Application of Bayesian Methods to Electrocardiography," Ph.D. thesis, Northeastern University, Boston, Massachusetts, 2002.

[32] Y. Rudy and R. Plonsey, "A comparison of volume conductor and source fgeometry effects on body surface and epicardial potentials," *Circ. Res.*, vol.46, pp. 283-291, 1980.

[33] A. Barnard, I. Duck, M. Lynn and W. Timlake, "The application of electromagnetic theory in electrocardiography II. Numerical solutions of the integral equations," *Biophys. J.*, vol. 7, pp. 463-490, 1967.

[34] R. C. Barr, M. Ramsey and M. S. Spach, " Relating epicardial to body surface potential distributions by means of transfer coefficients base on geometry measurements. ", *IEEE Transactions of Biomedical Engineering*, vol. BME-24, pp. 1-11, 1977.

[35] R. Plonsey, "Laws governing current flow in the volume conductor," *In The Theoritical Basis of Electrocardiography* (C. V. Nelson and D. B. Geselowitz, ads), pp. 165-174, Oxford, 1976.

[36] C. Johnson, R. MacLeod and P. Ershler, "Acomputer model for study of electrical flow in the human thorax," *Comp. in Biol. & Med*, vol.22, pp. 305-323, 1992.

[37] G. Shou, L. Xia, and M. Jiang, Q. Wei, F. Liu and S. Crozier, "Solving the ecg forward problem by means of standard h- and h-hierarchical adaptive linear boundary element method: Comparison with two refinement schemes," *IEEE Transactions on Biomedical Engineering*, vol. 56, no. 5, pp. 1454-1464, 2009.

[38] D. Yao, "Electric potential produced by a dipole in a homogeneous conducting sphere," *IEEE Transactions on Biomedical Engineering*, vol. 47, no. 7, pp. 964-966, 2000.

[39] C. R. Johnson, “Computational and numerical methods for bioelectric field problems,” *Critical Reviews in Biomedical Engineering*, vol. 25, pp. 1–81, 1997.

[40] D. Güllmar, J. R. Reichenebach, A. Anwander, T. Knösche, C. H.Wolters, M. Eiselt and J. Haueisen, “Influence of anisotropic conductivity of the white matter tissue on EEG source reconstruction—A FEM simulation study,” *Int. J. Bioelectromagn.*, vol. 7, pp. 108–110, 2005.

[41] S.E. Geneser, R. M. Kirby and R.S. MacLeaod, "Application of stochastic finite elementmethods to study the sensitivity of ECG forward modeling to organ conductivity," *IEEE Transactions on Biomedical Engineering*, vol. 55, no. 1, pp. 31-40, 01 2008.

[42] S. Ghosh and Y. Rudy,"Accuracy of quadratic versus linear interpolation in noninvasive electrocardiographic imaging (ECGI)," in *Annals of Biomedical Engineering*, 2005.

[43] R. C. Barr, M. Ramsey and M. S. Spach, "Relating epicardial to body surface potential distributions by means of transfer coefficients based on geometry measurements," *IEEE Transactions on Biomedical Engineering*, Vols. BME-24, no. 1, pp. 1-11, 1977.

[44] H. A. Schlitt, L. Heller, B. Aaron, E. Best and D. M. Ranken, "Evaluation of boundary element methods for the EEG forward problem: Effect of linear interpolation," *IEEE Transactions on Biomedical Engineering*, vol. 42, no. 1, pp. 52-58, 01 1955.

[45] A. S. Ferguson and G. Stroink, "Factors affecting the accuracy of the boundary element method in the forward problem-I: Calculating surface potentials," *IEEE Transactions on Biomedical Engineering*, vol. 44, no. 11, pp. 1139-1155, 1997.

[46] N. Gençer and I. Tanzer, "Forward problem solution of electromagnetic source imaging using a new BEM formulation with high-order elements," *Physics in Medicine and Biology*, vol. 44, no. 9, pp. 2275-2287, 09 1999.

[47] G. Fischer, B. Tilg, P. Wach, R. Modre, U. Leder and H. Nowak, "Application of high-order boundary elements to the electrocardiographic inverse problem," *Computer Methods and Programs in Biomedicine*, vol. 58, no. 2, pp. 119-131, 1999.

[48] J. H. M. Frijns, S. De Snoo and R. Schoonhoven, "Improving the accuracy of the boundary element method by the use of second-order interpolation functions," *IEEE Transactions on Biomedical Engineering*, vol. 47, no. 10, pp. 1336-1346, 10 2000.

[49] M. Fuchs, J. Kastner, M. Wagner, S. Hawes and J. Ebersole, "A standardized boundary element method volume conductor model," *Clinical Neurophysiology*, vol. 113, no. 5, pp. 702-712, 2002.

[50] Z.A. Acar and N. Gençer, "An advanced boundary element method (BEM) implementation for the forward problem of electromagnetic source imaging," *Physics in Medicine and Biology*, vol. 49, no. 21, pp. 5011-5028, 11 2004.

[51] R.M. Gulrajani, P. Savard and F.A. Roberge, " The inverse problem of electrocardiography: Solution in terms of equivalent sources, *" Critical reviews in biomedical engineering*, vol. 16, no. 3, pp. 171-214,1988.

[52] R.C. Barr and M.S. Spach, "Inverse calculation of QRS-T epicardial potentials from body surface potential distributions for normal and ectopic beats in the intact dog," *Circulation Research*, vol. 42, no. 5, pp. 661-675, 1978.

[53] P.C. Franzone, B. Taccardi and C. Viganotti, "An approach to inverse calculation of epicardial potentials from body surface maps," *Advances in Cardiology*, vol. 31, no. 8, pp. 50-54, 1978.

[54] Y. Rudy and B.J. Messinger Rapport "The inverse problem in electrocardiography: solutions in terms of epicardial potentials, " *Critical reviews in biomedical engineering*, vol.14, no.3, pp. 215-268, 1988.

[55] R.S. MacLeod and R.L. Lux and B. Taccardi, "Electrocardiographic mapping in a realistic torso tank preparation," in *Annual International Conference of the IEEE Engineering in Medicine and Biology*, vol. 17. no. 1, pp. 245-246, IEEE Press, 1995.

[56] R. MacLeod, B. Taccardi and R.L. Lux, "Mapping of cardiac ischemia in a realistic torso tank preparation," in *Building Bridges: International Congress on Electrocardiology International Meeting*, pp. 76-77, 1995.

[57] R.S. MacLeod and D.H. Brooks, "Recent progress in inverse problems in electrocardiology," *IEEE Engineering in Medicine and Biology Magazine*, vol. 17, no. 1, pp. 73-83, 1998.

[58] Y. Rudy, H.S. Oster and D.S. Khoury, "Inverse reconstruction of epicardial and endocardial potentials," *proceeding of International Conference of IEEE, EMBS*, pp. 2006-2008, 1992.

[59] D. Khoury, B. Taccardi, R. Lux, P. Ershler and Y. Rudy, "Reconstruction of endocardial potentials and activation sequences from intracavitary probe measurements: Localization of pacing sites and effects of myocardial structure," *Circulation*, vol. 91, no. 3, pp. 845-863, 1995.

[60] E. Velipasaoglu, H. Sun, F. Zhang, K. Barrier and D. Khoury, "Spatial regularization of the electrocardiographic inverse problem and its application to endocardial mapping," *IEEE Transactions on Biomedical Engineering*, vol. 47, no. 3, pp. 327-337, 2000.

[61] R.M. Gulrajani, "The forward and inverse problems of electrocardiography: Gaining a better qualitative and quantitative understanding of the heart's electrical activity," *IEEE Engineering in Medicine and Biology Magazine*, vol. 7, no. 5, pp. 84-101, 1998.

[62] P.R. Johnston and R.M. Gulrajani, "A new method for regularization parameter determination in the inverse problem of electrocardiography," *IEEE Transactions on Biomedical Engineering*, vol. 44, no. 1, pp. 19-39, 1997.

[63] G. Shou, M. Jiang, L. Xia, Q. Wei, F. Liu and S. Crozier, "A comparison of different choices for the regularization parameter in inverse electrocardiography models," in *Annual International Conference of the IEEE Engineering in Medicine and Biology* - Proceedings, New York, 2006.

[64] S. Twomey, "On the Numerical Solution of Fredholm Integral Equations of the First Kind by the Inversion of the Linear System Produced by Quadrature," *Journal of the ACM (JACM)*, vol. 10, no. 1, pp. 97-101, 1963.

[65] C.S. Liu, "A Dynamical Tikhonov Regularization for Solving Ill-posed Linear Algebraic Systems," *Acta Applicandae Mathematicae*, vol. 123, no. 1, pp. 285-307, 2013.

[66] L. Reichel, F. Sgallari and Q. Ye, "Tikhonov regularization based on generalized Krylov subspace methods," in *Applied Numerical Mathematics*, 2012.

[67] G. Shou, L. Xia and M. Jiang, "Solving the electrocardiography inverse problem by using an optimal algorithm based on the total least squares theory," in *3rd International Conference on Natural Computation*, ICNC, Haikou, Hanian, 2007.

[68] R. Fierro, G. Golub, P.C. Hansen and D. O'Leary, "Regularization by truncated total least squares," *SIAM Journal on Scientific Computing*, vol. 18, no. 4, pp. 1223-1241, 1997.

[69] G. Shou, L. Xia, M. Jiang, Q. Wei, F. Liu and S. Crozier, "Truncated Total Least Squares: A New Regularization Method for the Solution of ECG Inverse Problems," *IEEE Transactions On Biomedical Engineering*, vol. 55, no. 4, pp. 1327-1335, 2008.

[70] D. L. Phillips, "A Technique for the Numerical Solution of Certain Integral Equations of the First Kind," *Journal of the ACM (JACM)*, vol. 9, no. 1, pp. 84-97, 01 1962.

[71] L. Zhang, Y. Cao and Z. Yangc, "Novel Iterative Truncated Total Least Squares algorithm for Image Restoration," *Applied Mechanics and Materials*, Vols. 401-403, pp. 1397-1400, 2013.

[72] A. Güçlü, "Comparison of Five Regularization Methods for the Solution of Inverse Electrocardiography Problem," M.Sc. Thesis, Middle East Technical University, Ankara, 2013.

[73] M. Jiang, L. Xia, G. Shou and M. Tang, "Combination of the LSQR method and a genetic algorithm for solving the electrocardiography inverse problem," *Physics in Medicine and Biology*, vol. 52, no. 5, p. 1277–1294, 2007.

[74] J. Barzilai and J. Borwein, "Two-point step size gradient methods," *IMA Journal of Numerical Analysis*, vol. 8, no. 1, pp. 141-148, 1988.

[75] G. Shou, L. Xia, F. Liu, M. Jiang and S. Crozier, "On epicardial potential reconstruction using regularization schemes with the L1-norm data term," *Physics in Medicine and Biology*, vol. 56, no. 1, pp. 57-72, 2011.

[76] G. Shou, L. Xia, M. Jiang, F. Liu and S. Crozier, "Forward and Inverse Solutions of Electrocardiography Problem Using an Adaptive BEM Method," in *Lecture Notes in Computer Science (including subseries Lecture Notes in Artificial Intelligence and Lecture Notes in Bioinformatics)*, Salt Lake, 2007.

[77] R. Aster, B. Borcher and C. Thurber1, "Rank Deficiency and Ill-Conditioning," in *Parameter Estimation and Inverse Problems*, Academic Press, 2003, p. 08.

[78] A. Tikhonov and V.Y. Arsenin, Solutions of Ill-posed Problems, John Wiley & Sons Inc, 1977.

[79] P. Franzone, L. Guerri, B. Taccardi and C. Viganotti, "Finite element approximation of regularized solutions of the inverse potential problem of electrocardiography and applications to experimental data," vol. 22, no. 1, pp. 91-186, 1985.

[80] S. Morigi and F. Sgallari "A regularizing L-curve Lanczos method for underdetermined linear systems," *Applied Mathematics and Computation*, vol. 121, no. 1, pp. 55-73, 2001.

[81] Huffel and J. Vandewalle, “The Total Least Squares Problem: Computational Aspects and Analysis,” Philadelphia, Pennsylvania: *Society for Industrial and Applied Mathematics*, 1991.

[82] G. H. Golub and C. V. Loan, "An Analysis of the Total Least Squares Problem," *SIAM Journal of Numerical Analysis*, vol. 17, no. 6, pp. 883-893, 1980.

[83] M. Jiang, L. Xia1, G. Shou1 and M. Tang3, "Combination of the LSQR method and a genetic algorithm for solving the electrocardiography inverse problem," *Physics in Medicine and Biology*, vol. 52, pp. 1277-1294, 2007.

[84] R. MacLeod, R. Lux and B. Taccardi, "A possible mechanism for electrocardiographically silent changes in cardiac repolarization," *Journal of Electrocardiology*, 1998.

APPENDIX A

FIGURES

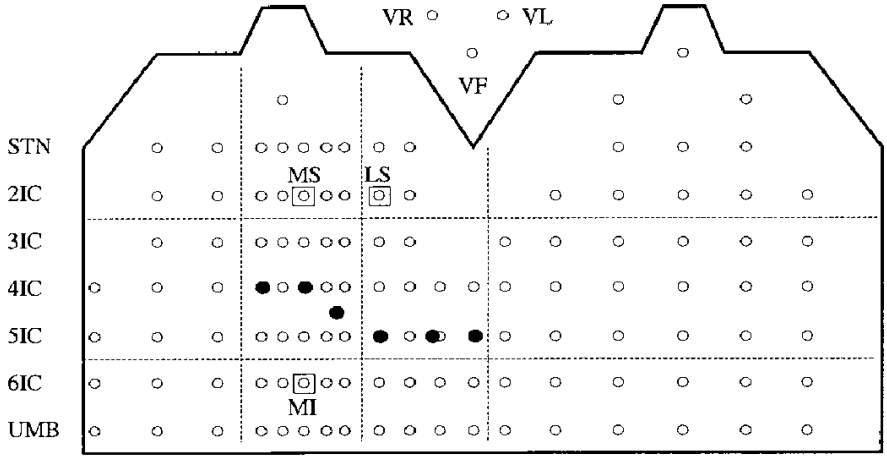

Figure A.1: Positions of the leads proposed by Kors *et al.*, [22].

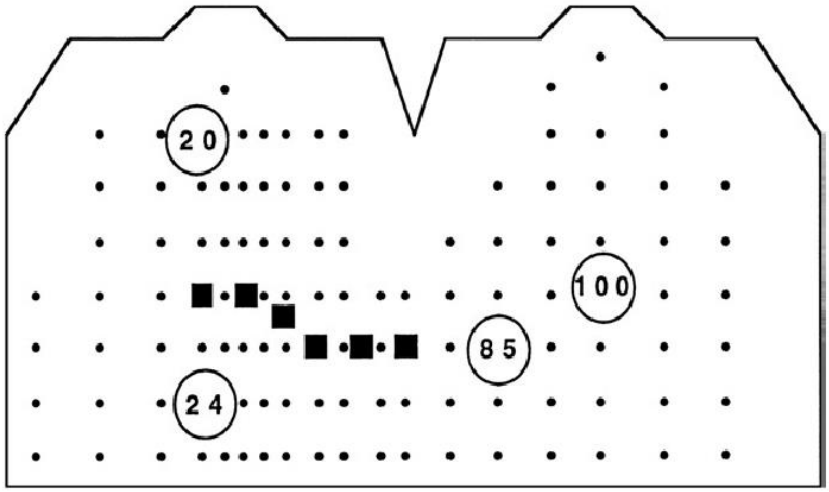

Figure A.2: Positions of the eigenleads proposed by Lux *et al.* [29].

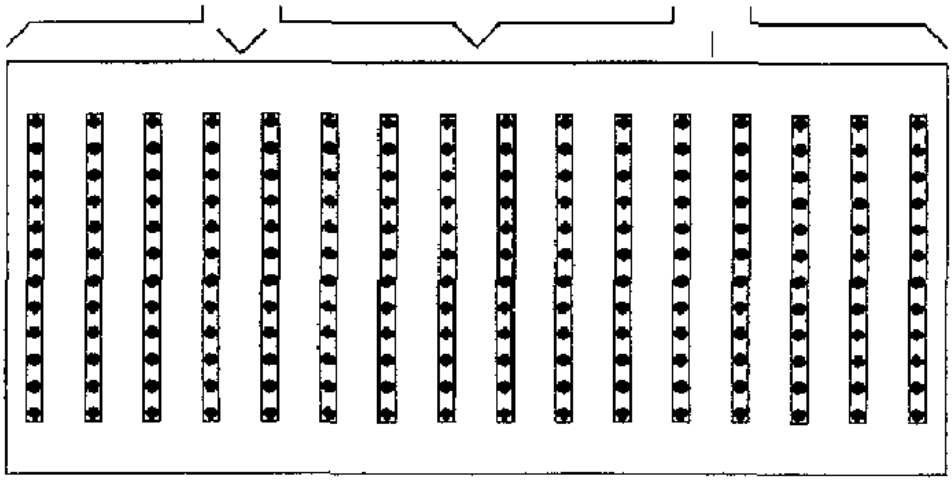

Figure A.3: Positions of the leads proposed by Lux *et al.* [27].

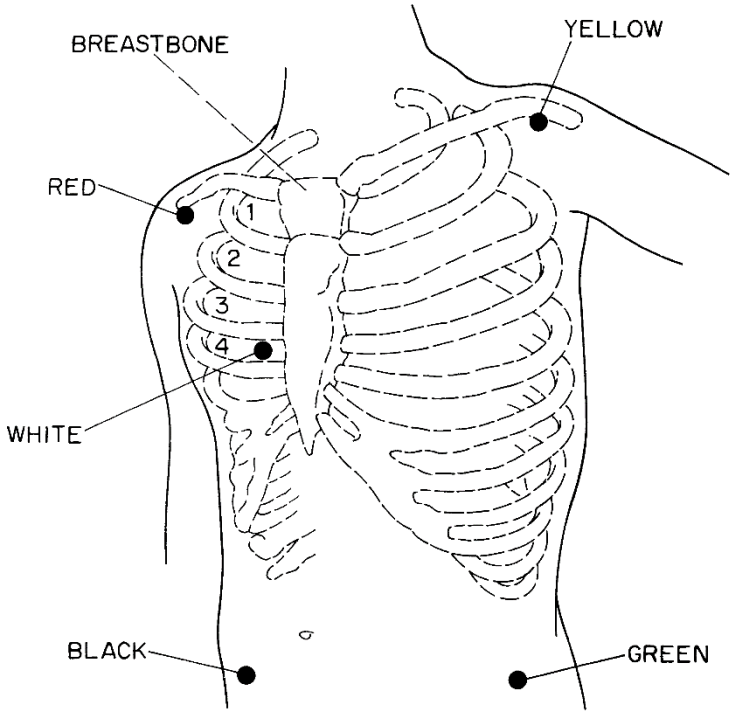

Figure A.4: Positions of the leads in EASI [30].

For natural numbers (taken to include 0) n and k, the binomial coefficient $\binom{n}{k}$ can be defined as the coefficient of the monomial X_k in the expansion of $(1 + X)^n$. The same coefficient also occurs (if $k \leq n$) in the binomial formula:

$$\binom{n}{k} = \frac{n!}{k!(n-k)!} \tag{A.1}$$